Synthesis and Property of Diborane(4) Dianion and Its Transition Metal Complexes

Seiji Akiyama

Table of Contents

Chapter 1

General Introduction

1.1 Boron

The boron (symbol B) is a chemical element and its atomic number 5. The feature of boron is the low electronegativity (Table 1.1). According to Mulliken's (χ_M) definition,[1] this property is based on boron's small ionization energy (I) and small electron affinity (E_a) (Figure 1.1). While, it corresponds small effective nuclear charge (Z_{eff}) and large covalent radii (r) in Allred Rochow's definition.[2] In addition, boron is an electron-deficient because the number of valence electron of boron is only three according to octet rule by Lewis.[3]

Table 1.1 Values of electronegativity of B, C, N, or O.

electronegativity (Pauling scale)	B	C	N	O
Pauling	2.04	2.25	3.04	3.44
Mulliken-Jaffe	2.04	2.48	2.90	3.42
Allred Rochow	2.01	2.50	3.07	3.50
Allen	2.051	2.544	2.066	3.610

$$\chi_{\mathrm{M}} = \frac{1}{2}(I + E_{\mathrm{a}}), \quad \chi_{\mathrm{AR}} = 0.744 + 3590\frac{Z_{\mathrm{eff}}}{(r/\mathrm{pm})^2}$$

Figure 1.1 The Definitions of electronegativity of Mulliken's and Allred Rochow's

The boron is also used well in our life (Figure 1.2). In material science, borosilicate glass is useful for cooking or experimental glasswares.[4] Borosilicate glass is useful as cooking or experimental glasswares because it shows resistance for thermal or chemical stress. Further, a neodymium magnet[5] which is known as one of the strongest magnets and a p-type semiconductor also contain boron. In radiochemistry, boron is a common chemical element of neutron absorption. In particular, boron carbide is applied for the control rod of a nuclear reactor. The drug including boron isotope ^{10}B is utilized in boron neutron capture therapy (BNCT).[6] In synthetic chemistry, the hydroboration-oxidation reaction by borane (BH_3) is a strong tool of anti-Markovnikov hydration of unsaturated hydrocarbons.[7] Of course, Suzuki-Miyaura cross-coupling is a common method of C–C bond formation to easily synthesize new drugs.[8]

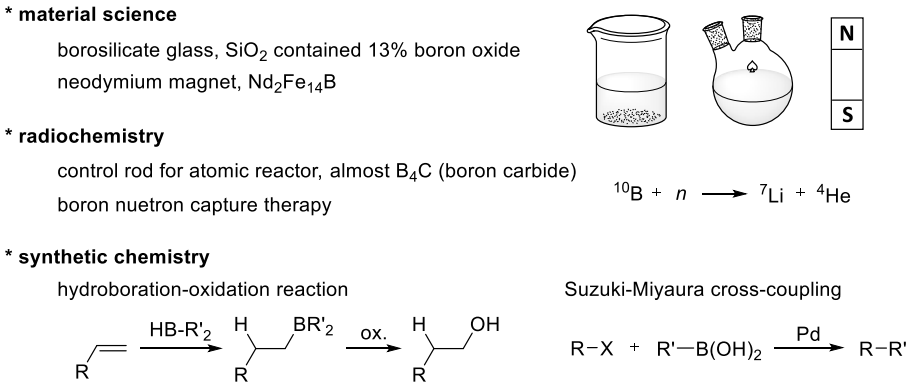

Figure 1.2 Examples of application of boron for life

1.2 Synthesis and Structures of Multiple Bond Between Borons

The simplest multiple bond between borons is a diborene HB=BH. The property of this diborene is quite different from ethylene ($H_2C=CH_2$) or diazene (HN=NH) of analogs (Figure 1.3). Ethylene and diazene have one occupied p-orbital and satisfy the octet rule. As a result, they are relatively stable and observable species. Needless to say, ethylene is the most important product of petrochemistry. It is applied as a plant hormone.[9)] On the other hand, diazene is metastable and decomposes to such as dinitrogen and hydrazine by disproportionation.[10)] It can be used for the *cis*-selective reduction of alkenes in organic synthesis.[11)] In particular, azo compounds, which have N=N double bond as a chromophore, are important as red artificial dyes. In contrast to examples of C or N, a diborene is highly unstable compounds. Actually, the first observation of diborene was recently reported by Ar matrix isolation method.[12)] Interestingly, it was reported that the diborene has the double bond character and triplet spin state by using Raman and ESR spectroscopy. Thus, the diborene has anomal semi-occupied and degenerated two p-orbitals.

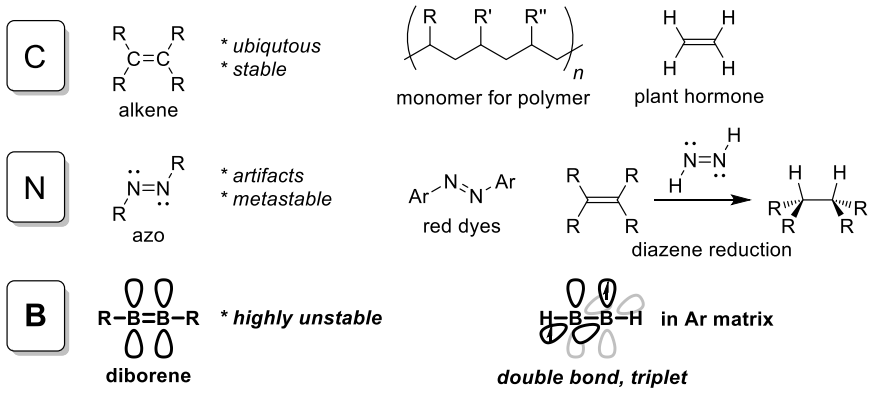

Figure 1.3 The comparison of C=C, N=N, and B=B double bond

The synthetic methods of diborene are limited. One of the synthesis methods is hydrogen abstraction from B_2H_6 by X-irradiation[12)b] or fluorine gas (Scheme 1.1).[12)c] Another method uses the reaction of H_2 gas with boron of gas-phase generated by pulsed-laser evaporation.[12)a] To isolate B=B double bond having compounds in the condensed phase, it is necessary to occupy the vacant orbital on two boron atoms with two bases. Compounds having a B=B double bond can be classified into the following two types. The first example of this class is reported by Robinson's group in 2007.[13] The synthesis of Lewis base stabilized diborene is achieved by the reduction of NHC-coordinated BBr_3. Many neutral diborenes are published in this method.[14)] The second class is stabilized by an anionic base, and it is called to diborane(4) dianion. The history of diborane(4) dianion is older than the former. The first example of diborane(4) dianion having a B=B double bond is reported by Power's group in 1992.[15)] This anionic compound is synthesized by two-electron reduction of tetraaryldiborane(4). A few examples of diborane(4) dianion are reported.[16)] The synthesis of compounds having a B≡B triple bond is also possible like alkynes or dinitrogen. This type of compound is called to a diboryne. The key precursor of synthesis of a diboryne is NHC-coordinated tetrabromodiborane(4). The four-electron reduction of the base coordinated tetrabromodiborane(4) gives a diboryn.[17)] This compound is a

milestone in organoboron chemistry. These B=B double or B≡B triple bonds are characterized by molecular structure. By single-crystal X-ray diffraction, the B=B / B≡B length of both neutral diborenes and diborane(4) dianions is shorter than that of a normal B–B single bond. Generally, the length of diborane(4) dianions is longer. The diborynes has the shortest B≡B length. The mechanical strength of B≡B triple bond of diborynes is evaluated by Raman spectroscopy.[18)] The frequency corresponding to the absorption of B≡B triple bond shows lower than those of the C≡C or N≡N triple bond.

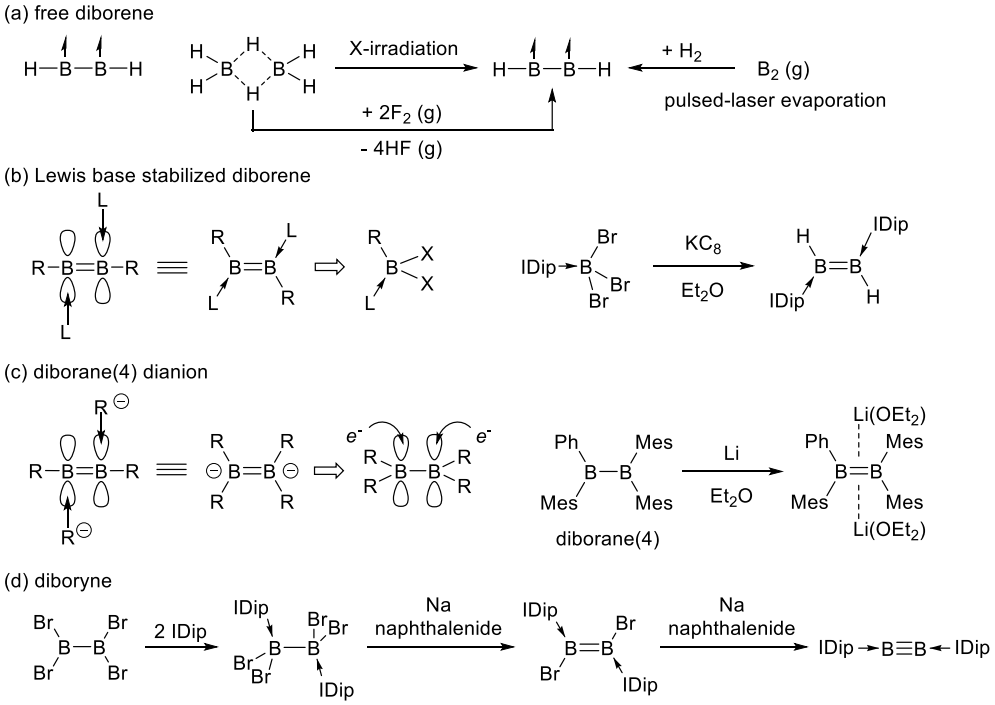

Scheme 1.1 Methods of synthesis of compounds having a B=B double bond

1.3 Reactivity of Multiple Bond Between Borons

Recently, various reactivities of multiple bond between borons are revealed (Scheme 1.2). In particular, the reactivity of neutral diborenes and diboynes is actively investigated. In the chemistry of a diborene, the reactivity for the B=B double bond similar to alkenes is found. For example, simple 1,2-addition of Se–Se,[19)b] B–B, [19)d] or B–H[19)a,e] bond, [4+2] pericyclic addition with diene,[19)c] carbene insertion (or 1,1-addition) of isocyanide,[20)] and p-coordination of metals. [21)] Interestingly, diborenes show the reactivity like electron-rich alkenes. Actually, [4+2] cycloadition with electron-rich diene does not proceed. In the chemistry of diborynes, a few examples of reactivity is reported. The insertion reaction of chalcogen (S, Se) to triple bond,[22)b] and formal [1+2] cycloaddition with carbon monoxide[22)a] are published. However, the most interesting molecule is the disubstituted diborenes formed by 1,2-addition of chalcogen to a cAAC-stabilized diboryne. [22)bc] Surprisingly, the product is a twisted B=B double bond. The completely twisted double bond is not achieved in C or N double bond still, thus this remarkable phenomenon would be based on the feature of electron-deficiency of vacant p-orbital on borons.

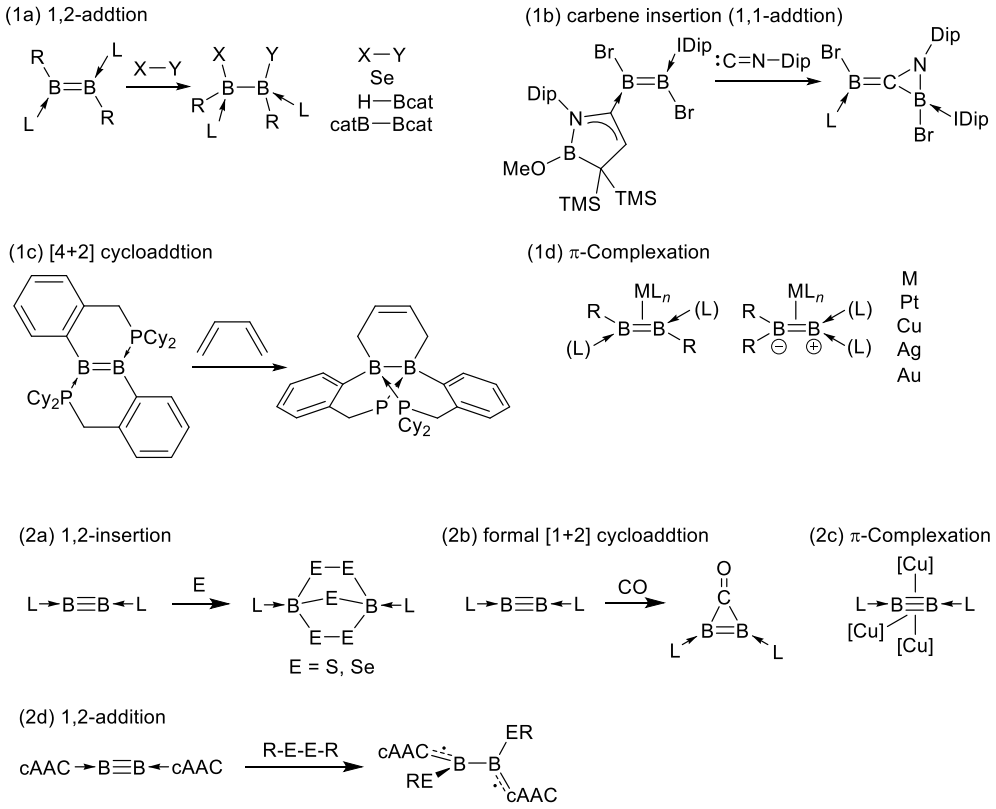

Scheme 1.2 reactivities of B=B double or B≡B triple bonds

On the other hand, the reactivity of diborane(4) dianion is not well known so far (Scheme 1.3). One of the reported reactivity is two-electron oxidation by 1,2-diboromoethane.[16)b] This reaction gives neutral diborane(4) hydrogen-bridged by oxidation. Another reactivity was found in diborane(4) dianion of planer constrained biphenyl skeleton, recently. The reaction of diborane(4) dianion with terminal dihaloalkanes obtain diborafluorenylalkane.[16)e] This reactivity means that the diborane(4) dianion is the behavior of diborane(4) dianion like two borafluorenyl anions. The detail of the mechanism is unclear, but the reaction would be through the pathway of ring-contracted rearrangement from a six-membered ring to a five-membered ring. It should be noted that the reaction with 1,2-dibromoethane gave a different product in the former or latter. In addition, as a related reaction to diborane(4) dianion, the reaction of a platinum complex with tetraiododiborane(4) is important. This reaction gave a formal tetraiododiborane(4) dianion π-complex of platinum via unclear multi redox steps.[23)] However, the direct synthesis of diborane(4) dianion π-complex with using diborane(4) dianions is still not achieved.

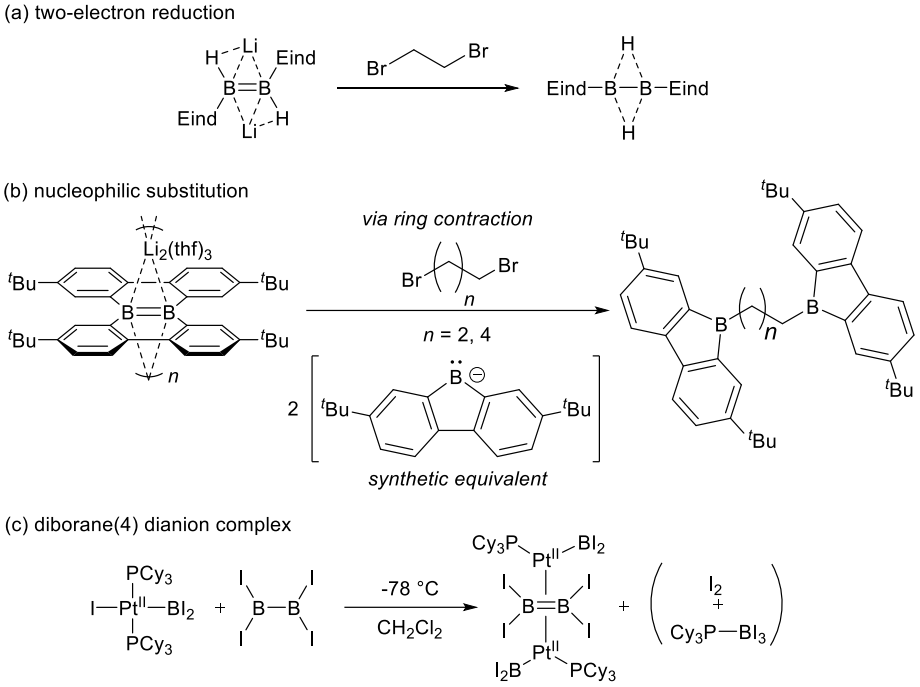

Scheme 1.3 Reactivities of diborane(4) dianion and related reaction

1.4 Summary

To summarize this chapter briefly, the chemistry of multiple bond between borons is actively developing. In particular, the chemistry of synthesis and reactivity of diborens is remarkably expanded. On the other hand, the chemistry of diborane(4) dianion still has many possibilities.

Based on these backgrounds, the author has unveiled the physical property and reactivity of diborane(4) dianion. In chapter 2, synthesis, property and reactivity of tetraaryldiborane(4) dianion are described. The reaction of diborane(4) with metallic lithium gave diborane(4) dianion. The property of B=B double of diborane(4) dianion was revealed by single-crystal X-ray diffraction analysis, NMR spectroscopy, CV measurement, DFT calculation. Particularly, the reaction of diborane(4) dianion with dichloromethane formed a diborylmethane. This result means the new reactivity of diborane(4) dianion as a two synthetic equivalent of diarylboryl anion.

In chapter 3, the synthesis and fully characterization of copper complexes having a dianionic diborane(4) ligand are discussed. The electronic structure and interaction between dianionic diborane(4) ligand and metal center is unveiled by X-ray crystallographic analysis, NMR spectroscopy, UV-Vis absorption, DFT and NBO calculation, XANES analysis.

In chapter 4, the synthesis and molecular structure of diborane(5) σ-Rh complex via aryl C-H activation is illustrated. The bonding character between anionic diborane(5) ligand and metal center is revealed by X-ray crystallographic analysis, NMR spectroscopy, UV-Vis absorption, DFT and NBO calculation.

In chapter 5, the reactivity and structure of diborylmethyl potassium salt, and the substituent effect of diarylboryl group is reported. In particular, the delocalization of lone pair of carbanion and negative hyperconjugation by the vacant p-orbital of the diarylboryl group was revealed by NMR

spectroscopy.

1.5 References

[1)] (a) Mulliken, R. S. *J. Chem. Phys.* **1934**, *2*, 782. (b) Mulliken, R. S. *J. Chem. Phys.* **1935**, *3*, 573.

[2)] Allred, A. L.; Rochow, E. G. *J. Inorg. Nuc. Chem.* **1958**, *5*, 264.

[3)] (a) Lewis, G. N. *J. Am. Chem. Soc.* **1916**, *38*, 762. (b) Langmuir, I. *J. Am. Chem. Soc.* **1919**, *41*, 868.

[4)] Abe, T. Borosilicate Glasses. *J. Am. Ceramic Soc.* **1952**, *35*, 284.

[5)] (a) Croat, J. J.; Herbst, J. F.; Lee, R. W.; Pinkerton, F. E. *J. App. Phys.* **1984**, *55*, 2078. (b) Sagawa, M.; Fujimura, S.; Togawa, N.; Yamamoto, H.; Matsuura, Y. *J. App. Phys.* **1984**, *55*, 2083.

[6)] (a) Barth, R. F.; Soloway, A. H.; Fairchild, R. G. *Scientific American* **1990**, *263*, 100. (b) Coderre, J. A.; Morris, G. M. *Radiation Research* **1999**, *151*, 1. (c) Barth, R. F.; Coderre, J. A.; Vicente, M. G. H.; Blue, T. E. *Clin. Cancer Res.* **2005**, *11*, 3987.

[7)] Brown, H. C.; Zweifel, G. *J. Am. Chem. Soc.* **1959**, *81*, 247.

[8)] (a) Miyaura, N.; Suzuki, A. *J. Chem. Soc., Chem. Commun.* **1979**, 866. (b) Miyaura, N.; Yamada, K.; Suzuki, A. *Tetrahedron Letters* **1979**, *20*, 3437. (c) Miyaura, Norio.; Suzuki, Akira. *Chem. Rev.* **1995**, *95*, 2457.

[9)] (a) Sisler, E. C.; Yang, S. F. Ethylene, the Gaseous Plant Hormone. *BioScience* **1984**, *34*, 234 (b) Ju, C.; Van de Poel, B.; Cooper, E. D.; Thierer, J. H.; Gibbons, T. R.; Delwiche, C. F.; Chang, C. *Nature Plants* **2015**, *1*, 1.

[10)] Wiberg, Nils; Holleman, A. F.; Wiberg, Egon, eds. (**2001**). "1.2.7 Diimine N2H2 [1.13.17]". *Inorganic Chemistry.* Academic Press. pp. 628–632. ISBN 978-0123526519.

[11)] (a) Corey, E. J.; Mock, W. L.; Pasto, D. J. *Tetrahedron Lett.* **1961**, *2*, 347. (b) Hünig, S.; Müller, H.-R.; Thier, W. *Tetrahedron Lett.* **1961**, *2*, 353. (c) Corey, E. J.; Pasto, D. J.; Mock, W. L. *J. Am. Chem. Soc.* **1961**, *83*, 2957. (d) van Tamelen, E. E.; Dewey, R. S.; Timmons, R. J. *J. Am. Chem. Soc.* **1961**, *83*, 3725. (e) Hamersma, J. W.; Snyder, E. I. *J. Org. Chem.* **1965**, *30,* 3985. (f) Cusack, J.; Reese, B.; Risius, C.; Roozpeikar, B. *Tetrahedron* **1976**, *32*, 2157.

[12)] (a) Tague, T. J.; Andrews, L. Reactions of Pulsed-Laser Evaporated Boron Atoms with Hydrogen. Infrared Spectra of Boron Hydride Intermediate Species in Solid Argon. *J. Am. Chem. Soc.* **1994**, *116* (11), 4970. (b) Knight, L. B.; Kerr, K.; Miller, P. K.; Arrington, C. A. *J. Phys. Chem.* **1995**, *99* (46), 16842. (c) Schleier, D.; Humeniuk, A.; Reusch, E.; Holzmeier, F.; Nunez-Reyes, D.; Alcaraz, C.; Garcia, G. A.; Loison, J.-C.; Fischer, I.; Mitric, R. *J. Phys. Chem. Lett.* **2018**, *9*, 5921.

[13)] Wang, Y.; Quillian, B.; Wei, P.; Wannere, C. S.; Xie, Y.; King, R. B.; Schaefer, H. F.; Schleyer, P. v. R.; Robinson, G. H. *J. Am. Chem. Soc.* **2007**, *129* , 12412.

[14)] (a) Y. Wang, B. Quillian, P. Wei, Y. Xie, C. S. Wannere, R. B. King, H. F. Schaefer, P. v. R. Schleyer, G. H. Robinson, *J. Am. Chem. Soc.* **2008**, *130*, 3298-3299. (b) H. Braunschweig, R. D. Dewhurst, K. Hammond, J. Mies, K. Radacki, A. Vargas, *Science* **2012**, *336*, 1420-1422. (c) (d) P. Bissinger, H. Braunschweig, A. Damme, T. Kupfer, I. Krummenacher, A. Vargas, *Angew. Chem.*

Int. Ed. **2014**, *53*, 5689-5693. (d) J. Böhnke, H. Braunschweig, W. C. Ewing, C. Hörl, T. Kramer, I. Krummenacher, J. Mies, A. Vargas, *Angew. Chem. Int. Ed.* **2014**, *53*, 9082-9085. (e) H. Braunschweig, R. D. Dewhurst, C. Hörl, A. K. Phukan, F. Pinzner, S. Ullrich, *Angew. Chem. Int. Ed.* **2014**, *53*, 3241-3244. (f) P. Bissinger, H. Braunschweig, M. A. Celik, C. Claes, R. D. Dewhurst, S. Endres, H. Kelch, T. Kramer, I. Krummenacher, C. Schneider, *Chem. Commun.* **2015**, *51*, 15917-15920. (g) P. Bissinger, H. Braunschweig, A. Damme, C. Hörl, I. Krummenacher, T. Kupfer, *Angew. Chem. Int. Ed.* **2015**, *54*, 359-362. (h) J. Böhnke, H. Braunschweig, T. Dellermann, W. C. Ewing, K. Hammond, J. O. C. Jimenez-Halla, T. Kramer, J. Mies, *Angew. Chem. Int. Ed.* **2015**, *54*, 13801-13805. (i) Arrowsmith, J. Böhnke, H. Braunschweig, M. A. Celik, T. Dellermann, K. Hammond, *Chem.-Eur. J.* **2016**, *22*, 17169-17172. (j) H. Braunschweig, P. Constantinidis, T. Dellermann, W. C. Ewing, I. Fischer, M. Hess, F. R. Knight, A. Rempel, C. Schneider, S. Ullrich, A. Vargas, J. D. Woollins, *Angew. Chem. Int. Ed.* **2016**, *55*, 5606-5609. (k) H. Braunschweig, I. Krummenacher, C. Lichtenberg, J. D. Mattock, M. Schäfer, U. Schmidt, C. Schneider, T. Steffenhagen, S. Ullrich, A. Vargas, *Angew. Chem. Int. Ed.* **2017**, *56*, 889-892. (m) S. R. Wang, M. Arrowsmith, J. Böhnke, H. Braunschweig, T. Dellermann, R. D. Dewhurst, H. Kelch, I. Krummenacher, J. D. Mattock, J. H. Müssig, T. Thiess, A. Vargas, J. Zhang, *Angew. Chem. Int. Ed.* **2017**, *56*, 8009-8013. (l) D. Auerhammer, M. Arrowsmith, P. Bissinger, H. Braunschweig, T. Dellermann, T. Kupfer, C. Lenczyk, D. K. Roy, M. Schäfer, C. Schneider, *Chem.-Eur. J.* **2018**, *24*, 266-273. (m) J. Bohnke, T. Bruckner, A. Hermann, O. F. Gonzalez-Belman, M. Arrowsmith, J. O. C. Jimenez-Halla, H. Braunschweig, *Chem. Sci.* **2018**, *9*, 5354-5359. (n) J. Böhnke, T. Dellermann, M. A. Celik, I. Krummenacher, R. D. Dewhurst, S. Demeshko, W. C. Ewing, K. Hammond, M. Heß, E. Bill, E. Welz, M. I. S. Röhr, R. Mitrić, B. Engels, F. Meyer, H. Braunschweig, *Nature Commun.* **2018**, *9*, 1197. (o) T. E. Stennett, J. D. Mattock, L. Pentecost, A. Vargas, H. Braunschweig, *Angew. Chem. Int. Ed.* **2018**, *57*, 15276-15281. (p) J. H. Muessig, M. Thaler, R. D. Dewhurst, V. Paprocki, J. Seufert, J. D. Mattock, A. Vargas, H. Braunschweig, *Angew. Chem. Int. Ed.* **2019**, *58*, 4405-4409. (q) A. Hermann, J. Cid, J. D. Mattock, R. D. Dewhurst, I. Krummenacher, A. Vargas, M. J. Ingleson, H. Braunschweig, *Angew. Chem. Int. Ed.* **2018**, *57*, 10091-10095. (r) T. E. Stennett, J. D. Mattock, I. Vollert, A. Vargas, H. Braunschweig, *Angew. Chem. Int. Ed.* **2018**, *57*, 4098-4102. (s) W. Lu, Y. Li, R. Ganguly, R. Kinjo, *J. Am. Chem. Soc.* **2017**, *139*, 5047-5050; (v) W. Lu, Y. Li, R. Ganguly, R. Kinjo, *J. Am. Chem. Soc.* **2018**, *140*, 1255-1258. (t) S. Morisako, R. Shang, Y. Yamamoto, H. Matsui, M. Nakano, *Angew. Chem. Int. Ed.* **2017**, *56*, 15234-15240. (u) T. E. Stennett, P. Bissinger, S. Griesbeck, S. Ullrich, I. Krummenacher, M. Auth, A. Sperlich, M. Stolte, K. Radacki, C.-J. Yao, F. Wgrthner, A. Steffen, T. B. Marder, H. Braunschweig *Angew. Chem. Int. Ed.* **2019**, *58*, 6449–6454. (v) T. Brückner, R. D. Dewhurst, T. Dellermann, M. Müller, H. Braunschweig, *Chem. Sci.* **2019**, *10*, 7375–7378.

[15)] A. Moezzi, R. A. Bartlett, P. P. Power, *Angew. Chem. Int. Ed. Engl.* **1992**, 31, 1082-1083.

[16)] (a) H. Nöth, J. Knizek, W. Ponikwar, *Eur. J. Inorg. Chem.* **1999**, *1999,* 1931-1937. (b) Y. Shoji,

T. Matsuo, D. Hashizume, H. Fueno, K. Tanaka, K. Tamao, *J. Am. Chem. Soc.* **2010**, *132*, 8258-8260. (c) A. Moezzi, M. M. Olmstead, P. P. Power, *J. Am. Chem. Soc.* **1992**, *114*, 2715-2717. (d) A. Hübner, M. Bolte, H.-W. Lerner, M. Wagner, *Angew. Chem. Int. Ed.* **2014**, *53*, 10408-10411. (e) T. Kaese, A. Hübner, M. Bolte, H.-W. Lerner, M. Wagner, *J. Am. Chem. Soc.* **2016**, *138*, 6224-6233.

[17)] Braunschweig, H.; Dewhurst, R. D.; Hammond, K.; Mies, J.; Radacki, K.; Vargas, A. *Science* **2012**, *33*, 1420–1422.

[18)] Böhnke, J.; Braunschweig, H.; Constantinidis, P.; Dellermann, T.; Ewing, W. C.; Fischer, I.; Hammond, K.; Hupp, F.; Mies, J.; Schmitt, H.-C.; Vargas, A. *J. Am. Chem. Soc.* **2015**, *137*, 1766.

[19)] (a, BH) Böhnke, J.; Braunschweig, H.; Ewing, W. C.; Hörl, C.; Kramer, T.; Krummenacher, I.; Mies, J.; Vargas, A. *Angew. Chem. Int. Ed.* **2014**, *53*, 9082–9085. (b, Se) Braunschweig, H.; Krummenacher, I.; Lichtenberg, C.; Mattock, J. D.; Schäfer, M.; Schmidt, U.; Schneider, C.; Steffenhagen, T.; Ullrich, S.; Vargas, A. *Angew. Chem. Int. Ed.* **2017**, *56*, 889–892. (c, 4+2) Stennett, T. E.; Mattock, J. D.; Pentecost, L.; Vargas, A.; Braunschweig, H. *Angew. Chem. Int. Ed.* **2018**, *57*, 15276–15281. (d, BB) Stennett, T. E.; Bertermann, R.; Braunschweig, H. *Angew. Chem. Int. Ed.* **2018**, *57*, 15896–15901. (e, BH) Dömling, M.; Arrowsmith, M.; Schmidt, U.; Werner, L.; Castro, A. C.; Jiménez-Halla, J. O. C.; Bertermann, R.; Müssig, J.; Prieschl, D.; Braunschweig, H. *Angew, Chem. Int. Ed.* **2019**, *58*, 9782–9786.

[20)] Lu, W.; Li, Y.; Ganguly, R.; Kinjo, R. *J. Am. Chem. Soc.* **2017**, *139*, 5047–5050.

[21)] (a) Bissinger, P.; Braunschweig, H.; Damme, A.; Kupfer, T.; Vargas, A. *Angew. Chem. Int. Ed.* **2012**, *51*, 9931–9934. (b) Braunschweig, H.; Damme, A.; Dewhurst, R. D.; Vargas, A. *Nat. Chem.* **2013**, *5*, 115–121. (c) Bissinger, P.; Steffen, A.; Vargas, A.; Dewhurst, R. D.; Damme, A.; Braunschweig, H. *Angew. Chem. Int. Ed.* **2015**, *54*, 4362–4366. (d) Wang, S. R.; Arrowsmith, M.; Braunschweig, H.; Dewhurst, R. D.; Dömling, M.; Mattock, J. D.; Pranckevicius, C.; Vargas, A. *J. Am. Chem. Soc.* **2017**, *139*, 10661–10664. (e) Wang, S. R.; Arrowsmith, M.; Braunschweig, H.; Dewhurst, R. D.; Paprocki, V.; Winner, L. *Chem. Commun.* **2017**, *53*, 11945–11947. (f) Lu, W.; Kinjo, R. *Chem. Commun.* **2018**, *54*, 8842–8844.

[22)] (a) Braunschweig, H.; Dellermann, T.; Dewhurst, R. D.; Ewing, W. C.; Hammond, K.; Jimenez-Halla, J. O. C.; Kramer, T.; Krummenacher, I.; Mies, J.; Phukan, A. K.; Vargas, A. *Nat. Chem.* **2013**, *5*, 1025–1028. (b) Braunschweig, H.; Dellermann, T.; Ewing, W. C.; Kramer, T.; Schneider, C.; Ullrich, S. *Angew. Chem. Int. Ed.* **2015**, *54*, 10271–10275. (c) Böhnke, J.; Dellermann, T.; Celik, M. A.; Krummenacher, I.; Dewhurst, R. D.; Demeshko, S.; Ewing, W. C.; Hammond, K.; Heß, M.; Bill, E.; Welz, E.; Röhr, M.; Mitrić, R.; Engels, B.; Meyer, F.; Braunschweig, H. *Nat. Comm.* **2018**, *9*, 1–7.

[23)] Braunschweig, H.; Dewhurst, R. D.; Jiménez-Halla, J. O. C.; Matito, E.; Muessig, J. H. *Angew. Chem. Int. Ed.* **2018**, *57*, 412–416.

Chapter 2

Synthesis and Reactivity of Diborane(4) Dianions

2.1 Introduction

A B=B double bond is a fundamental target in boron chemistry[2] and is isoelectronic to a C=C double bond in alkenes, but it is not as ubiquitous as C=C double bond. In the last decades, many B=B double bond species were synthesized. These compounds can be generally classified into a neutral diborene[3] or dianionic diborane(4),[4] in which the boron atom has an oxidation state of one. The latter class of compounds were relatively limited to the former compounds (Figure 2.1a). It was reported the synthesis of amino-substituted diborane(4) dianions **A** and **B** with stabilization through coordination of the amino groups to the lithium cation.[4a,b] Hydrogen- and carbon-substituted diborane(4) dianion **C** was also synthesized by a reduction of the Eind-substituted boron difluoride.[4c] All-carbon-substituted diborane(4) dianions **D** and **E** were synthesized by a reduction of tetraaryldiborane(4)[4d] or hydrogen-bridged diarylborane dimer.[4e,f] Since the most of studies on diborane(4) dianion focused on their structures around the B=B double bond, the information about physical property and reactivity was limited, probably due to the large substituents around the B=B bond. Only two reactions of diborane(4) dianion having B=B double bond were reported. First example is a formation of neutral hydride bridged diborane(4) by the reaction of **C** with 1,2-diboromoethane (Figure 2.1b). This case means simple oxidation of dianionic species **C**. In contrast, second one is the similar reaction of **E** with 1,2-dibromoethane, but this reaction gave quite different B-alkylateds derivatives **F** with a rearrangement of the boron-containing six-membered ring to a five-membered ring (Figure 2.1c).[5] In this transformation, boron-containing cyclic system in **E** can be considered as two equivalents of diarylboryl anion **G**.[6] Considering about Wanzlick equilibrium between tetraaminoethylene and two equivalents of *N*-heterocyclic carbene (Figure 2.1d),[7] a half of diborane(4) dianion having B=B double bond could be considered as a synthetic equivalent of boryl anion. However, there has been no report for such reactivity of diborane(4) dianion.

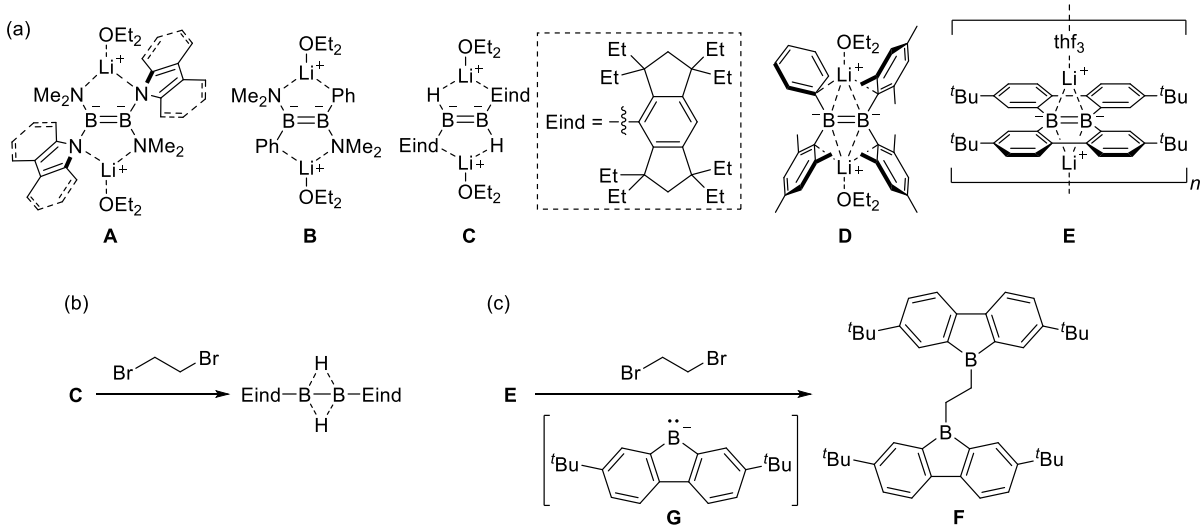

Figure 2.1 (a) Previous examples of dianionic B-B double bond. (b) Reaction of E with 1,2-diboromoethane.

2.2 Synthesis and Characterization of Tetra(*o*-tolyl)diborane(4) Dianion

We recently reported an easy and scalable synthesis of the tetra(*o*-tolyl)diborane(4) **1** and its reactivity toward dihydrogen,[8a] carbon monoxide, isocyanide,[8b] nitrile, and azo-compounds.[8c] DFT calculations suggested the high reactivity of **1** toward these molecules would originate from a low-lying LUMO consisting of two vacant p-orbitals on two boron atoms and a reactive B–B single bond contributing to HOMO.[8a] Considering a simple structure and scalable synthesis of **1**, one can expect that dianion of **1** would have a variety of reactivity in comparison with those of other diborane(4) dianions. Herein, we describe the synthesis of tetraaryldiborane(4) dianions by reduction of **1**, detailed study on their photophysical and electrochemical properties, and their reactivity as two equivalents of diarylboryl anion, toward electrophiles.

Lithium salt of diborane(4) dianion **2** was obtained as a dark-red solid in 98% yield by two electron reduction of tetra(*o*-tolyl)diborane(4) **1** with metallic lithium in toluene/THF (Scheme 2.1). Similarly, magnesium salt of dianion **3** was synthesized by a reaction of 1 with metallic magnesium in the presence of catalytic amount of anthracene. The ^{1}H NMR spectra of the isolated diborane(4) dianions **2** in C_6D_6 and **3** in THF-d_8 showed four magnetically equivalent *o*-tol groups. The ^{11}B NMR spectra of diborane(4) dianions **2** and **3** exhibited one broad signal (**2**: δ_B = 31 ppm in C_6D_6, **3**: δ_B = 38 ppm in THF-d_8). The remarkable upfield-shift of the ^{11}B signals of **2** and **3** related to that of **1** (δ_B = 88 ppm) clearly reflects change in electronic state rather than in hybridization of boron centers.

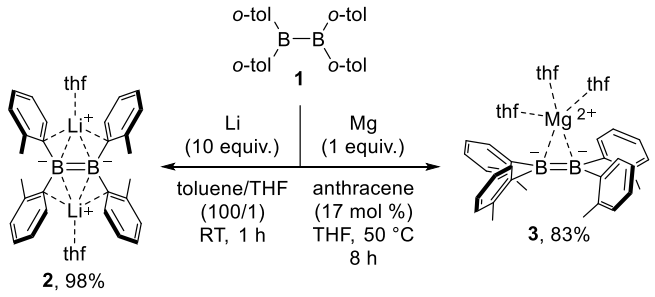

Scheme 2.1 Synthesis of B_2(*o*-tolyl)$_4$ (4) dianions **2** and **3**.

The molecular structures of **2** and **3** were determined by single-crystal X-ray diffraction analysis (Figure 2.2). The lithium salt **1** crystallized as a contact ion pair with two THF molecules and an inversion center located on the midpoint of the two boron atoms. The lithium cation was coordinated by one THF molecule and two ipso carbon atoms in *o*-tol groups [Li1–C1: 2.244(3), Li1–C8*:2.277(3)]. The structure of the magnesium salt **3** was also contact ion pair and the magnesium cation was bound to B_2(*o*-tol)$_4^{2-}$ anion in η^2-fashion. As a result, all of four methyl groups of *o*-tol groups pointed to the opposite side of magnesium cation. Major structural parameters of **2** and **3** were compared with those of **1** (Table 2.1). Most notable difference appears as C–B–B–C torsion angles. The C–B–B–C torsion angles in **1** [75.7(7)-93.2(7)°] were almost orthogonal, while those of **2** and **3** were almost orthogonal.[8a] Furthermore, the B–B lengths [1.633(3), 1.639(6) Å] in **2** and **3** were shortened in comparison with that of **1** [1.686(9), 1.694(9) Å]. These features are

consistent with those of the previously reported C-substituted diborane(4) dianions **D** and **E**,[4d,e] suggesting a formation of B=B π-bond in **2** and **3**. It should be noted that the B–Li lengths in **2** [2.243(2), 2.277(3) Å] were slightly shorter than those in tetraaryldiborane(4) dianions **D** and **E**. The B–Mg lengths in **3** [2.476(5), 2.647(4) Å] were longer than those in borylmagnesium species,[9] boratabenzene-magnesium complexes,[10] borole dianion-magnesium complex,[11] and unsymmetrical diborene-magnesium complexes.[12]

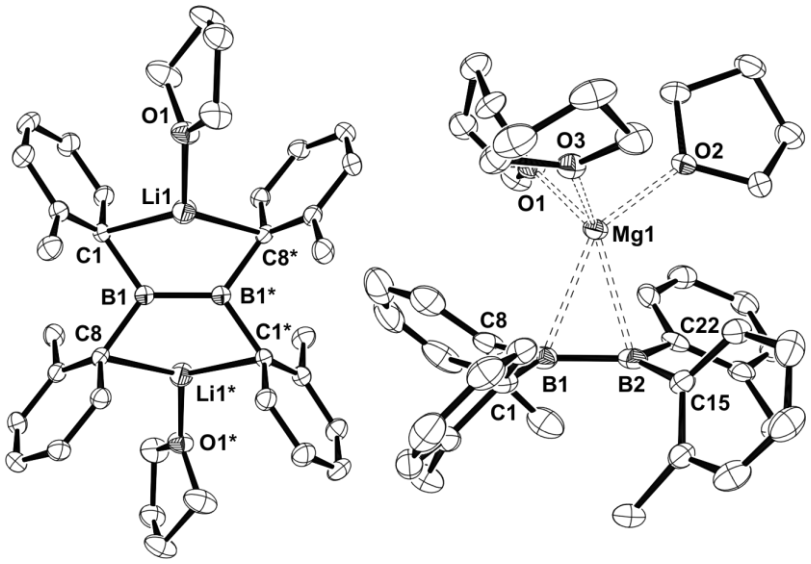

Figure 2.2 Molecular structures of **2** and **3** (thermal ellipsoids set at 50% probability; Hydrogen atoms, minor parts of disordered THF molecules for **2**, and co-crystallized toluene molecule for **3** are omitted for clarity).

Table 2.1 Selected bond lengths (Å) and torsion angles (°) in **1**, **2**, and **3**.

	1	**2**	**3**
B–B	1.686(9)	1.633(3)	1.639(6)
	1.694(9)		
C–B–B–C	75.7(7)	0	−0.6(5)
	~ 93.2(7)		2.2(6)
B–C	1.562(9)	1.626(2)	1.619(5)
	~ 1.592(8)	1.628(2)	1.622(6)
B–M		2.243(2)	2.647(4)
		2.277(3)	2.476(5)

To investigate the electronic structure of **2** and **3**, DFT calculations were conducted at the M06-2X/6-31G(d) level of theory. The HOMO of **2** and **3** is mainly contributed by the π-orbital on two boron atoms (Figure 2.3, **Figure 2.25**). The HOMO−1 of **2** exhibited a significant contribution of the B–B σ-orbital. These two orbitals would originate from LUMO and HOMO of neutral diborane(4) **1**. These results of calculation have supported the nucleophilicity of π-orbitals on two

boron atoms like alkenes. NBO analysis revealed the B=B double bond character in **2** and **3** with WBI values of 1.65 and 1.56, which are significantly larger than that of **1** (0.96) (Table 2.2). Also, natural population analysis (NPA) showed the natural charges of the two boron atoms in **2** and **3** become negative upon reduction of **1** (–0.18 *e* for **2**, –0.14 *e* and –0.17 *e* for **3**, 0.60 *e* for **1**).

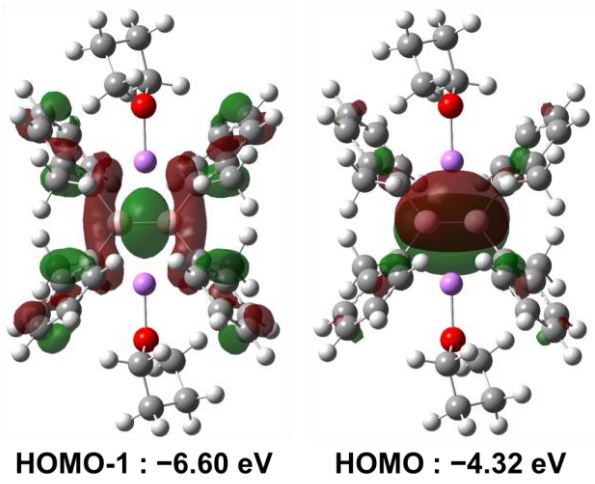

Figure 2.3 Molecular orbitals of **2** calculated at M06-2X/6-31G(d) level of theory (hydrogen atoms omitted for clarity).

Table 2.2 WBI and NPA charges of **1**, **2**, and **3**.

	1	**2**	**3**
WBI of B–B bond	0.96	1.65	1.56
NPA charge of boron atoms (Q)	0.60 *e*	−0.18 *e*	−0.14 *e*
	0.60 *e*	−0.18 *e*	−0.17 *e*
difference of Q from **1** (ΔQ)	-	−0.77 *e*	−0.73 *e*
	-	−0.77 *e*	−0.77 *e*
sum of ΔQ	-	−1.55 *e*	−1.50 *e*
ratio for 2 *e*	-	78%	75%

To estimate further electronic states and HOMO level of **2**, measurement of UV-vis spectra and cyclic voltammetry were performed. The UV-vis spectrum of a toluene solution of **2** at −30 °C exhibited an absorption maximum at 439 nm (Figure S16), which can be assigned as a transition from π-orbital of the B=B bond (HOMO) to the π*-orbitals of *o*-tolyl groups (LUMO) with intramolecular charge transfer character. It should be noted that the UV-vis spectrum of **2** showed a notable solvatochromism (**Figure 2.1**). An absorption maximum of **2** in THF appeared at 570 nm with a significant longer-wavelength shift in comparison with that in toluene. This red-shift would suggests that the Li cation(s) partially dissociates from diborane(4) dianion moiety to generate solvent-separated ion pairs (**2'**)[Li(thf)$_n$] and (**2''**)[Li(thf)$_n$]$_2$ (**Scheme 2.2**). Similar but small hypsochromic shift indused by interaction between diboryne with alkaline metals (Li and Na cation)

was reported.[13] However, the THF solution magnesium salt **3** did not show solvatochromism, reflecting stronger Coulomb interaction between $[B_2(o\text{-tol})_4]^{2-}$ and Mg^{2+} based on the large charge than that of **2**. In fact, TD-DFT calculations for counter-cation-free **2'** and **2''** predict their red-shifted absorptions vs. that of the contact ion pair **2** (**Figure 2.26Figure 2.31**). It should be noted that leaving a dark purple THF solution of **2** at room temperature induced a decomposition of **2** as judged by UV-vis spectroscopy (**Figure 2.22**). Next, we experimentally evaluated HOMO level of **2** with electrochemistry. In the cyclic voltammogram obtained at −30 °C, a THF solution of **2** showed two reversible oxidation waves (**Figure 2.1**). The first oxidation event to form radical anion of **1** was observed at $E_{1/2}$ = −2.97 V (vs. Fc/Fc^+), indicating that **2** in THF could be one of the strongest boron-containing reductants. In fact, this value was more negative than related boron cotained compounds: IPr-stabilized neutral diborene (−1.95 V),[3d] sodium salt of aromatic triboracyclopropenyl dianion (−2.42 V),[14a] which have unsaturated BB bond, simple trimesitylborane (−2.57 V).[14b] The second oxidation of **2** was observed at $E_{1/2}$ = −2.09 V, which is identical to the reduction potential of the previously reported **1**.[8a]

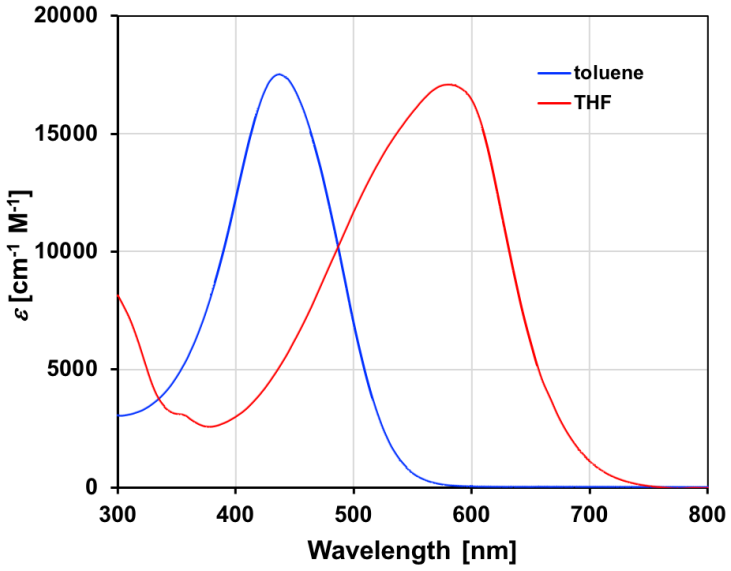

Figure 2.4 UV-Vis spectra of **2** [toluene 1.0 mM, THF, 0.92 mM, −30 °C]

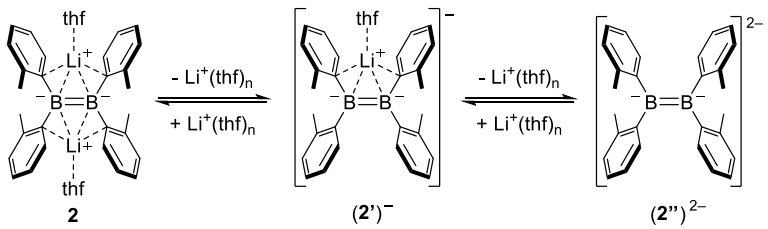

Scheme 2.2 Dissociation equilibrium of **2** in THF

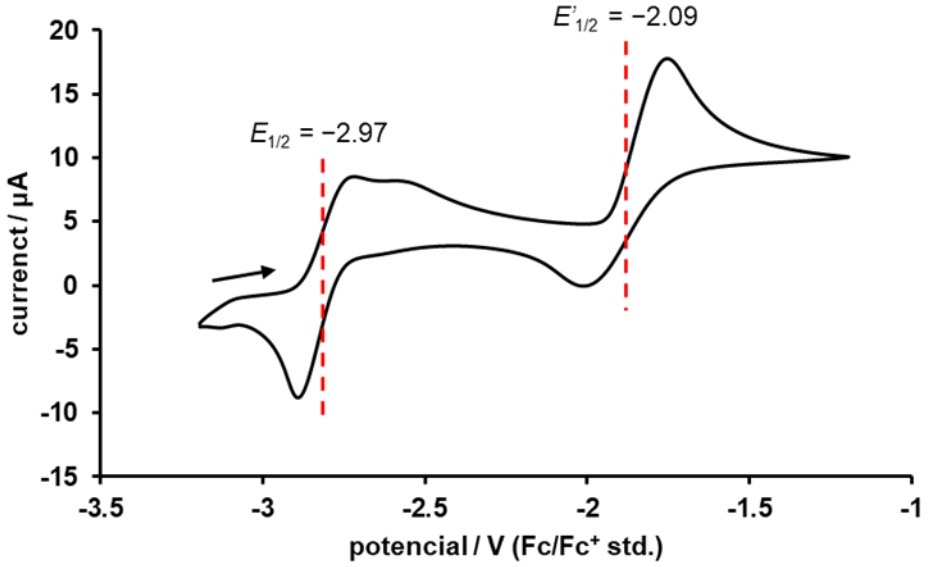

Figure 2.5 Cyclic voltammogram of **2** in THF at room temperature (vs Fc/Fc^+; supporting electrolyte, $LiPF_6$ (0.1 mol L^{-1}); scan rate, 10 mV s^{-1}).

2.3 Reactivity of Tetra(*o*-tolyl)diborane(4) Dianion

Reaction of dianion **2** with CH_2Cl_2 and S_8 gave diarylborylated compounds via a formal nucleophilic substitution by diarylboryl anion (**Scheme 2.3**). Treatment of **2** with CH_2Cl_2 immediately afforded a geminal diborated product, bis(diarylboryl)methane **4**, with a generation of small amount of neutral diborane(4) **1**. This result indicates that dianion **2** behaves as two equivalents of nucleophilic diarylboryl anion, although the details about reaction mechanism is not clear so far.

Two potential mechanisms for the formation of **4** by the reaction of **2** and CH_2Cl_2: (Path A) a nucleophilic attack of π-electron in the B=B double bond of **2** to CH_2Cl_2 and a subsequent migration of the diarylborylgroup in sp^2-sp^3 diboron intermediate **6**;[15] (Path B) two single-electron transfer (SET) processes from **2** to CH_2Cl_2 involving a generation of lithium carbenoid species **9** and neutral **1** (via **7**[16] and **8**), in which the former can be a nucleophile attacking to the latter compound to generate the same intermediate **6** in Path A (**Scheme 2.4**).

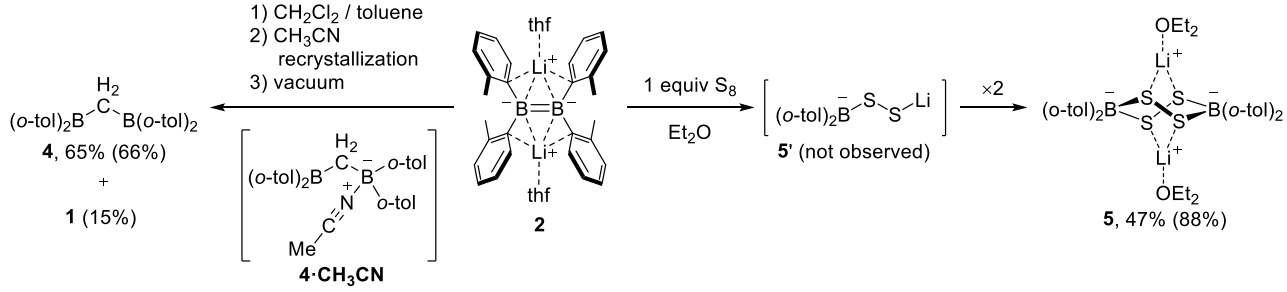

Scheme 2.3 Reactivity of Dianion **2** with CH_2Cl_2 or S_8 as two equivalents of Ar_2B^- anion (NMR yield in parentheses).

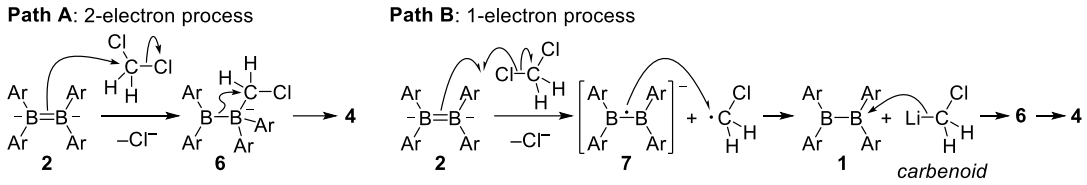

Scheme 2.4 Two possible mechanism for formation of **4**. (a) simple double nucleophilic 2-electron process. (b) 1-electron process following B–B insertion by carbenoid.

Compound **4** crystalized from acetonitrile solution as acetonitrile-coordinated **4·CH$_3$CN** as judged by a single-crystal X-ray diffraction analysis (**Figure 2.6**). Evacuation of **4·CH$_3$CN** allowed to release acetonitrile molecule to regenerate **4** as an analytically pure colorless oil. Reaction of **2** with S_8 furnished a six-membered ring compound **5** consisting of two boron and four sulfur atoms with a twist-boat conformation. This compound **5** would be considered as a dimer of (*o*-tol)$_2$B–S–S$^-$ anion, **5'**, which was generated by a formal nucleophilic attack of diarylboryl anion to S_8 molecule. The structure of **5** was confirmed by a single-crystal X-ray diffraction analysis (**Figure 2.21**). Each two lithium cations were coordinated with two sulfur atoms and one diethyl ether molecule. A similar B_2S_4 six-membered ring compound was obtained by a reaction of cAAC-substituted dicyanodiborene toward S_8, in which a monomeric cAAC-cyanoborylene would presumably form as a nucleophilic intermediate.[17] It should be noted that **2** underwent electron-transfer instead of nucleophilic attack toward benzophenone to generate diphenyl ketyl radical as was confirmed by UV-vis spectrum (**Figure 2.24**). Thus, introduction of non-heteroatom-substituted boryl group in a nucleophilic fashion would allow us to synthesize a new class of boron-containing molecules.

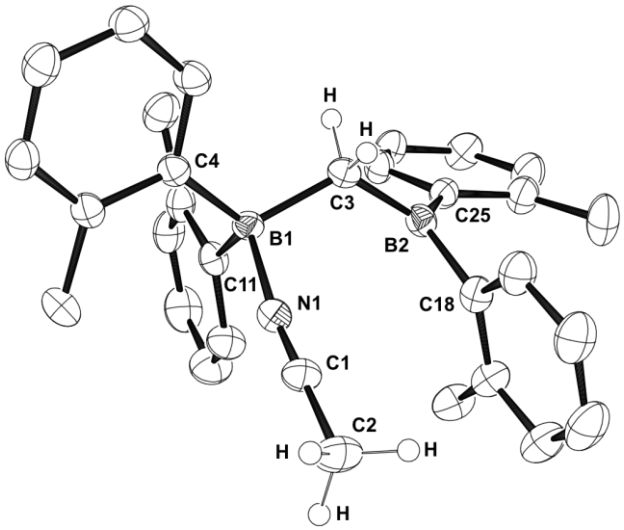

Figure 2.6 Molecular structure of **4·CH$_3$CN** (thermal ellipsoids set at 50% probability; hydrogen atoms except for methylene moiety are omitted for clarity). Selected bond distances (Å): B1–C3 1.571(5), B2–C3 1.658(4), B1–N1 1.622(4), N1–C1 1.140(4).

2.4. Conclusion

In summary, we reported the synthesis of lithium and magnesium salts of tetraaryldiborane(4) dianion **2** and **3** having the B=B double bond character as judged by X-ray

diffraction analysis. The spectroscopic and electrochemical study on the lithium salt **2** revealed a very high-lying HOMO corresponding to the B=B π-orbital, which was perturbed by a dissociation of Li^+ cation in THF. Treatment of the lithium salt **2** with CH_2Cl_2 and S_8 produced diarylborylated species, indicating that **2** could be considered as a synthetic equivalent of diarylboryl anion.

1 2.5 Experimental Section

General Methods

All manipulations involving the air- and moisture-sensitive compounds were carried out under an argon atmosphere using standard Schlenk and glovebox (Korea KIYON, Korea and ALS Technology, Japan) technique. THF, Et_2O and n-hexane were purified by passing through a solvent purification system (Grass Contour). C_6D_6 was dried by distillation over sodium/benzophenone followed by vacuum transfer. Tetra(*o*-tolyl)diborane(4) (**1**) was synthesized according to the literature.[8a] The nuclear magnetic resonance (NMR) spectra were recorded on a JEOL ECS-400 (399 MHz for ^1H, 100 MHz for ^{13}C, 155 MHz for ^7Li, 128 MHz for ^{11}B) or a Bruker AVANCE III HD 500 spectrometers (500 MHz for ^1H, 128 MHz for ^{13}C). Chemical shifts (δ) are given by definition as dimensionless numbers and relative to ^1H or ^{13}C NMR chemical shifts of the residual C_6D_5H for ^1H (δ = 7.16), C_6D_6 itself for ^{13}C (δ = 128.0). The ^7Li and ^{11}B NMR NMR spectra were referenced using an external standard of LiCl in D_2O and $BF_3(OEt_2)$. The absolute values of the coupling constants are given in Hertz (Hz). Multiplicities are abbreviated as singlet (s), doublet (d), triplet (t), quartet (q), multiplet (m) and broad (br). NMR yield was decieded by using phenanthrene as internal standard and ^1H NMR spectra. Melting points were determined on MPA100 OptiMelt (Tokyo Instruments, Inc.) and were uncorrected. Elemental analyses were performed on a Perkin Elmer 2400 series II CHN analyzer. High-resolution mass spectra were measured on a Bruker micrOTOF II mass spectrometer with an atmospheric pressure chemical ionization (APCI) probe.

Synthesis of 2

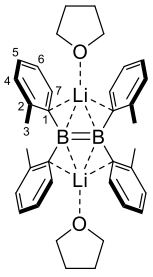

A suspension of lithium powder (71.3 mg, 10.3 mmol) in toluene (12 mL) and THF (0.25 mL) was stirred with a glass-coated stirring bar for 15 min at −35 °C to activate the surface of lithium. A solution of **1** (386 mg, 0.989 mmol) in toluene (12 mL) and THF (0.25 mL) was added to the suspension of Li and the resulting mixture was stirred for 1 h at −35 °C. The resulting suspension was filtered through a pad of celite to remove an excess amount of lithium and the residue was washed with hexane. The volatiles were removed from the filtrate under reduced pressure to give **1** as analytically pure crystalline dark-red solids (529 mg, 0.972 mmol, 92%). The crystals recrystallized from toluene were suitable for X-ray analysis. ^1H NMR (399 MHz, C_6D_6) δ 8.67 (d, $^3J_{HH}$ = 7 Hz, 4H, H7), 7.27 (t, $^3J_{HH}$ = 7 Hz, 4H, H6), 7.01 (t, $^3J_{HH}$ = 7 Hz, 4H, H4), 6.97 (d, $^3J_{HH}$ = 7 Hz, 4H, H5), 2.56 (m, 8H, THF), 2.38 (s, 12H, H3), 0.87 (m, 8H, THF); $^7Li\{^1H\}$ NMR (155 MHz, C_6D_6), δ −0.04 (br); $^{11}B\{^1H\}$ NMR (128 MHz, C_6D_6) δ 31 (br s); $^{13}C\{^1H\}$ NMR (C_6D_6) δ 154.38 (br s, 4°, C1), 142.06 (4°, C2), 141.26 (3°, C7), 129.97 (3°,

C4), 124.48 (3°, C5), 124.26 (3°, C6), 67.97 (2°, CH_2O of THF), 25.40 (1°, C3), 25.01 (2°, CH_2CH_2O of THF). mp: 162-165 °C. (decomp.) Anal. Calc. for $C_{36}H_{44}B_2Li_2O_2$: C, 79.45; H, 8.15; Found: C, 79.57; H, 8.00; N, 0.03.

Synthesis of 3

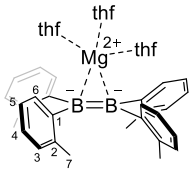

To a THF solution (5 mL) of **1** (121 mg, 0.314 mmol), Mg turnings (76.3 mg, 3.14 mmol) and anthracene (9.5 mg, 0.0533 mmol) were added and the resulting suspension was heated at 60 °C for 5 h. The resulting reaction mixture was filtrated through a pad of celite and the residue was washed with toluene. The volatiles were removed from the filtrate. The residue was washed with toluene (20 mL×2) and hexane (20 mL×2) and dried under vacuum to afford **3** as a dark red powder (163.7 mg, 0.261 mmol, 83% yield). The crystals recrystallized from THF/pentane were suitable for X-ray analysis. ^{1}H NMR (500 MHz, THF-d_8) δ 7.15 (d, $^3J_{HH}$ = 7 Hz, 4H, H6), 6.62 (d, $^3J_{HH}$ = 7 Hz, 4H, H3), 6.49 (td, $^3J_{HH}$ = 7 Hz, 4H, H5), 6.45 (t, $^3J_{HH}$ = 7 Hz, 4H, H4), 1.84 (s, 12H, H7); ^{11}B{^{1}H} NMR (128 MHz, THF-d_8) δ 38 (br s); ^{13}C{^{1}H} NMR (126 MHz, THF-d_8) δ 162.14(br s, 4°, C1), 141.45 (4°, C2), 136.25 (3°, C6), 130.06 (3°, C3), 122.30 (3°, C5), 121.62 (3°, C4), 24.36 (1°, C7). mp: 130-138 °C. (decomp.) Anal. Calc. for $C_{40}H_{52}B_2MgO_3$: C, 76.65; H, 8.36; Found: C, 76.32; H, 8.58; N, 0.02.

Synthesis of 4

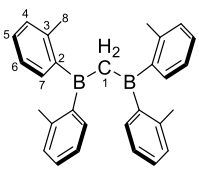

A solution of **2** (54.9 mg, 0.101 mmol) in toluene (2 mL) was added to dichloromethane (2.0 mL, 31 mmol) and the color of the solution immediately changed from deep red to colorless. The volatile was evaporated from the reaction mixture and the residue was extracted with hexane (5 mL). The hexane solution was filtrated and the filtrate was evaporated to dryness. The residue was recrystallized from acetonitrile at −35°C to give colorless crystals of **4·MeCN**, which was structurally characterized by a single-crystal X-ray diffraction analysis. These crystals of **4·MeCN** were dried under vacuum to give **4** as a colorless oil (65% yield). ^{1}H NMR (399 MHz, C_6D_6) δ 7.44 (dd, $^3J_{HH}$ = 7 Hz, $^4J_{HH}$ = 2 Hz, 4H, H7), 7.09 (td, $^3J_{HH}$ = 7 Hz, $^4J_{HH}$ = 2 Hz, 4H, H6), 7.02 (t, $^3J_{HH}$ = 7 Hz, 4H, H5), 6.92 (d, $^3J_{HH}$ = 7 Hz, 4H, H4), 3.13 (s, 2H, H1), 1.97 (s, 12H, H6); ^{11}B{^{1}H} NMR (128 MHz, C_6D_6) δ 79 (br s); ^{13}C{^{1}H} NMR (100 MHz, C_6D_6) δ 146.69 (br s, 4°, C2), 140.62 (4°, C3), 132.85 (2°, C7), 130.16 (3°, C4), 129.93 (3°, C6), 125.30 (3°, C5), 43.50 (br s, C1), 23.01 (1°, C8); HRMS (APCI−) Calcd for $C_{29}H_{30}B_2$ [M^-]: 399.2460, found; 399.2467.

Measurement of NMR yield: To a reaction mixture obtained from **2** (27.2 mg, 0.0500 mmol) and CH_2Cl_2 (0.5 mL, 7.8 mmol), phenanthrene (11.3 mg, 0.0634 mmol) as an internal standard and C_6D_6 were added. An aliquot was pipetted to an NMR tube to take ^{1}H NMR spectrum to determine NMR yield (**4**: 66%, **1**: 15%, **Figure 2.16**).

Synthesis of 5

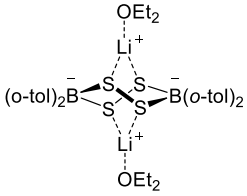

A solution of **2** (54.8 mg, 0.0998 mmol) in toluene (5 mL) was added to S_8 (25.8 mg, 0.101 mmol) and the color of the resulting solution immediately changed from deep red to colorless. The reaction mixture was filtrated and the filtrate was evaporated. The residue was recrystallized from Et_2O/toluene to afford pale yellow crystals of **5** (31.6 mg, 0.0467 mmol, 47% yield). ^{1}H NMR (399 MHz, C_6D_6) δ 8.67 (d, $^3J_{HH}$ = 7 Hz, 4H, ortho to B), 7.05 (m, 12H, ArH), 2.49 (q, $^3J_{HH}$ = 7 Hz, 8H, CH_2 of Et_2O), 2.32 (s, 12H, CH_3 of tol), 0.50 (t, $^3J_{HH}$ = 7 Hz, 12H, CH_3 of Et_2O); ^{7}Li{^{1}H} NMR (155 MHz, C_6D_6) δ −0.1(s); ^{11}B{^{1}H} NMR (128 MHz, C_6D_6) δ 6.2 (br); ^{13}C{^{1}H} NMR (100 MHz, C_6D_6) δ 148.05 (br s, 4°, *ipso* to B), 142.25 (4°, *ipso* to CH_3), 131.34 (ArH), 131.29 (ArH), 127.09 (ArH), 126.55 (ArH), 65.88 (CH_2 of Et_2O), 23.64 (CH_3 of tolyl), 14.32 (CH_3 of Et_2O); mp: 124-129 °C. (decomp.) Anal. Calc. for $C_{36}H_{48}B_2MgLi_2O_6S_6$: C, 63.91; H, 7.15; Found: C, 64.06; H, 6.77; N, 0.04.

Measurement of NMR yield: To a reaction mixture obtained from **2** (27.8 mg, 0.0511 mmol) and S_8 (13.2 mg, 0.0515 mmol), phenanthrene (13.0 mg, 0.0729 mmol) as an internal standard and C_6D_6 were added. An aliquot was pipetted to an NMR tube to take ^{1}H NMR spectrum to determine NMR yield (**5**: 88%, **Figure 2.20**).

2. NMR spectra of new compounds

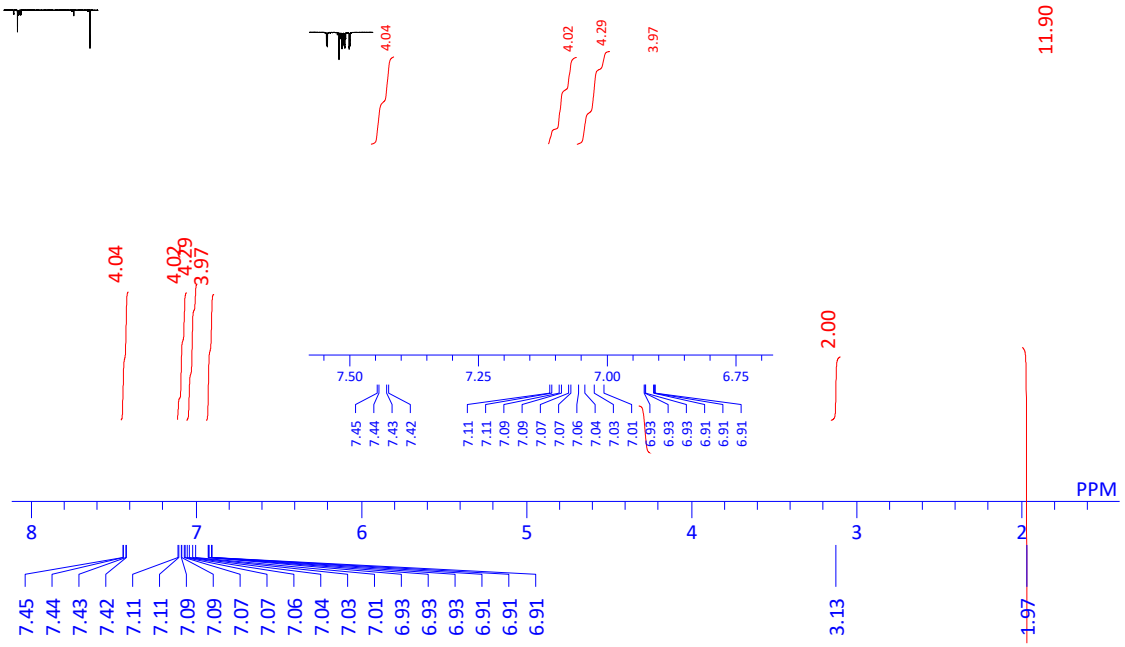

Figure 2.7 The ^{1}H NMR spectrum (benzene-d_6) of **2**

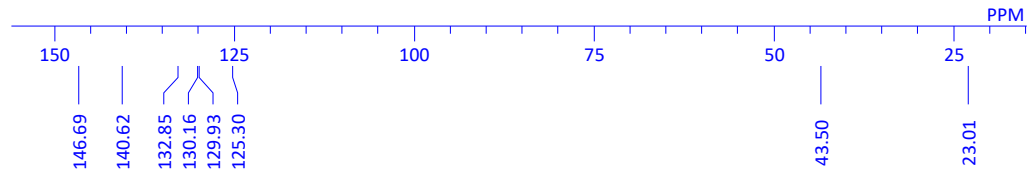

Figure 2.8 The $^{13}C\{^{1}H\}$ NMR spectrum (benzene-d_6) of **2**

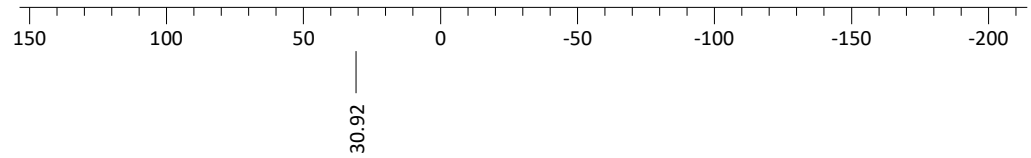

Figure 2.9 The $^{11}B\{^{1}H\}$ NMR spectrum (benzene-d_6) of **2**

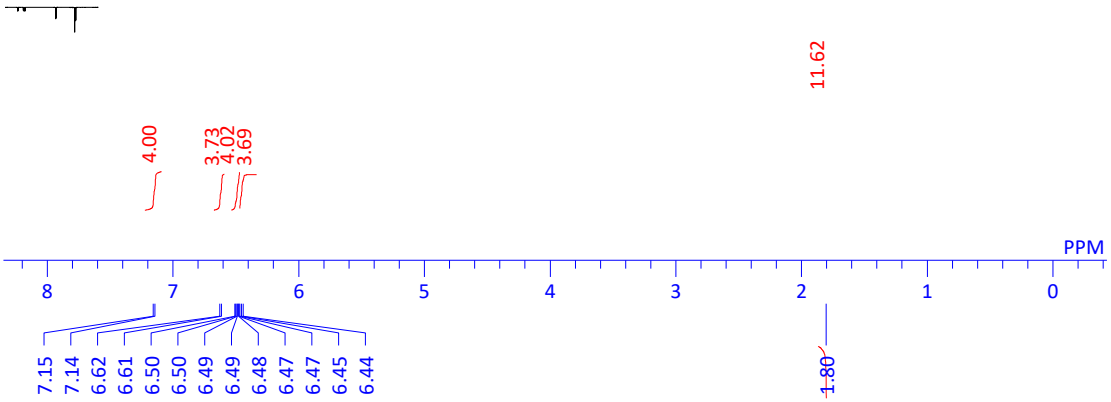

Figure 2.10 The ^{1}H NMR spectrum (THF-d_8) of **3**

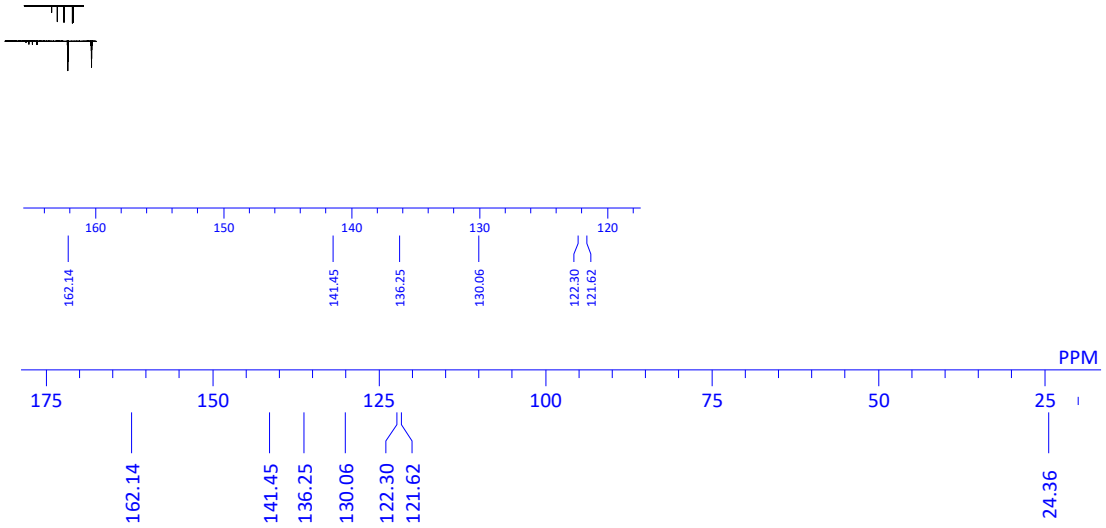

Figure 2.11 The ^{13}C{^{1}H} NMR spectrum (THF-d_8) of **3**

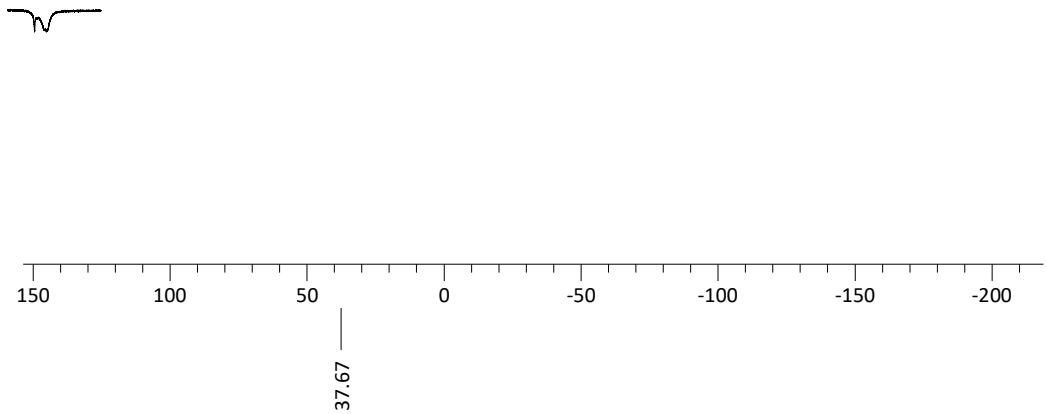

Figure 2.12 The ^{11}B{^{1}H} NMR spectrum (THF-d_8) of **3**

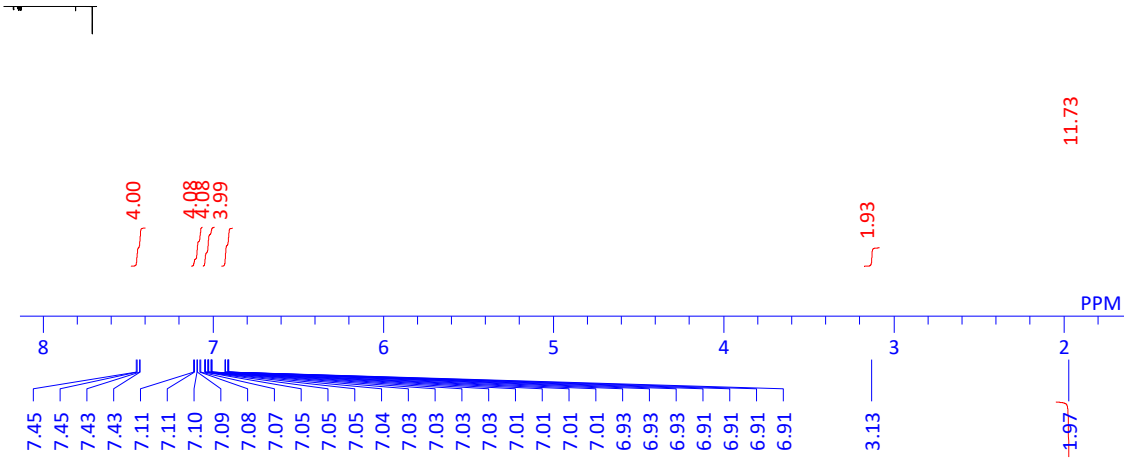

Figure 2.13 The ^{1}H NMR spectrum (C_6D_6) of **4**

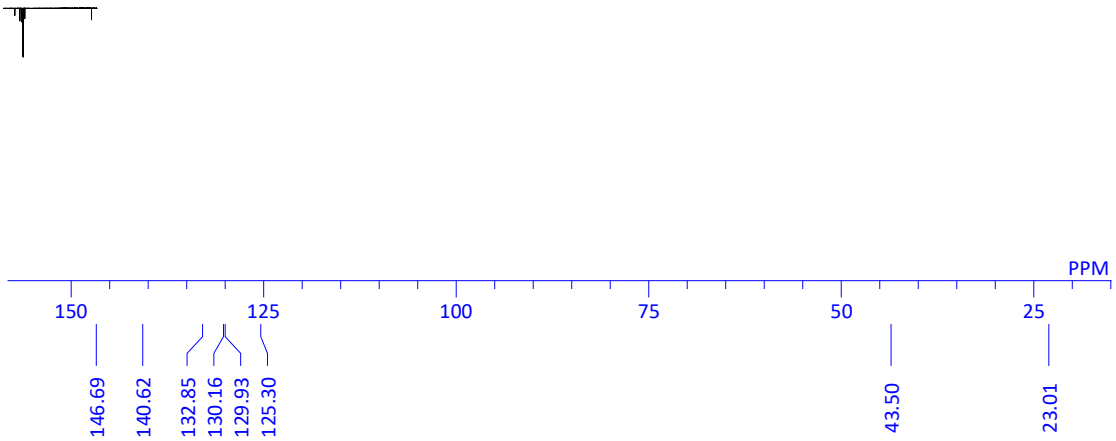

Figure 2.14 The $^{13}C\{^{1}H\}$ NMR spectrum (C_6D_6) of **4**

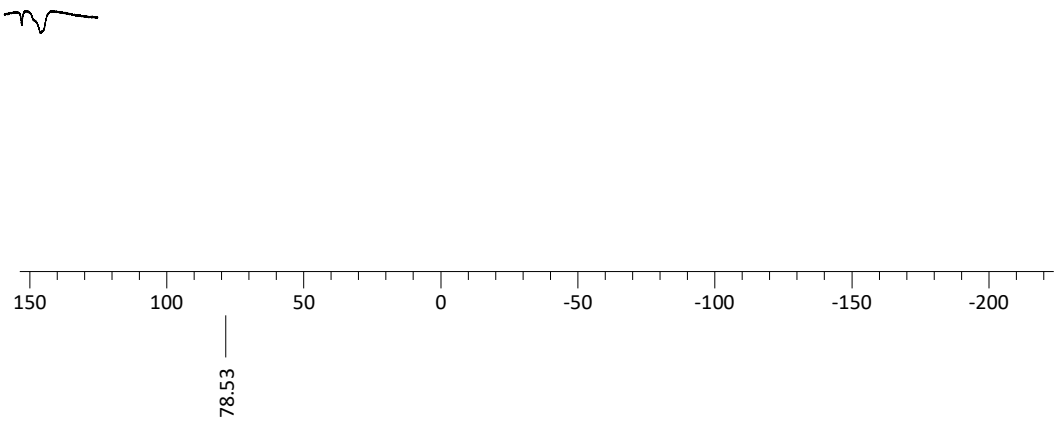

Figure 2.15 The $^{11}B\{^{1}H\}$ NMR spectrum (C_6D_6) of **4**

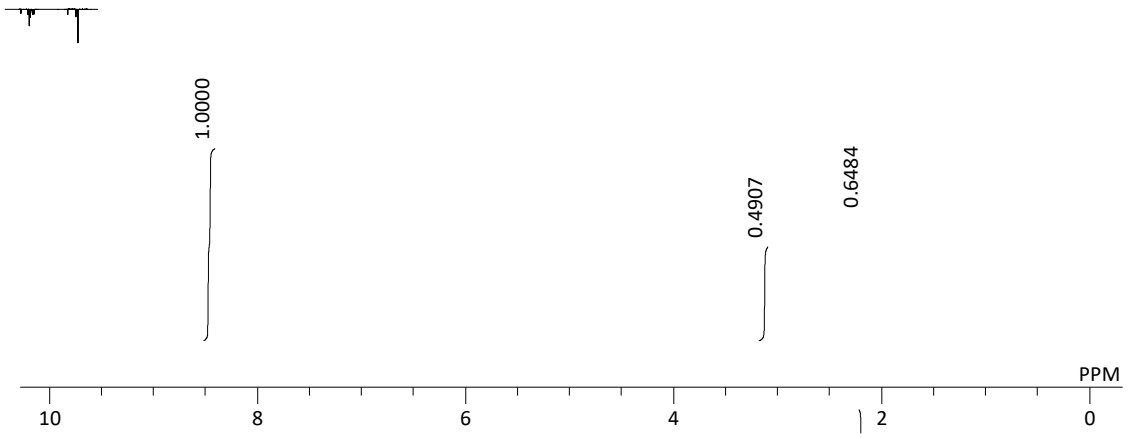

Figure 2.16 The ^{1}H NMR spectrum (C_6D_6) of the crude mixture for the reaction of **2** with CH_2Cl_2 to estimate NMR yield (**4**: 66%, **1**: 15%)**.**

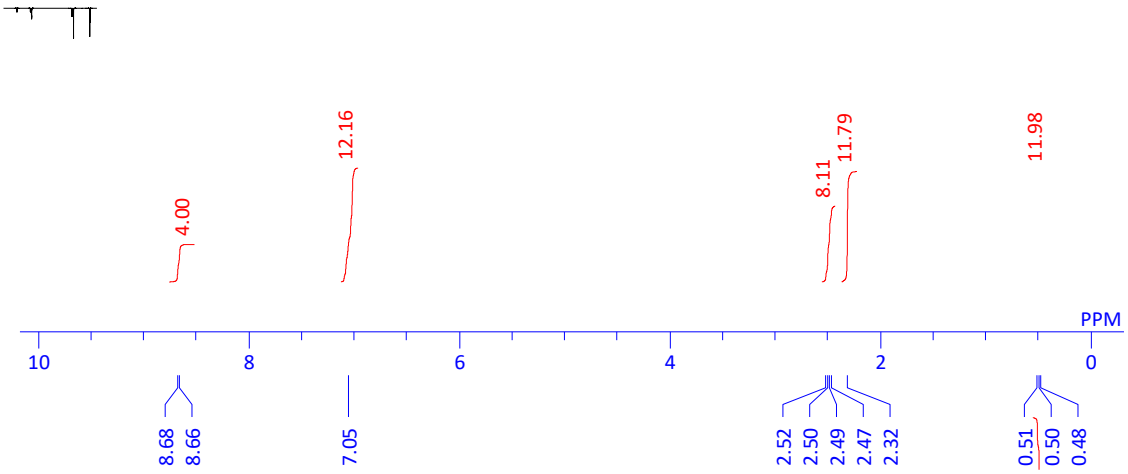

Figure 2.17 The ^{1}H NMR spectrum (C_6D_6) of **5**

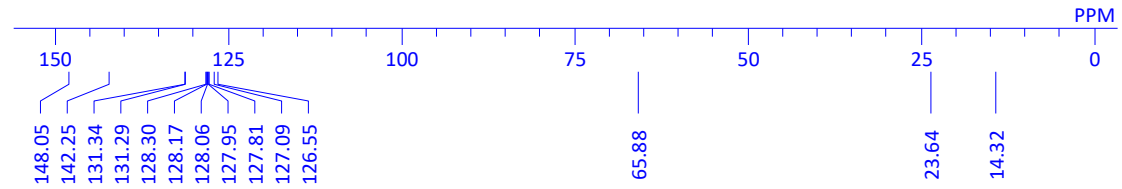

Figure 2.18 The $^{13}C\{^{1}H\}$ NMR spectrum (C_6D_6) of **5**

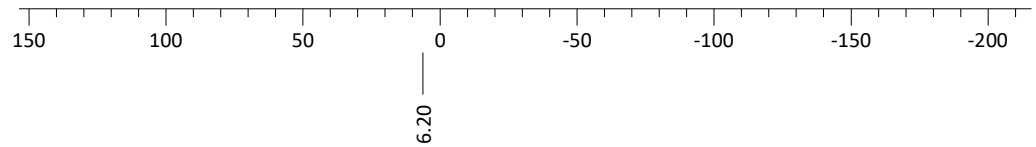

Figure 2.19 The $^{11}B\{^{1}H\}$ NMR spectrum (C_6D_6) of **5**

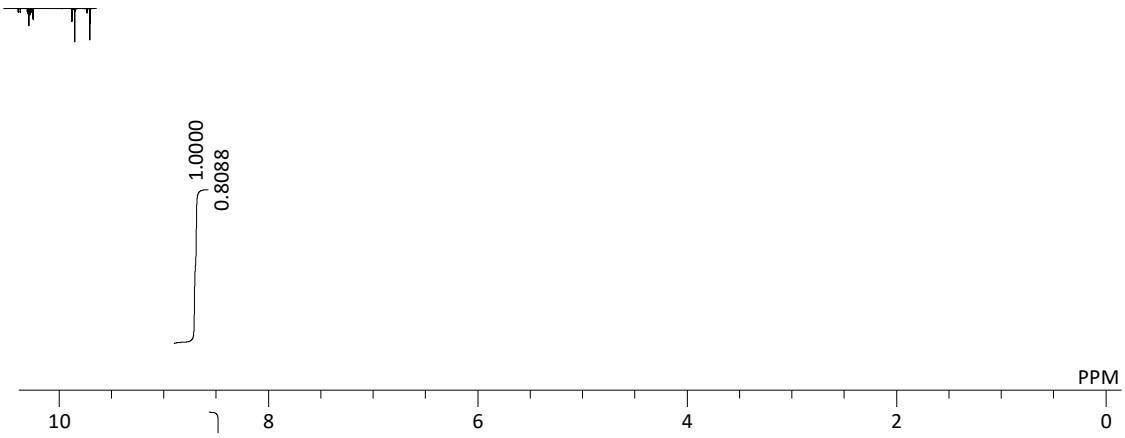

Figure 2.20 The ^{1}H NMR spectrum (C_6D_6) of the crude mixture for the reaction of **2** with S_8 to estimate NMR yield (**5**: 88%).

3. X-ray Crystallographic Analysis

Details of the crystal data and a summary of the intensity data collection parameters for **2**, **3**, **4**, **5** are listed in **Table 2.3**. The crystals were coated with mineral oil and put on a MicroMount^{TM} (MiTeGen, LLC), and then mounted on diffractometer. Diffraction data were collected on a Bruker Photon or Rigaku HyPix-6000 detectors using Mo*K*α radiation. The Bragg spots were integrated using CrysAlisPro program package.[18] Absorption corrections were applied. All the following procedure for analysis, Yadokari-XG 2009 was used as a graphical interface.[19] The structure was solved by a direct method with programs of SHELXT and refined by a full-matrix least squares method with the program of SHELXL-2016.[20] Anisotropic temperature factors were applied to all non-hydrogen atoms. The hydrogen atoms were put at calculated positions, and refined applying riding models. The detailed crystallographic data have been deposited with the Cambridge Crystallographic DataCentre: Deposition code CCDC 1921451 (**2**), CCDC 1921452 (**3**), CCDC 1921453 (**4**), CCDC 1921454 (**5**). A copy of the data can be obtained free of charge via http://www.ccdc.cam.ac.uk/products/csd/request.

Table 2.3 Crystallographic data for **2-5**

	2	**3**	**4**	**5**
CCDC #	1921451	1921452	1921453	1921454
formula	$C_{36}H_4B_2Li_2O_2$	$C_{47}H_{60}MgO_3$	$C_{31}H_{33}B_2N$	$C_{36}H_{48}B_2Li_2O$
formula	544.21	718.88	441.20	676.48
T / K	113	113	93	93
color	red	red	colorless	colorless
size / mm	0.16×0.12×0.0	0.26×0.10×0.	0.29×0.11×0.	0.23×0.08×0.
crystal system	*Monoclinic*	*Monoclinic*	*Monoclinic*	*Monoclinic*
space group	$P2_1/n$ (#14)	$P2_1/n$ (#14)	Cc (#9)	$P2_1/c$ (#14)
a / Å	10.5120(6)	10.1811(8)	10.4002(5)	13.6457(5)
b / Å	12.1150(5)	31.340(3)	25.2303(11)	21.4156(5)
c / Å	12.6651(5)	12.9725(17)	9.8661(5)	13.8407(5)
α / °	90	90	90	90
β / °	101.554(4)	99.936(10)	94.834(4)	114.708(4)
γ / °	90	90	90	90
V / Å^3	1580.25(13)	4077.1(17)	2579.7(2)	3674.4(2)
Z	2	4	4	4
D_x / g cm^{-3}	1.144	1.171	1.136	1.223
μ / mm^{-1}	0.066	0.084	0.064	0.289
F(000)	584	1552	944	1440
θ range / °	2.303 to	1721 to	1.614 to	1.878 to
reflns	12133	31400	12138	40083
Indep reflns	3394	8587	6658	8422
param	229	483	312	423
GOF on F^2	1.058	1.079	1.105	1.036
$R1$ [$I > 2\sigma(I)$][a]	0.00456	0.0858	0.0616	0.0369
w$R2$ [$I >$	0.1089	0.1817	0.1385	0.0833
$R1$ (all data)[a]	0.0566	0.1584	0.0797	0.0545
w$R2$ (all	0.1181	0.2161	0.1658	0.0905
$\Delta\rho_{min,\ max}$ / e	−0.225, 0.207	−0.459, 0.597	−0.286, 0.305	−0.302, 0.561

[a] $R1 = \Sigma\ ||Fo| - |Fc|| / \Sigma\ |Fo|$, [b] $wR2 = [\Sigma\ \{w(Fo^2 - Fc^2)^2 / \Sigma\ w(Fo^2)^2\}]^{1/2}$

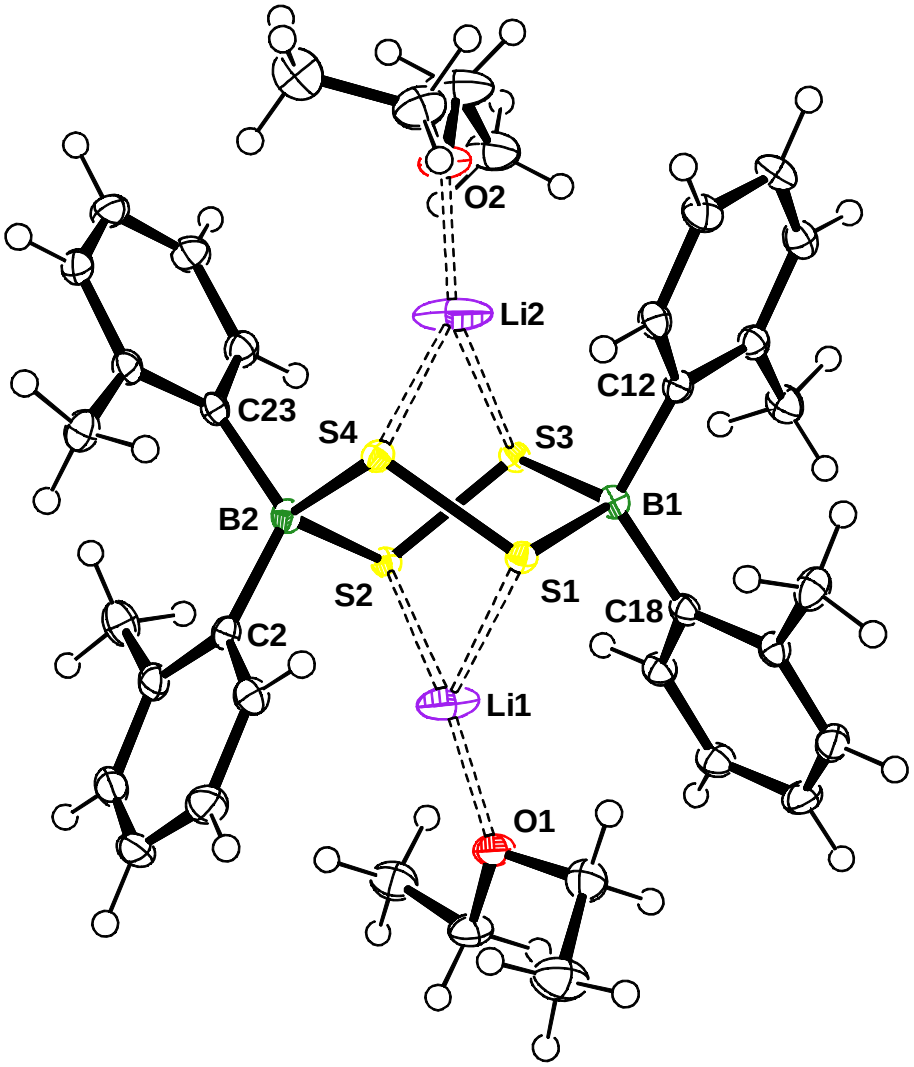

Figure 2.21 Molecular structure of **5** (thermal ellipsoid probability at 50%). Selected bond distances (Å) and angles (°) for **5**: B1−S1 1.967(2), B1−S3 1.974(2), B2−S2 1.970(2), B2−S4 1.978(2), B1−C12 1.627(3), B1−C18 1.623(3), B2−C2 1.626(2), B2−C23 1.626(2), Licv1−S1 2.411, Li1−S2 2.423(3), Li2−S3 2.399(5), Li2−S4: 2.415(3), Li1−O1: 1.871(4), Li2−O2 1.846(5); S1−B1−S3 107.73(9), C12−B1−C18 119.0(1), S2−B2−S4 108.16(9), C2−B2−C23 120.3(1), S1−Li1−S2 88.2(1), S3−Li2−S4 88.7(1).

4. UV-vis Absorption Spectra

UV-vis absorption spectra were measured with an UV-3600 spectrometer (Shimadzu) using a 1 mm width quartz cell. Toluene, Et_2O, hexane, and THF were dried over potassium mirror for the preparation of sample solution.

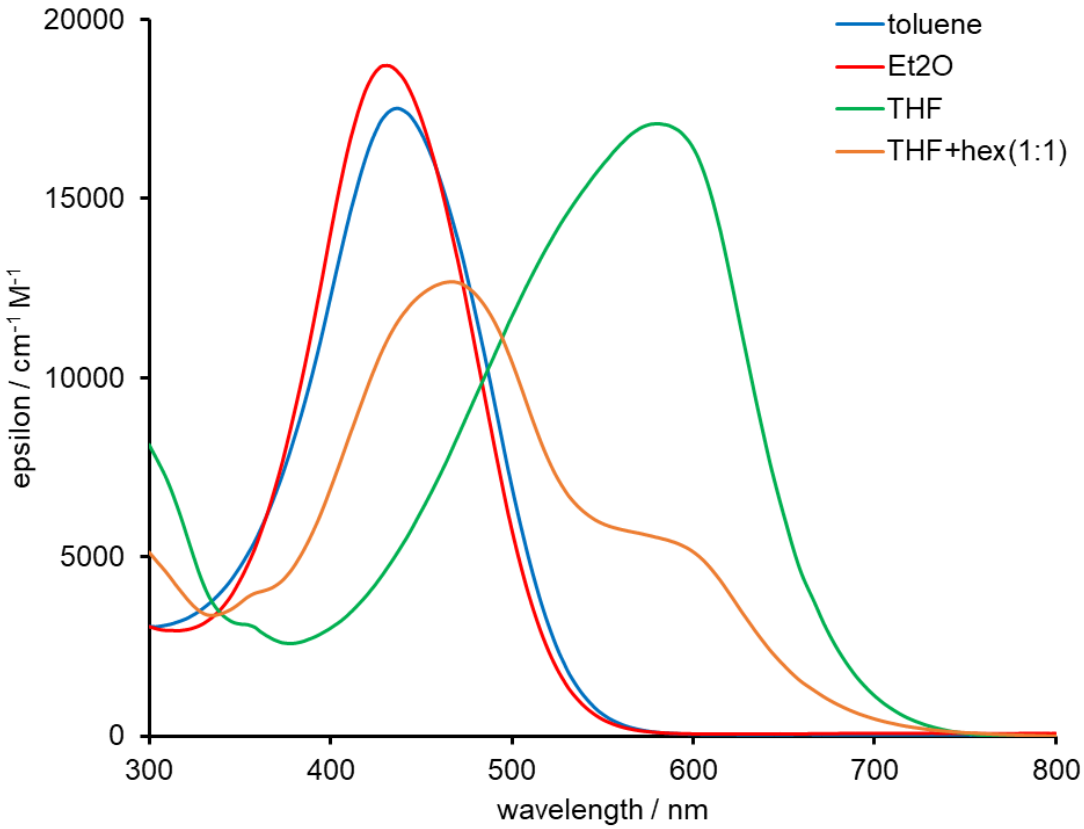

Figure 2.22 UV-Vis Spectra of **2** [toluene (1.0 mM), Et_2O (1.0 mM), THF (0.92 mM), or hexane/THF (1:1) (1.0 mM), −30 °C]

Table 2.4 Wavelengths of absorption maxima (λ_{max}) and molar absorption coefficient (ε) for each solvent

solvents	λ_{max} [nm]	ε [cm^{-1} M^{-1}]
toluene	439	1.7×10^4
Et_2O	440	1.9×10^4
THF	570	1.8×10^4

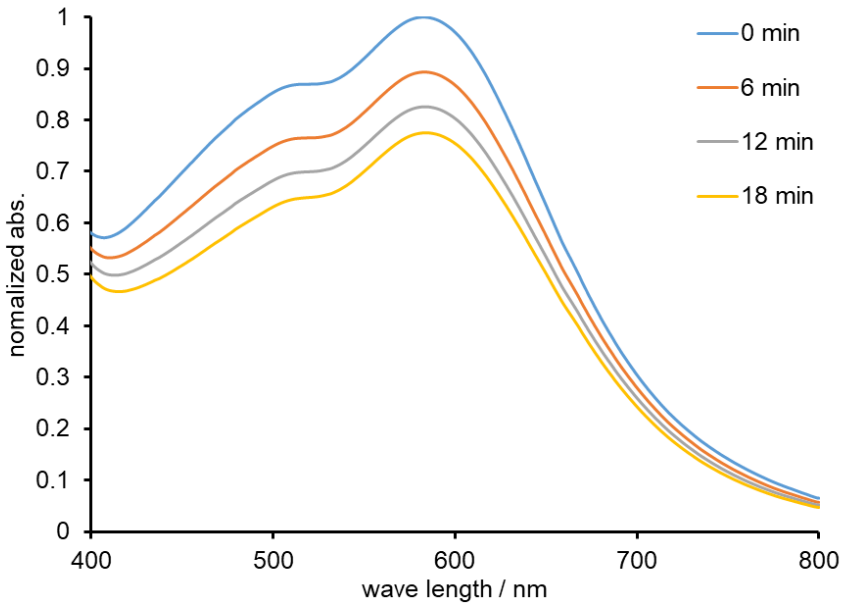

Figure 2.23 Monitoring the decomposition of **2** in THF at room temperature

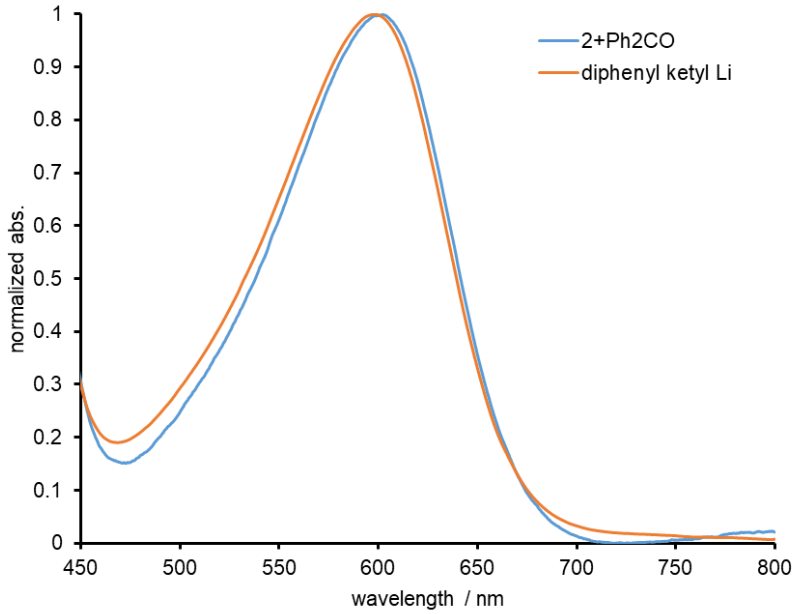

Figure 2.24 Monitoring the generation of diphenyl ketyl radical by UV-Vis spectrum

5. Cyclic voltammetry

The electrochemical experiments were carried out by using ALS 600D potentiostat/galvanostat, a glassy carbon disk working electrode, a Pt wire counter electrode, and Ag/Ag^+ (0.01 M $AgNO_3$ and $^nBu_4N^+PF_6^-$ acetornitrile solution as Ag^+ source) reference electrode. The measurements of cyclic voltammetry were carried out with a THF solution of **2** (0.50 mM) containing $LiPF_6$ (0.10 M) as a supporting electrolyte with scan rates of 10 mV/s in a glovebox filled with argon at −30 °C. The half wave potentials of **2** were compensated with that of Cp_2Fe/Cp_2Fe^+ redox cycle.

6. Theoretical Calculations

DFT calculations were performed by using Gaussian 16, Revision B.01 program package.[21] The geometry optimizations were performed at the M06-2X[22]/6-31G(d)[23] level of theory. The Wiberg bond index (WBI) and natural population analysis (NPA) charge distribution were calculated by natural bond orbital (NBO) method.[24] TD-DFT calculations were performed to estimate UV-vis spectrum of **2**, **2'** and **2''** with M06-2X/6-31G(d) level (nstates=3) of theory. Initial structures of **2'** and **2''** was generated by deleting Li^+(thf) fragment(s) from optimized structure of **2**. These structures were used for TD-DFT calculation with geometry optimizations by M06-2X/6-31G(d) level of theory.

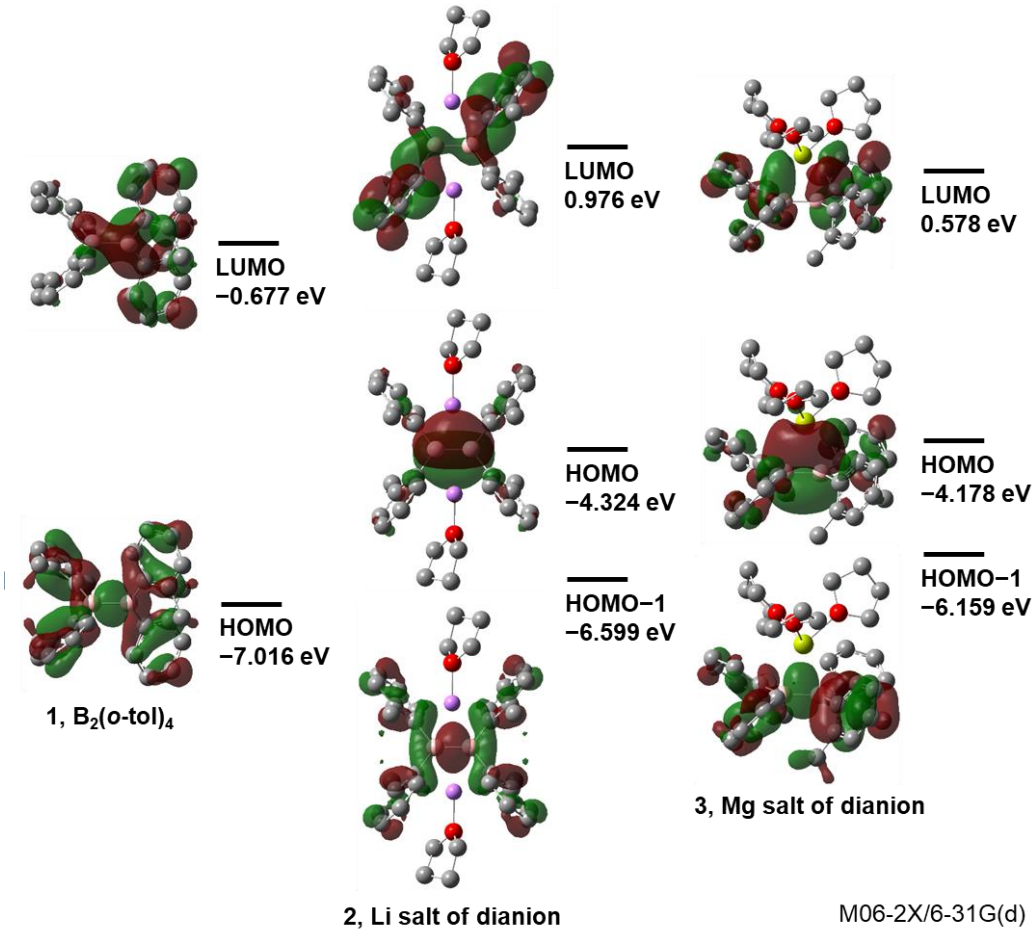

Figure 2.25 Selected MOs of **1**, **2** and **3** calculated at the M06-2X/6-31G(d) level of theory.

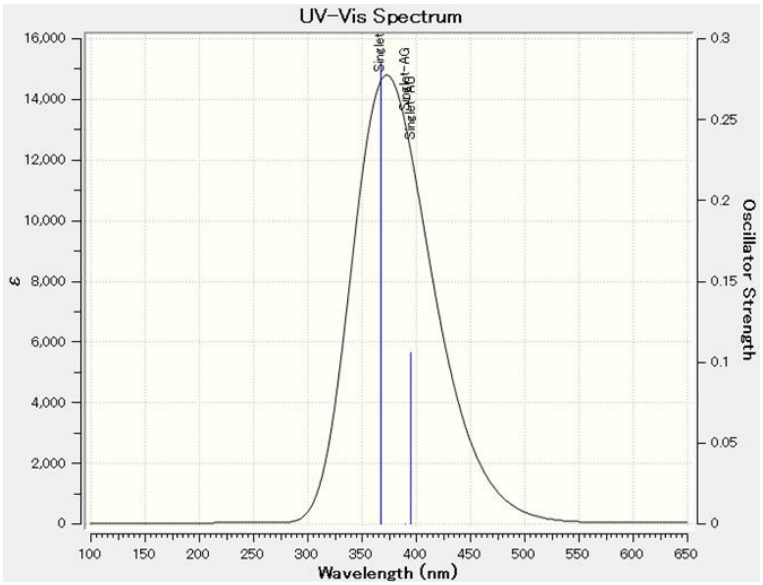

Figure 2.26 The simulated UV-vis spectrum of **2** by TD-DFT calculations

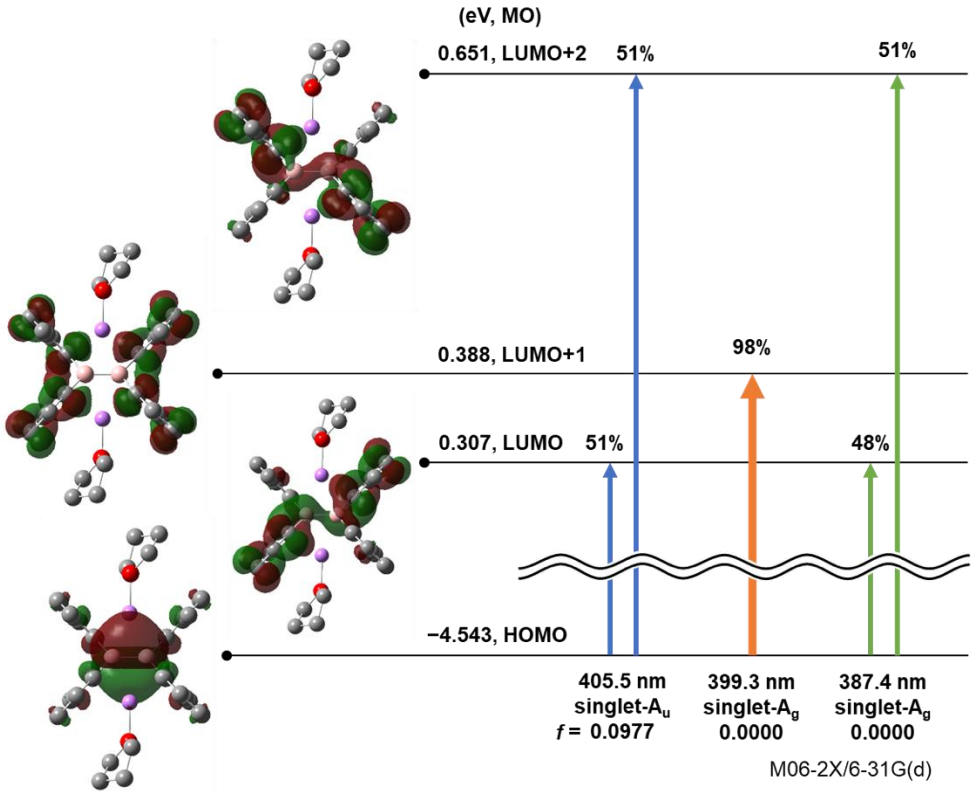

Figure 2.27 The calculated transition modes of **2**

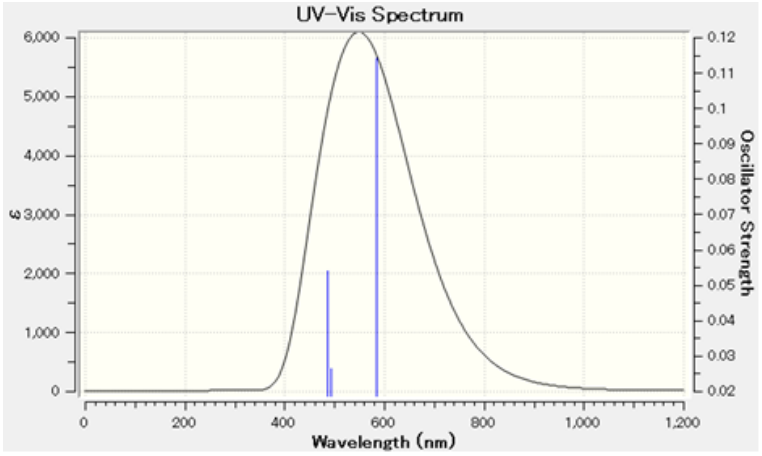

Figure 2.28 The simulated UV-vis spectrum of **2'** by TD-DFT calculations

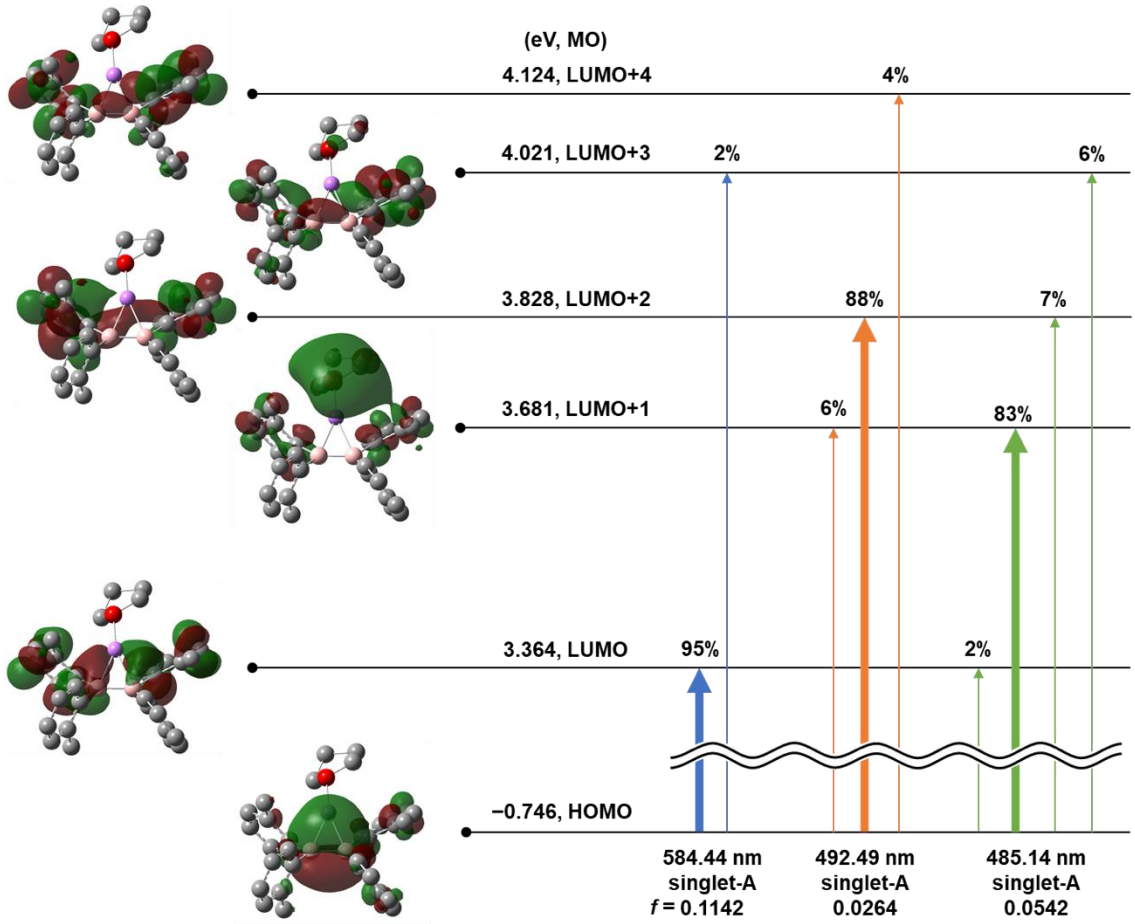

Figure 2.29 The calculated transition modes of **2'**

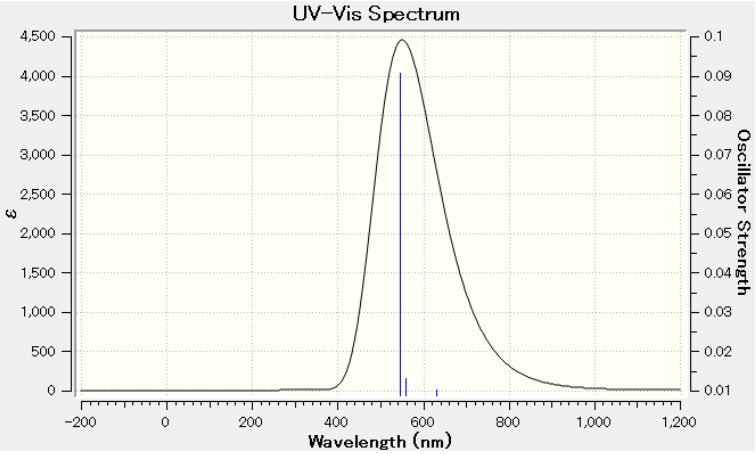

Figure 2.30 The simulated UV-vis spectrum of **2''** by TD-DFT calculations

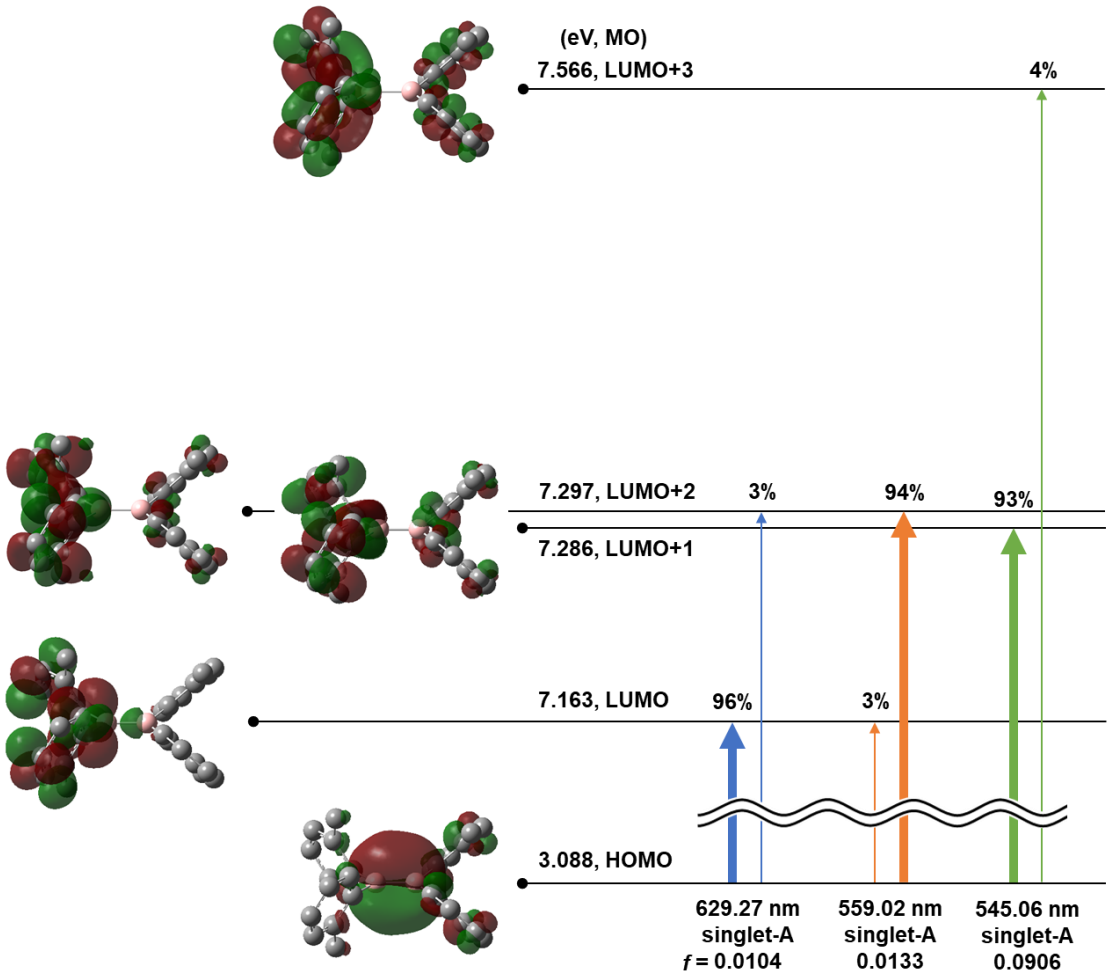

Figure 2.31 The calculated transition modes of **2''**

2.6. References

[2] M. Arrowsmith, H. Braunschweig, T. E. Stennett, *Angew. Chem. Int. Ed.* **2017**, *56*, 96-115.

[3] (a) Y. Wang, B. Quillian, P. Wei, C. S. Wannere, Y. Xie, R. B. King, H. F. Schaefer, P. v. R. Schleyer, G. H. Robinson, *J. Am. Chem. Soc.* **2007**, *129*, 12412-12413.

(b) Y. Wang, B. Quillian, P. Wei, Y. Xie, C. S. Wannere, R. B. King, H. F. Schaefer, P. v. R. Schleyer, G. H. Robinson, *J. Am. Chem. Soc.* **2008**, *130*, 3298-3299.
(c) H. Braunschweig, R. D. Dewhurst, K. Hammond, J. Mies, K. Radacki, A. Vargas, *Science* **2012**, *336*, 1420-1422.
(d) P. Bissinger, H. Braunschweig, A. Damme, T. Kupfer, I. Krummenacher, A. Vargas, *Angew. Chem. Int. Ed.* **2014**, *53*, 5689-5693.
(e) J. Böhnke, H. Braunschweig, W. C. Ewing, C. Hörl, T. Kramer, I. Krummenacher, J. Mies, A. Vargas, *Angew. Chem. Int. Ed.* **2014**, *53*, 9082-9085.
(f) H. Braunschweig, R. D. Dewhurst, C. Hörl, A. K. Phukan, F. Pinzner, S. Ullrich, *Angew. Chem. Int. Ed.* **2014**, *53*, 3241-3244.
(g) P. Bissinger, H. Braunschweig, M. A. Celik, C. Claes, R. D. Dewhurst, S. Endres, H. Kelch, T. Kramer, I. Krummenacher, C. Schneider, *Chem. Commun.* **2015**, *51*, 15917-15920.
(h) P. Bissinger, H. Braunschweig, A. Damme, C. Hörl, I. Krummenacher, T. Kupfer, *Angew. Chem. Int. Ed.* **2015**, *54*, 359-362.
(i) J. Böhnke, H. Braunschweig, T. Dellermann, W. C. Ewing, K. Hammond, J. O. C. Jimenez-Halla, T. Kramer, J. Mies, *Angew. Chem. Int. Ed.* **2015**, *54*, 13801-13805.
(j) Arrowsmith, J. Böhnke, H. Braunschweig, M. A. Celik, T. Dellermann, K. Hammond, *Chem.-Eur. J.* **2016**, *22*, 17169-17172.
(k) H. Braunschweig, P. Constantinidis, T. Dellermann, W. C. Ewing, I. Fischer, M. Hess, F. R. Knight, A. Rempel, C. Schneider, S. Ullrich, A. Vargas, J. D. Woollins, *Angew. Chem. Int. Ed.* **2016**, *55*, 5606-5609.
(l) H. Braunschweig, I. Krummenacher, C. Lichtenberg, J. D. Mattock, M. Schäfer, U. Schmidt, C. Schneider, T. Steffenhagen, S. Ullrich, A. Vargas, *Angew. Chem. Int. Ed.* **2017**, *56*, 889-892.
(m) S. R. Wang, M. Arrowsmith, J. Böhnke, H. Braunschweig, T. Dellermann, R. D. Dewhurst, H. Kelch, I. Krummenacher, J. D. Mattock, J. H. Müssig, T. Thiess, A. Vargas, J. Zhang, *Angew. Chem. Int. Ed.* **2017**, *56*, 8009-8013.
(n) D. Auerhammer, M. Arrowsmith, P. Bissinger, H. Braunschweig, T. Dellermann, T. Kupfer, C. Lenczyk, D. K. Roy, M. Schäfer, C. Schneider, *Chem.-Eur. J.* **2018**, *24*, 266-273.
(o) J. Bohnke, T. Bruckner, A. Hermann, O. F. Gonzalez-Belman, M. Arrowsmith, J. O. C. Jimenez-Halla, H. Braunschweig, *Chem. Sci.* **2018**, *9*, 5354-5359.
(p) J. Böhnke, T. Dellermann, M. A. Celik, I. Krummenacher, R. D. Dewhurst, S. Demeshko, W. C. Ewing, K. Hammond, M. Heß, E. Bill, E. Welz, M. I. S. Röhr, R. Mitrić, B. Engels, F. Meyer, H. Braunschweig, *Nature Commun.* **2018**, *9*, 1197.
(q) T. E. Stennett, J. D. Mattock, L. Pentecost, A. Vargas, H. Braunschweig, *Angew. Chem. Int. Ed.* **2018**, *57*, 15276-15281.
(r) J. H. Muessig, M. Thaler, R. D. Dewhurst, V. Paprocki, J. Seufert, J. D. Mattock, A. Vargas, H. Braunschweig, *Angew. Chem. Int. Ed.* **2019**, *58*, 4405-4409.
(s) A. Hermann, J. Cid, J. D. Mattock, R. D. Dewhurst, I. Krummenacher, A. Vargas, M. J.

Ingleson, H. Braunschweig, *Angew. Chem. Int. Ed.* **2018**, *57*, 10091-10095.
(t) T. E. Stennett, J. D. Mattock, I. Vollert, A. Vargas, H. Braunschweig, *Angew. Chem. Int. Ed.* **2018**, *57*, 4098-4102.
(u) W. Lu, Y. Li, R. Ganguly, R. Kinjo, *J. Am. Chem. Soc.* **2017**, *139*, 5047-5050; (v) W. Lu, Y. Li, R. Ganguly, R. Kinjo, *J. Am. Chem. Soc.* **2018**, *140*, 1255-1258.
(w) S. Morisako, R. Shang, Y. Yamamoto, H. Matsui, M. Nakano, *Angew. Chem. Int. Ed.* **2017**, *56*, 15234-15240.
(x) T. E. Stennett, P. Bissinger, S. Griesbeck, S. Ullrich, I. Krummenacher, M. Auth, A. Sperlich, M. Stolte, K. Radacki, C.-J. Yao, F. Wgrthner, A. Steffen, T. B. Marder, H. Braunschweig *Angew. Chem. Int. Ed.* **2019**, *58*, 6449–6454.
(y) T. Brückner, R. D. Dewhurst, T. Dellermann, M. Müller, H. Braunschweig, *Chem. Sci.* **2019**, *10*, 7375–7378.

[4] (a) A. Moezzi, R. A. Bartlett, P. P. Power, *Angew. Chem. Int. Ed. Engl.* **1992**, *31*, 1082-1083.
(b) H. Nöth, J. Knizek, W. Ponikwar, *Eur. J. Inorg. Chem.* **1999**, *1999*, 1931-1937.
(c) Y. Shoji, T. Matsuo, D. Hashizume, H. Fueno, K. Tanaka, K. Tamao, *J. Am. Chem. Soc.* **2010**, *132*, 8258-8260.
(d) A. Moezzi, M. M. Olmstead, P. P. Power, *J. Am. Chem. Soc.* **1992**, *114*, 2715-2717.
(e) A. Hübner, M. Bolte, H.-W. Lerner, M. Wagner, *Angew. Chem. Int. Ed.* **2014**, *53*, 10408-10411.
(f) T. Kaese, A. Hübner, M. Bolte, H.-W. Lerner, M. Wagner, *J. Am. Chem. Soc.* **2016**, *138*, 6224-6233.

[5] T. Kaese, T. Trageser, H. Budy, M. Bolte, H.-W. Lerner, M. Wagner, *Chem. Sci.* **2018**, *9*, 3881-3891.

[6] for the general review papers of boryl anion: see
(a) M. Yamashita, K. Nozaki, *J. Synth. Org. Chem., Jpn.* **2010**, *68*, 359-369.
(b) M. Yamashita, *Bull. Chem. Soc. Jpn.* **2011**, *84*, 983-999.
(c) M. Yamashita, K. Nozaki, in *Synthesis and Application of Organoboron Compounds* (Eds.: E. Fernández, A. Whiting), Springer International Publishing, **2015**, pp. 1-37.

[7] (a) H. W. Wanzlick, E. Schikora, *Angew. Chem.* **1960**, *72*, 494-494.
(b) V. P. W. Böhm, W. A. Herrmann, *Angew. Chem. Int. Ed.* **2000**, *39*, 4036-4038.
(c) W. Kirmse, *Angew. Chem. Int. Ed.* **2010**, *49*, 8798-8801.

[8] (a) N. Tsukahara, H. Asakawa, K.-H. Lee, Z. Lin, M. Yamashita, *J. Am. Chem. Soc.* **2017**, *139*, 2593-2596.
(b) Y. Katsuma, N. Tsukahara, L. Wu, Z. Lin, M. Yamashita, *Angew. Chem. Int. Ed.* **2018**, *57*, 6109-6114.
(c) Y. Katsuma, L. Wu, Z. Lin, S. Akiyama, M. Yamashita, *Angew. Chem. Int. Ed.* **2019**, *58*, 317-321.

[9] (a) M. Yamashita, Y. Suzuki, Y. Segawa, K. Nozaki, *J. Am. Chem. Soc.* **2007**, *129*, 9570-9571.

(b) W. Lu, H. Hu, Y. Li, R. Ganguly, R. Kinjo, *J. Am. Chem. Soc.* **2016**, *138*, 6650-6661.
(c) A.-F. Pécharman, A. L. Colebatch, M. S. Hill, C. L. McMullin, M. F. Mahon, C. Weetman, *Nature Commun.* **2017**, *8*, 15022.

[10] X. Zheng, U. Englert, G. E. Herberich, J. Rosenplänter, *Inorg. Chem.* **2000**, *39*, 5579-5585.

[11] H. Braunschweig, A. Damme, D. Gamon, H. Kelch, I. Krummenacher, T. Kupfer, K. Radacki, *Chem.-Eur. J.* **2012**, *18*, 8430-8436.

[12] W. Lu, R. Kinjo, *Chem. Commun.* **2018**, *54*, 8842-8844.

[13] R. Bertermann, H. Braunschweig, P. Constantinidis, T. Dellermann, R. D. Dewhurst, W. C. Ewing, I. Fischer, T. Kramer, J. Mies, A. K. Phukan, A. V.argas, *Angew. Chem. Int. Ed.* **2015**, *54*, 13090–13094.

[14] (a) T. Kupfer, H. Braunschweig, K. Radacki, *Angew. Chem. Int. Ed.* **2015**, *54*, 15084-15088.
(b) C.-W. Chiu, Y. Kim, F. P. Gabbaï, *J. Am. Chem. Soc*. **2009**, *131*, 60–61.

[15] (a) D. S. Matteson, R. W. H. Mah, *J. Am. Chem. Soc.* **1963**, *85*, 2599-2603.
(b) D. S. Matteson, D. Majumdar, *J. Am. Chem. Soc.* **1980**, *102*, 7588-7590.
(c) D. S. Matteson, R. Ray, *J. Am. Chem. Soc.* **1980**, *102*, 7590-7591.
(d) D. S. Matteson, K. M. Sadhu, *J. Am. Chem. Soc.* **1983**, *105*, 2077-2078.
(e) D. S. Matteson, K. M. Sadhu, M. L. Peterson, *J. Am. Chem. Soc.* **1986**, *108*, 810-819.
(f) D. S. Matteson, R. Soundararajan, O. C. Ho, W. Gatzweiler, *Organometallics* **1996**, *15*, 152-163.
(g) R. P. Singh, D. S. Matteson, *J. Org. Chem.* **2000**, *65*, 6650-6653.
(h) D. S. Matteson, *J. Org. Chem.* **2013**, *78*, 10009-10023.

[16] (a) J. E. Leffler, G. B. Watts, T. Tanigaki, E. Dolan, D. S. Miller, J. Am. Chem. Soc. 1970, 92, 6825–6830.
(b) A. Berndt, H. Klusik, K. Schlüter, *J. Organomet. Chem.* **1981**, 222, c25–c27.
(c) H. Klusik, A. Berndt, *Angew. Chem. Int. Ed. Engl.* **1981**, 20, 870–871.
(d) H. Klusik, A. Berndt, *Angew. Chem.* **1981**, *93*, 903–904.
(e) W. J. Grigsby, P. P. Power, *Chem. Commun.* **1996**, 2235–2236.
(f) W. J. Grigsby, P. Power, *Chem. Eur. J.* **1997**, *3*, 368–375.

[17] D. Auerhammer, M. Arrowsmith, R. D. Dewhurst, T. Kupfer, J. Bohnke, H. Braunschweig, *Chem. Sci.* **2018**, *9*, 2252-2260.

[18] CrysAlisPRO, Oxford Diffraction/Agilent Technologies UK Ltd, Yarnton, England, 2015.

[19] C. Kabuto, S. Akine, E. Kwon, *J. Cryst. Soc. Jpn.* **2009**, *51*, 218-224.

[20] (a) G. Sheldrick, *Act. Cryst. Sec. A* **2008**, *64*, 112-122; (b) G. Sheldrick, *Act. Cryst. Sec. C* **2015**, *71*, 3-8.

[21] M. J. Frisch, G. W. Trucks, H. B. Schlegel, G. E. Scuseria, M. A. Robb, J. R. Cheeseman, G. Scalmani, V. Barone, G. A. Petersson, H. Nakatsuji, X. Li, M. Caricato, A. V. Marenich, J. Bloino, B. G. Janesko, R. Gomperts, B. Mennucci, H. P. Hratchian, J. V. Ortiz, A. F. Izmaylov, J. L. Sonnenberg, Williams, F. Ding, F. Lipparini, F. Egidi, J. Goings, B. Peng, A. Petrone, T.

Henderson, D. Ranasinghe, V. G. Zakrzewski, J. Gao, N. Rega, G. Zheng, W. Liang, M. Hada, M. Ehara, K. Toyota, R. Fukuda, J. Hasegawa, M. Ishida, T. Nakajima, Y. Honda, O. Kitao, H. Nakai, T. Vreven, K. Throssell, J. A. Montgomery Jr., J. E. Peralta, F. Ogliaro, M. J. Bearpark, J. J. Heyd, E. N. Brothers, K. N. Kudin, V. N. Staroverov, T. A. Keith, R. Kobayashi, J. Normand, K. Raghavachari, A. P. Rendell, J. C. Burant, S. S. Iyengar, J. Tomasi, M. Cossi, J. M. Millam, M. Klene, C. Adamo, R. Cammi, J. W. Ochterski, R. L. Martin, K. Morokuma, O. Farkas, J. B. Foresman, D. J. Fox, Wallingford, CT, **2016**.

[22] Y. Zhao, D. G. Truhlar, *Theor. Chem. Acc.* **2008**, 120, 215.

[23] (a) R. Ditchfield, W. J. Hehre, J. A. Pople, *J. Chem. Phys.* **1971**, 54, 724.
(b) W. J. Hehre, R. Ditchfield, J. A. Pople, *J. Chem. Phys.* **1972**, *56*, 2257–2261.
(c) P. C. Hariharan and J. A. Pople, Theo. Chim. Acta, **1973**, *28*, 213.
(d)P. C. Hariharan, J. A. Pople, *Mol. Phys.* **1974**, *27*, 209.
(e) M. M. Francl, W. J. Pietro, W. J. Hehre, J. S. Binkley, M. S. Gordon, D. J. DeFrees, J. A. Pople, *J. Chem. Phys.* **1982**, *77*, 3654.
(f) G. A. Petersson, A. Bennett, T. G. Tensfeldt, M. A. Al-Laham, W. A. Shirley, J. Mantzaris, *J. Chem. Phys.* **1988**, *89*, 2193.
(g) R. C. Binning Jr., L. A. Curtiss, *J. Comp. Chem.* **1990**, *11*, 1206.
(h) J.-P. Blaudeau, M. P. McGrath, L. A. Curtiss, L. Radom, *J. Chem. Phys.* **1997**, *107*, 5016.
(i) V. A. Rassolov, J. A. Pople, M. A. Ratner, T. L. Windus, *J. Chem. Phys.* **1998**, *109*, 1223.
(j) V. A. Rassolov, M. A. Ratner, J. A. Pople, P. C. Redfern, L. A. Curtiss, *J. Comp. Chem.* **2001**, *22*, 976.

[24] (a) J. P. Foster, F. Weinhold, *J. Am. Chem. Soc.* **1980**, *102*, 7211-7218; (b) A. E. Reed, F. Weinhold, *J. Chem. Phys.* **1983**, *78*, 4066-4073; (c) A. E. Reed, F. Weinhold, *J. Chem. Phys.* **1985**, *83*, 1736-1740; (d) A. E. Reed, R. B. Weinstock, F. Weinhold, *J. Chem. Phys.* **1985**, *83*, 735-746; (e) A. E. Reed, L. A. Curtiss, F. Weinhold, *Chem. Rev.* **1988**, *88*, 899-926.

Chapter 3

Complexes Bearing a Diborane(4) Dianion Ligand

3.1 Introduction

A B=B double bond is the simplest π-system consisting of only boron atom and is isoelectronic to an alkene. Similar to transition metal π-complexes of alkenes or alkynes, π-electrons of B–B multiple bond[2] are known to be able to bind to transition metals. Such π-complexes of the B–B multiple bond can be classified into three types with: (a) neutral diborene,[3] (b) neutral diboryne,[4] and (c) dianionic diborane(4) ligand[5] as described in Figure 3.1. Diborene-Pt(0) complexes have been reported to exhibit strengthening B=B bond upon coordination.[3a,b] Subsequently, diborene-Mo or -W trinuclear complexes were discovered.[6] Doubly base-stabilized symmetrical diborene complexes showed a simple η^2-coordination mode of B=B double bond toward Ag(I), Cu(I), Zn(II), and Cd(II).[3c-f] Similar, but slightly different unsymmetrical diborene could also coordinate to Cu(I), Ag(I), Au(I), and Mg(II).[3g, h] In contrast, a B(triple)B triple bond compound, diboryne, could bind two or more Cu(I) atoms[4] or one or two alkaline metal atom(s) (Li^+, Na^+)[7] through their π-bonds. A dinuclear Pt(II)-B_2I_4 complex was reported as the sole example of dianionic diborane(4)-transition metal π-complex.[5] This Pt(II)-B_2I_4 complex was synthesized from $Pt(PCy_3)_2$ and B_2I_4 through multiple redox processes on the platinum and boron atoms. It should be noted that related base-stabilized or metal-fragment-stabilized diborane(4) complexes have been reported with their unique coordination mode due to flexible structures of diborane(4).[6,8] Thus, there has been no example of direct synthesis of dianionic diborane(4)-transition metal π-complex from dianionic diborane(4).[9] On the other hand, we recently reported the synthesis of the dianionic tetra(*o*-tolyl)diborane(4) and its reactivity as a synthetic equivalent of diarylboryl anion.[10]

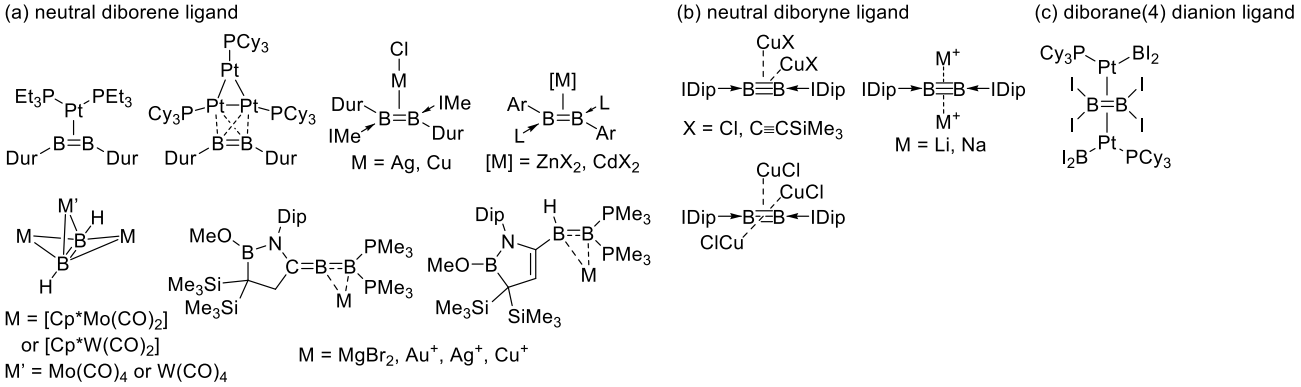

Figure 3.1 Examples of BB multiple bond-metal π-complexes

3.2 Synthesis and Structures Complexes having Diborane(4) Dianion Ligand

Herein, we report the synthesis of the copper-dianionic tetra(*o*-tolyl)diborane(4) complexes **2**-**4** by an isolated diborane(4) dianion **1** with copper salt. All of these complexes were structurally characterized by X-ray crystallographic analysis. All of these complexes exhibited visible absorption due to π-π* transition of B=B bond as assigned by DFT calculations. The X-ray absorption near edge structure (XANES) spectra revealed the electron richness of the copper center of **2**-**4**.

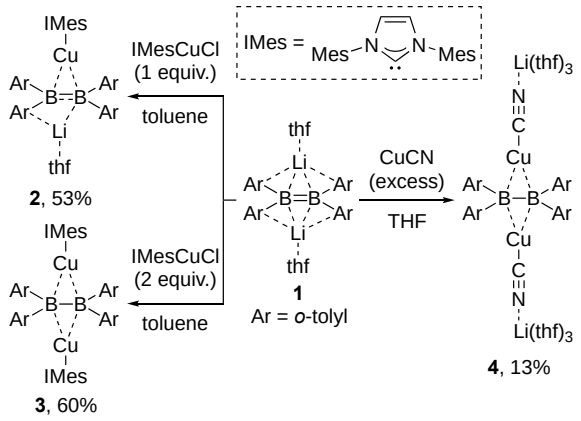

Scheme 3.1 Synthesis of dianionic tetra(*o*-tolyl)diborane(4)-copper complexes **2**-**4**.

The molecular structures of **2**, **3** and **4** were determined by a single-crystal X-ray diffraction analysis (**Figure 3.2**). The complex **2** crystallized as a contact ion pair contained lithium cation with one coordinating THF molecule. The lithium cation is close to ipso-carbon of one tolyl group and the one of two boron atoms [Li1–C22 2.354(9), Li1–B1 2.27(1) Å], while two boron atoms which are bonded with 1.684(6) Å in **2** similarly coordinate to the copper center [B–Cu 2.221(5), 2.231(5) Å]. Two angles around the boron atoms are 359.6° and 358.9°, indicating their planarity. Bis(NHC-copper) complex **3** equally coordinates to the two copper atoms on the both sides of the B=B bond [1.719(4) Å] with slightly shorter B–Cu lengths [2.178(3), 2.189(3), 2.183(3), 2.186(3) Å] than those of **2**. The two boron atoms in **3** are completely planar as judged by the sum of angles around the boron atoms (Σ∠B = 360° for both B atoms). It should be noted that Cu–C lengths in **3** [1.946(3), 1.946(3) Å] are longer than that of the previously reported (σ-boryl)Cu(IMes) complex [1.918(2) Å],[12] indicating stronger trans-influence of the dianionic diborane(4) ligand in comparison with that of σ-boryl ligand. Bis(cyanocuprate) complex **4** bears two lithium cations binding one nitrogen atom and three THF molecules. Two boron atoms which are bonded with 1.726(4) Å in **4** also equally coordinate to the two copper atoms with further shorter B–Cu distances [2.135(3), 2.171(3), 2.142(3), 2.153(3) Å] than those of **3**. It should be noted that all B–Cu lengths of **2**-**4** [2.135(3)-2.231(5) Å] are longer than those of σ-borylcopper complex [1.979(7)-2.002(3) Å][12-13] and similar to those of diborene π-complex of copper [2.133(3)-2.149(3) Å].[3d,3e] All the B–B bonds of complex **2**-**4** [1.684(6) for **2**, 1.719(4) for **3**, 1.726(4) Å for **4**] are elongated than that of **1** [1.633(3) Å].[10] The dihedral angles of C–B–B–C [**2**: 19.6(4)°, **3**: 10.6(4)°, **4**: 4.6(4)°] are larger than that of **1** (0°).[10]

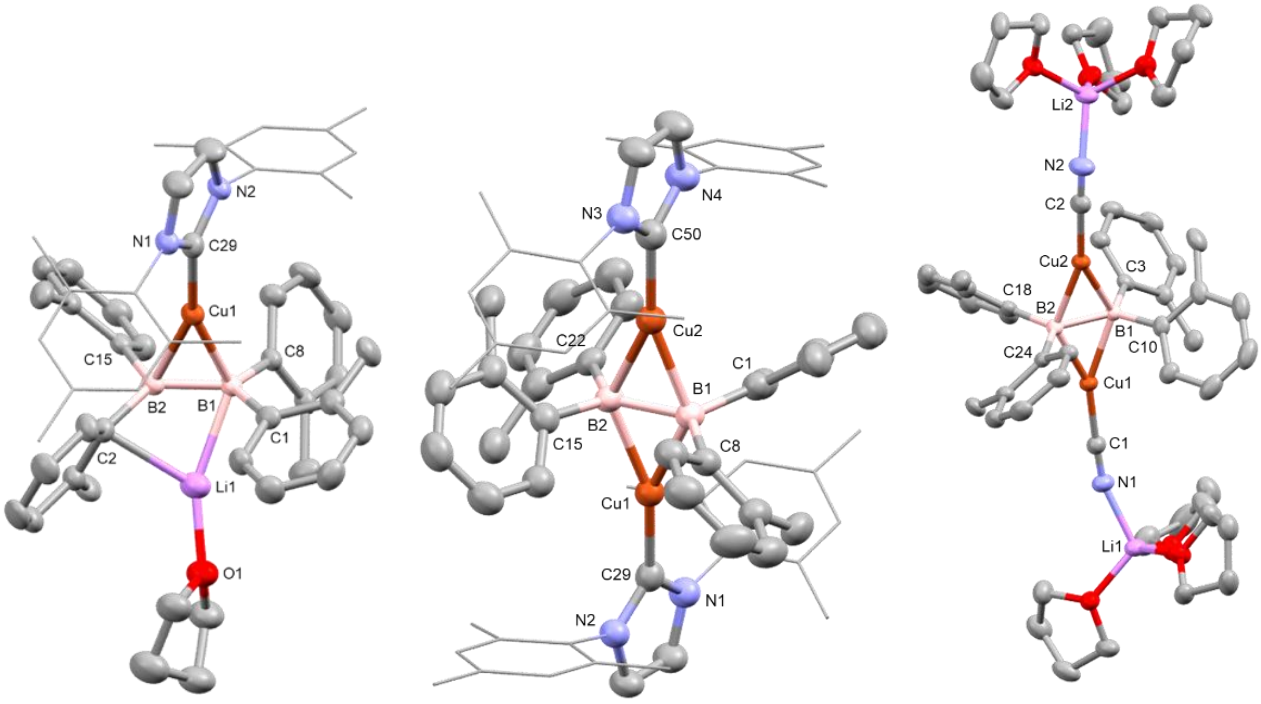

Figure 3.2 Molecular structure of **2**(left), **3**(center), and **4**(right) (thermal ellipsoids set at 50% probability; hydrogen atoms are omitted for clarity).

3.3 Characterization of Diborane(4) Dianion as a Ligand

To investigate the electronic structure of complexes **2**-**4**, DFT calculations were carried out at B3PW91/Def2SVP level of theory. The theoretically optimized structures of **2**-**4** are in good agreement with the experimentally determined crystal structures. Characteristic molecular orbitals are summarized in **Figure 3.3** (for **2**) and **Figure 3.18**, **Figure 3.19** (for **3** and **4**). The HOMO of **2** clearly shows π-orbital of B=B bond in the dianionic diborane(4) ligand with no significant contribution of Cu d-orbital. The HOMO-1 mainly consists of σ-orbitals of the four *o*-tolyl groups, π-orbital of the B–B bond, and d-orbital on the Cu atom. The combination of the π*-orbital of the B=B bond and the antibonding orbital of NCN moiety in the carbene ligand constructs LUMO. Similar composition has been observed for these orbitals of **3** and **4**. Natural bond orbital (NBO) analysis was performed to estimate the bonding mode between the B=B bond and the Cu atom. The second-order perturbation theory analysis for **2** indicates that donor-acceptor interaction from π-orbital of the B=B bond to a vacant d-orbital on the Cu atom (64.89 kcal/mol, **Table 3.1**, **Figure 3.4**) is dominant, while interactions from B–B π-bond to a vacant d-orbital on the Cu atom (π-coordination, 13.65 kcal/mol) and from an occupied d-orbital on the Cu atom to a π*-orbital on the B=B bond (π-backdonation, 7.63 kcal/mol) are far less significant. Similar tendency is observed for the complexes **3** and **4** (**Table 3.8** and **Table 3.9**, **Figure 3.25** and **Figure 3.26**).[9] In contrast, donor-accepter interaction in $[IMesCu(CH_2{=}CH_2)]^+$ (**5**), an isoelectronic model complex to **2**, shows slightly more effective π-backdonation (19.27 kcal/mol, **Table 3.10**, **Figure 3.1**). The weaker π-backdonation from Cu to B=B than that to C=C would be explained by that the π*-orbital of B=B bond is raised by dianionic charge of B=B bond in

comparison with that of neutral C=C bond.

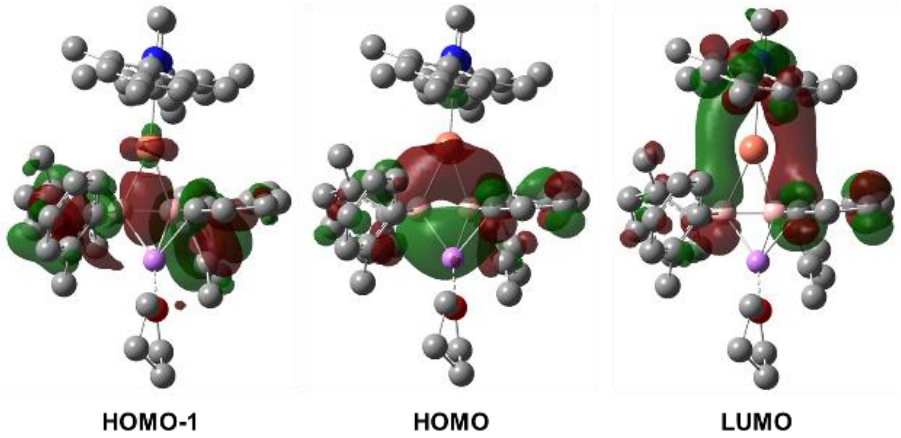

Figure 3.3 Molecular orbitals of **2** with a contour value of 0.03 atomic units. All hydrogen atoms are omitted for clarity.

Table 3.1 Selected second order perturbation energies $E^{(2)}$ in NBO analysis of compound **2**

donor NBOs	accecpter NBOs	$E^{(2)}_{ij}$ / kcal mol^{-1}
78, σ(B-B)	222, vacant d(Cu)	13.65
79, π(B=B)	222, vacant d(Cu)	64.89
73, occupied d(Cu)	225, π*(B=B)	7.63

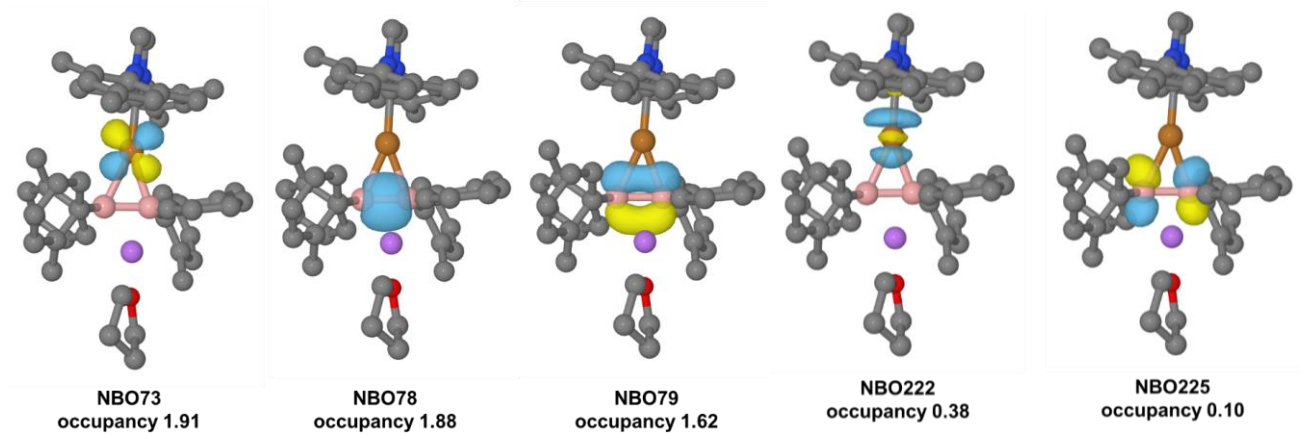

Figure 3.4 NBOs related to the donor-acceptor interaction in **2** summarized in **Table 3.1**.

The UV-Vis absorption spectrum of **2** shows two absorption maxima [418 nm (ε = 3200), 330 nm (ε = 11000)] and a broad edge to ca. 650 nm (**Figure 3.5**). TD-DFT calculations on **2** suggest two strong absorptions at 423 nm and 301 nm. The former was assigned to the HOMO (π-orbital of B=B bond)-LUMO (consisting of π*-orbitals of the B=B bond, the NCN moiety of carbene, and Mes groups) transition, while the latter was assigned to a transition from HOMO-1 (B–B σ-bond and π-orbital of *o*-tol groups) to LUMO and transitions from HOMO to π*-orbitals of *o*-tol groups. The broad

absorption around 460-650 nm would be explained by a formation of anionic complex **2'** through dissociation of Li^+(thf) moiety (**Scheme 3.2**) as assigned by TD-DFT calculations. The anionic complex **2'** has a higher HOMO and narrower HOMO-LUMO gap in comparison with those of **2** (**Figure 3.20** and **Figure 3.21**, **Table 3.4** and **Table 3.5**) giving the longer-wavelength shifted absorption probably due to the anionic charge, as previously found for **1**.[78] In the case of **3**, similar absorption maxima at 419 nm (ε = 12000) and 329 nm (ε = 9600) were observed. The spectrum of **4** has a shorter wavelength of the absorption maxima [λ_{max} (ε) = 382 nm (19000), 329 (17000)] than those of **2** and **3**. The former could be assigned as a transition from the π-orbital of B=B bond (HOMO) to combined two π*-orbitals of B=B and C≡N bonds (LUMO+2), based on the TD-DFT calculations (**Figure 3.24**, **Table 3.7**).

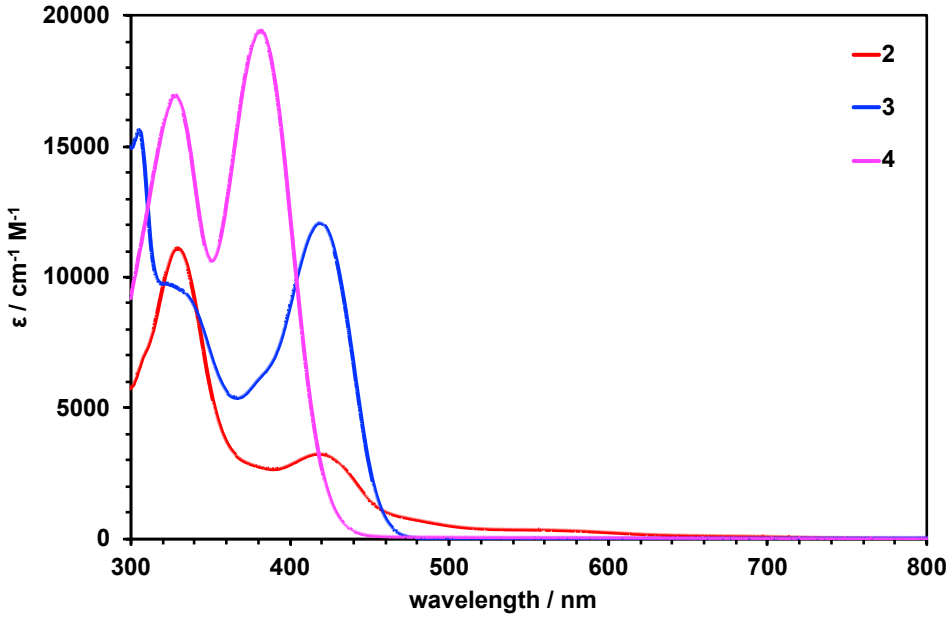

Figure 3.5 UV-Vis spectra of **2**-**4** (0.1 mM; toluene solution for **2** and **3**, THF solution for **4**).

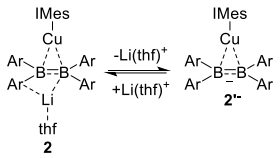

Scheme 3.2 Dissociation of Li^+ cation for **2**

To estimate electron-donating ability of the diborane(4) dianion ligand from the electron density on the copper center of **2**-**4**, XANES (x-ray absorption near edge structure) spectra of them have been measured. The Cu K-edge XANES spectra of **2**-**4** are summarized in **Figure 3.6** with those for Cu foil (Cu^0), CuCl, IMesCuCl, CuCl (Cu^I), and $CuCl_2$ (Cu^{II}) as reference compounds. The edge energies of **2**-**4** were slightly lower than those of Cu(I) com-pounds, indicating that the oxidation number of copper center in **2**-**4** is almost one and electron density on the copper is higher than those of the Cu(I) compounds. The order of edge energy is **4** < **2** < **3**. Thus, the diborane(4) dianion ligand

in the complexes **2-4** should be considered as relatively strong donor ligand in comparison with Cl and CN anions.

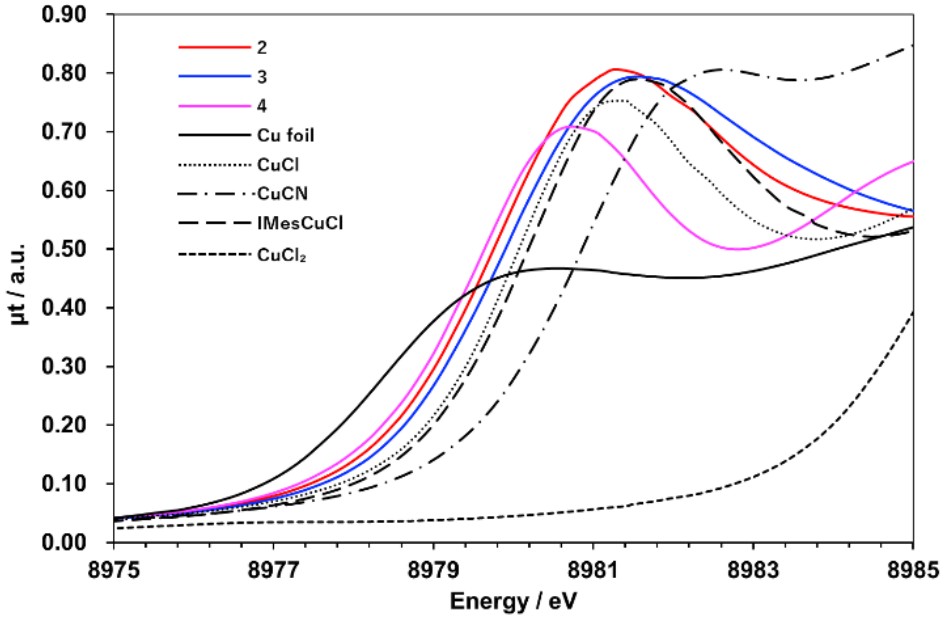

Figure 3.6 Normalized Cu K-edge XANES spectra at the pre-edge region for **2-4** (colored solid lines), Cu foil, $CuCl_2$, CuCl, CuCN, IMesCuCl.

3.4. Conclusion

In conclusion, a series of mono- and dinuclear copper complexes **2-4** having a dianionic diborane(4) ligand were synthesized by the reaction of diborane(4) dianion with copper salt. The strong σ-donating ability of the dianionic diborane(4) ligand was proven by IR spectroscopic analysis, X-ray crystallographic analysis, XANES spectra, and DFT calculations. The NBO calculations revealed that the π-backdonation to dianionic diborane(4) ligand was significantly weaker than that to the ethylene ligand due to the dianionic charges on the boron atoms.

3.5. Experimental Procedures

General Methods

All manipulations involving the air- and moisture-sensitive compounds were carried out under an argon atmosphere using standard Schlenk and glovebox (Korea KIYON, Korea and ALS Technology, Japan) technique. THF, Et_2O, toluene and n-hexane were purified by passing through a solvent purification system (Grass Contour). C_6D_6 was dried by distillation over sodium/benzophenone followed by vacuum transfer. Lithium salt of tetra(o-tolyl)diborane(4) dianion 11 and $IMesCuCl_2$ were synthesized according to the literature. The nuclear magnetic resonance (NMR) spectra were recorded on a JEOL ECS-400 (399 MHz for ^{1}H, 100 MHz for ^{13}C, 155 MHz for ^{7}Li, 128 MHz for ^{11}B) or a Bruker AVANCE III HD 500 spectrometers (500 MHz for ^{1}H, 128 MHz for ^{13}C). Chemical shifts (δ) are given by definition as dimensionless numbers and relative to 1H or 13C NMR chemical shifts of

the residual C_6D_5H for ^1H (δ = 7.16), C_6D_6 itself for ^{13}C (δ = 128.0). The ^7Li and ^{11}B NMR spectra were referenced using an external standard of LiCl in D_2O and $BF_3(OEt_2)$. The absolute values of the coupling constants are given in Hertz (Hz). Multiplicities are abbreviated as singlet (s), doublet (d), triplet (t), quartet (q), multiplet (m) and broad (br). The ATR-IR spectra were recorded on an Agilent Cary 630 spectrometer with a resolution of 4 cm^{-1}. Melting points were determined on MPA100 OptiMelt (Tokyo Instruments, Inc.) and were uncorrected. UV-vis absorption spectra were measured with an UV-3600 spectrometer (Shimadzu) using a 1 cm width quartz cell. Emission spectra were measured on a JASCO FP-8200 spectrometer. Elemental analyses were performed on a Perkin Elmer 2400 series II CHN analyzer.

Synthesis of 2, [Li(thf)][IMesCu(B_2(*o*-tol)$_4$)]

A toluene (1 mL) was added to mixture of 1 (21.8 mg, 0.040 mmol) and IMesCuCl (16.1 mg, 0.040 mmol). After stirring at room temperature for 10 minute and the volatile was evaporated. Resulting solid was extracted by hexane and red solution was recrystallized at −35 °C to give **2** as red crystals (19.5 mg, 53% yield).

^1H NMR (399 MHz, C_6D_6) δ 7.26 (4H, d, $^3J_{HH}$ = 7 Hz, 6-CH of *o*-tolyl), 7.04 (8H, m, 3- and 4-CH of *o*-tolyl), 6.82 (8H, m, 5-CH of *o*-tolyl + ArH of Mes), 5.98 (2H, s, vinyl-H), 2.79 (4H, m, Li-thf), 2.24 (6H, s, 4-Me of Mes), 2.08 (12H, s, Me of *o*-tolyl), 1.93 (12H, s, 2,6-Me of Mes), 0.89 (4H, m, Li-thf); $^{13}C\{^1H\}$ NMR (100 MHz, C_6D_6) δ: 181.47 (4°, carbene), 158.19 (4°,C_{ipso} of *o*-tolyl), 139.55 (4°, CMe of *o*-tolyl), 138.80 (4°, C_{ipso} of Mes), 137.24 (3°, 6-CH of *o*-tolyl), 135.97 (4°, 4-CMe of Mes), 135.31 (4°, 2,6-CMe of Mes), 129.74 (3°, 3,5-CH of Mes), 129.62 (3°, 5-CH of *o*-tolyl), 124.27 (3°, 3-CH of *o*-tolyl), 122.72 (3°, 4-CH of *o*-tolyl), 121.34 (3°, vinyl), 68.39 (2°, OCH_2 of Li(thf)), 25.61 (1°, CH_3 of *o*-tolyl), 24.98 (2°, OCH_2CH_2 of Li(thf)), 21.25 (1°, 4-CH3 of Mes), 17.69 (2,6-$(CH_3)_2$ of Mes); 11B{1H} NMR (128 MHz, C_6D_6) δ 30 (br). $^7Li\{^1H\}$ (155 MHz, C_6D_6) δ: 7.27 (br); mp. 78-83 °C; Anal. Calc. for $C_{59}H_{74}B_2CuLiN_2O$: C, 77.08; H, 8.11; N, 3.05; Found: C, 75.02; H, 8.10; N, 3.11.

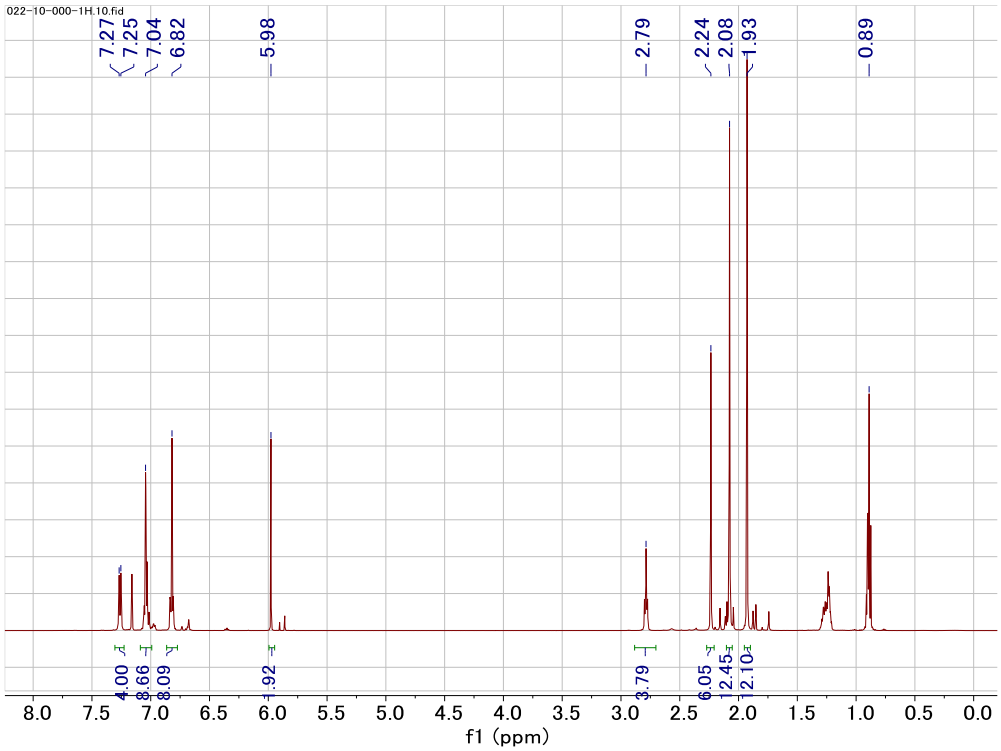

Figure 3.7 The 1H NMR spectrum (benzene-d_6) of **2**. Hexane and THF are contaminated as a crystal solvent.

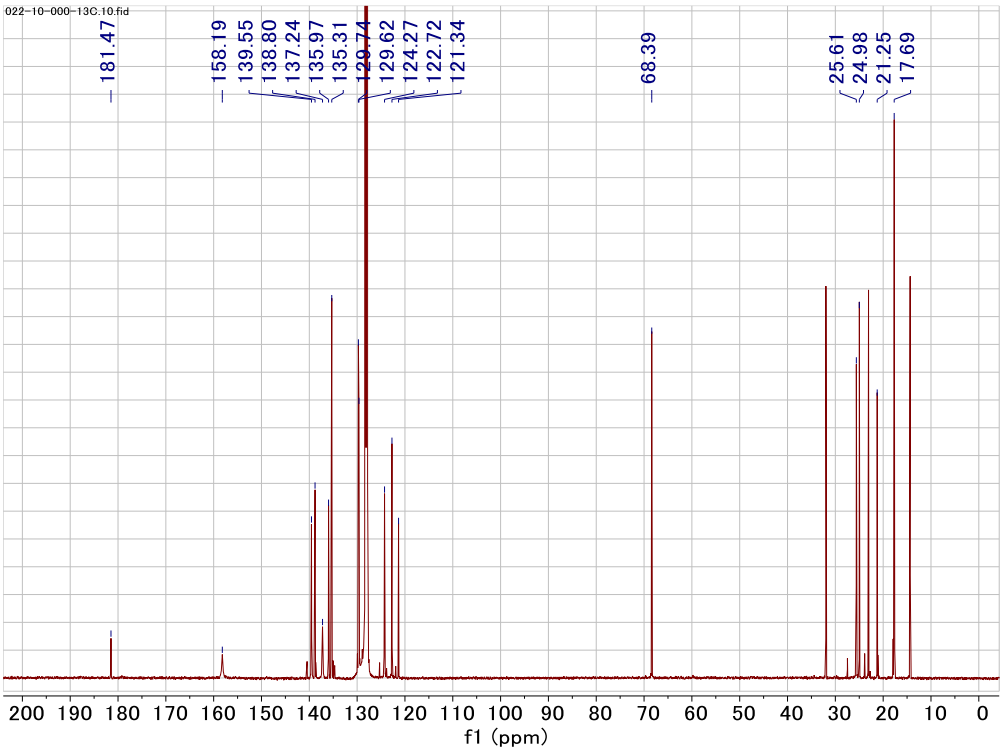

Figure 3.8 The $^{13}C\{^1H\}$ NMR spectrum (benzene-d_6) of **2**. Hexane and THF is contaminated as a crystal solvent.

Synthesis of 3, [IMesCu]$_2$[B$_2$(*o*-tol)$_4$]

A toluene (2 mL) was added to mixture of **1** (10.9 mg, 0.020 mmol) and IMesCuCl (16.0 mg, 0.040 mmol). After stirring at room temperature for 10 minutes and changing the color of the solution from dark red to yellow, the resulting solution was filtrated. The filtration was concentrated and recrystallized with vapor diffusion method using toluene/pentane to give **3** as yellow crystals (25.6 mg, 97%).

^{1}H NMR (300 MHz, CD_2Cl_2) δ 6.79 (8H, br s, CH of Mes), 6.77 (4H, s, vinyl-H), 6.52 (12H, ArH of Mes and *o*-tolyl), 5.92 (4H, t, $^3J_{HH}$ = 7 Hz, ArH of *o*-tol), 2.33 (12H, s, Me of *o*-tolyl), 1.77 (12H, br s, 2 or 6-Me of Mes), 1.72 (12H, br s, 2 or 6-Me of Mes), 1.55 (12H, s, 4-Me of Mes); ^{13}C{^{1}H} NMR (100 MHz, CD_2Cl_2) δ 181.12 (4°, carbene), 154.95 (br, 4°, C$_{ipso}$ of *o*-tolyl), 139.36 (3°, *o*-tol), 139.22 (4°, C$_{ipso}$ of Me in *o*-tolyl), 138.79 (4°, C$_{ipso}$ of 4-Me in Mes), 135.79 (4°, C$_{ipso}$ of 2,6-Me in Mes), 135.62 (4°, C$_{ipso}$ of 4-Me in Mes), 134.87 (4°, C$_{ipso}$ of Mes), 129.27 (3°, CH of Mes), 128.25 (3°, CH of *o*-tolyl), 123.06 (3°, CH of *o*-tolyl), 122.59 (3°, vinyl), 121.56 (3°, CH of *o*-tolyl), 26.82 (1°, Me of *o*-tolyl), 21.20 (1°, 4-Me of Mes), 18.01 (1°, 2,6-Me of Mes), 17.87 (1°, 2,6-Me of Mes); mp. 185-195 °C. (decomp); Anal. Calc. for $C_{70}H_{76}B_2Cu_2N_4$: C, 74.93; H, 6.83; N, 4.99; Found: C, 75.22; H, 6.65; N, 4.99.

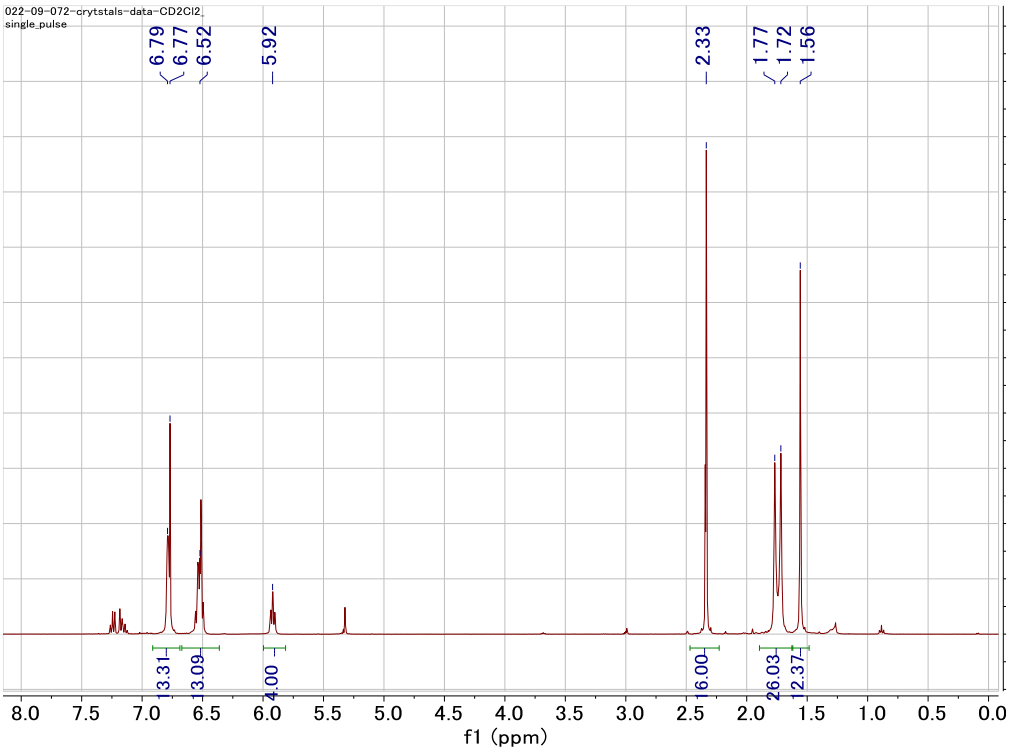

Figure 3.9 The 1H NMR spectrum (CH_2CD_2) of **3**. Toluene is contaminated as a crystal solvent.

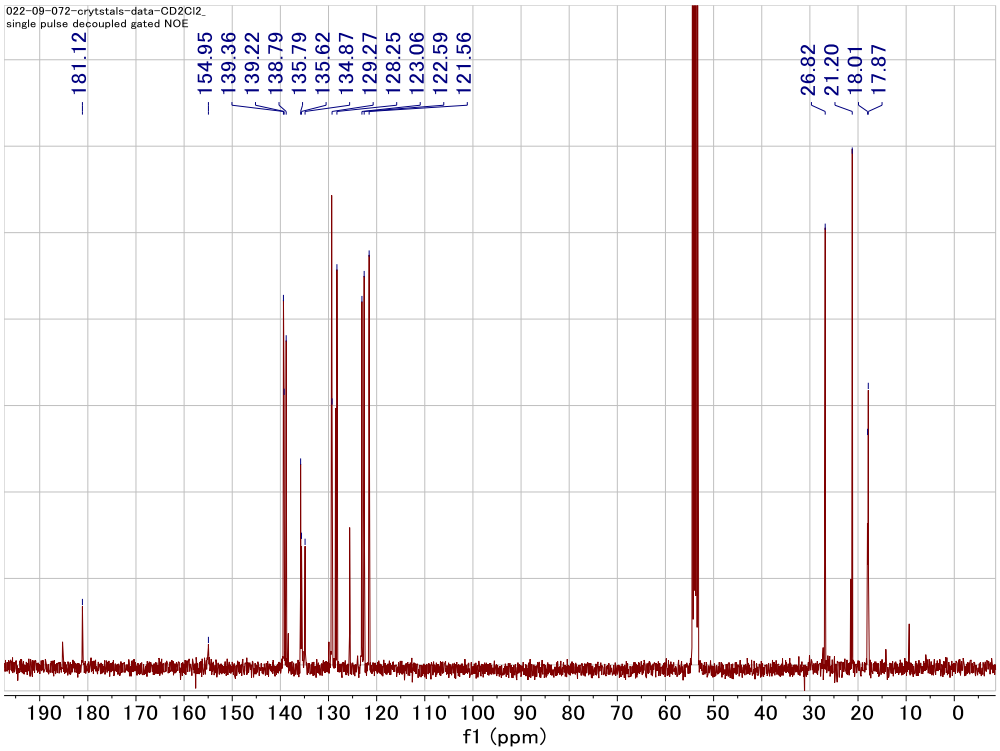

Figure 3.10 The $^{13}C\{^{1}H\}$ NMR spectrum (CH_2CD_2) of **3**. Toluene is contaminated as a crystal solvent.

Synthesis of 4, [CuCNLi(thf)$_3$]$_2$[(B$_2$(o-tol)$_4$)]

A THF solution (1 mL) of 1 (21.9 mg, 0.040 mmol) was dropwised to THF solution (1 mL) of CuCN (7.2 mg, 0.083 mmol) for 1 min. After stirring at room temperature for 2 h, the volatile was evaporated and the residue was washed with toluene (15 mL). The resulting green yellow residue was dissolve in THF and recrystallized with vapor diffusion method using THF/pentane to give **4** as green yellow crystals (5.2 mg, 13% yield).

^{1}H NMR (300 MHz, CD_2Cl_2) δ 6.79 (8H, br s, CH of Mes), 6.77 (4H, s, vinyl-H), 6.52 (12H, ArH of Mes and *o*-tolyl), 5.92 (4H, t, $^{3}J_{HH}$ = 7 Hz, ArH of *o*-tol), 2.33 (12H, s, Me of *o*-tolyl), 1.77 (12H, br s, 2 or 6-Me of Mes), 1.72 (12H, br s, 2 or 6-Me of Mes), 1.55 (12H, s, 4-Me of Mes); $^{13}C\{^{1}H\}$ NMR (100 MHz, CD_2Cl_2) δ 181.12 (4°, carbene), 154.95 (br, 4°, C_{ipso} of *o*-tolyl), 139.36 (3°, *o*-tol), 139.22 (4°, C_{ipso} of Me in *o*-tolyl), 138.79 (4°, C_{ipso} of 4-Me in Mes), 135.79 (4°, C_{ipso} of 2,6-Me in Mes), 135.62 (4°, C_{ipso} of 4-Me in Mes), 134.87 (4°, C_{ipso} of Mes), 129.27 (3°, CH of Mes), 128.25 (3°, CH of *o*-tolyl), 123.06 (3°, CH of *o*-tolyl), 122.59 (3°, vinyl), 121.56 (3°, CH of *o*-tolyl), 26.82 (1°, Me of *o*-tolyl), 21.20 (1°, 4-Me of Mes), 18.01 (1°, 2,6-Me of Mes), 17.87 (1°, 2,6-Me of Mes); mp. 185-195 °C. (decomp); Anal. Calc. for $C_{70}H_{76}B_2Cu_2N_4$: C, 74.93; H, 6.83; N, 4.99; Found: C, 75.22; H, 6.65; N, 4.99.

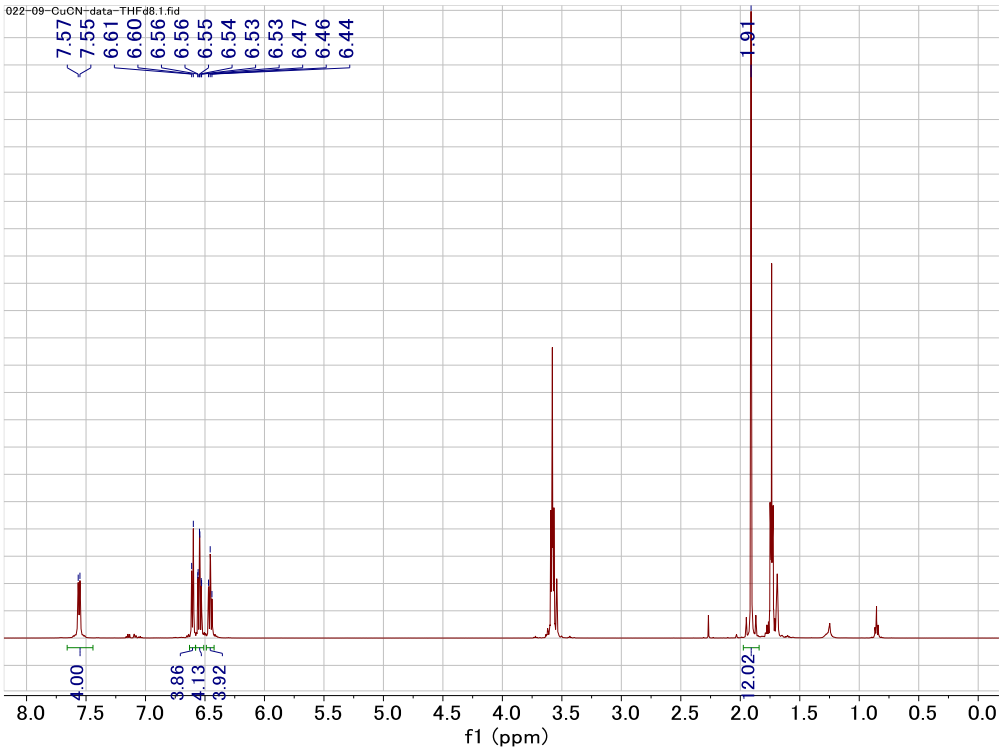

Figure 3.11 The ^{1}H NMR spectrum (THF-d_8) of **4**.

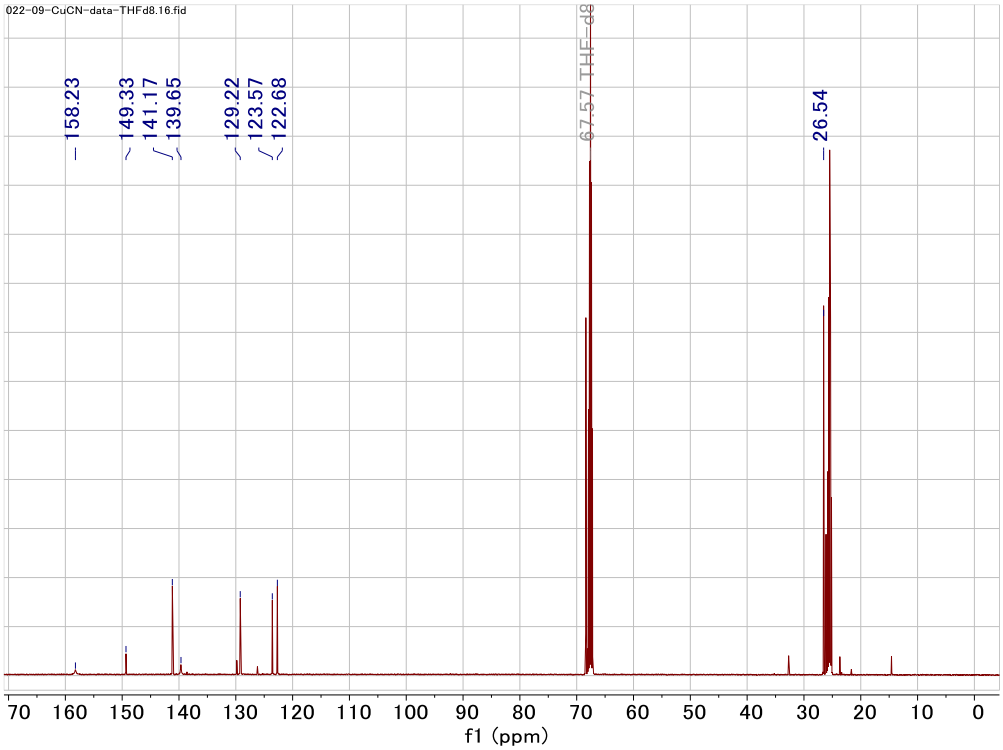

Figure 3.12 The ^{13}C{^{1}H} NMR spectrum (THF-d_8) of **4**

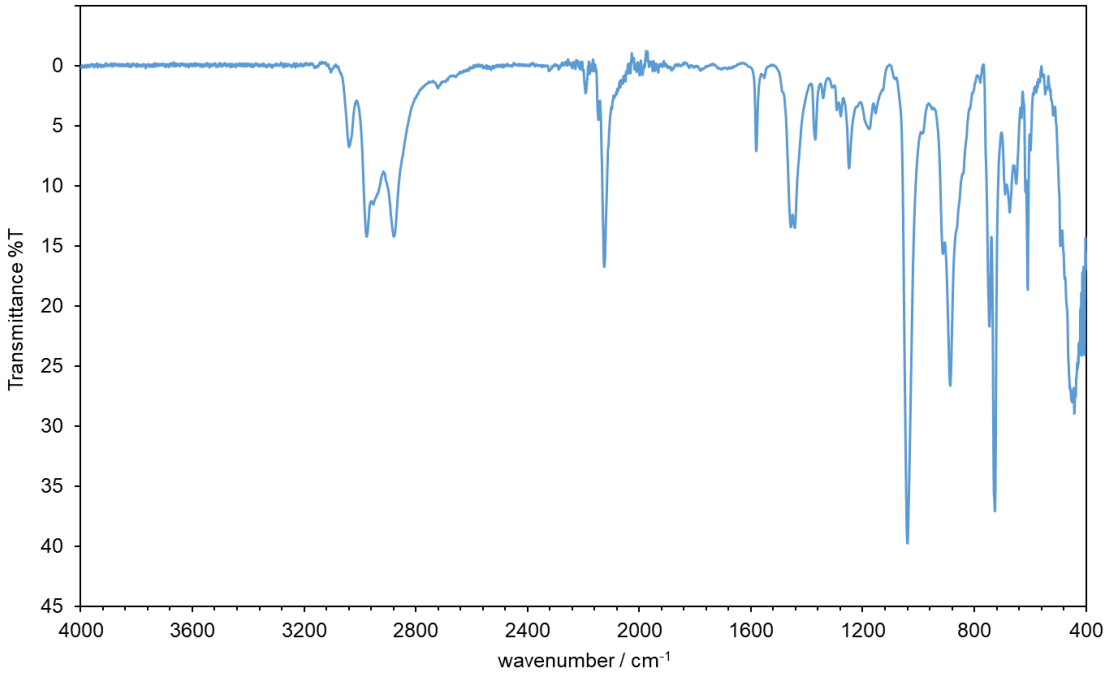

Figure 3.13 ATR-IR spectra of compound **4** (solid state).

X-ray Crystallographic Analysis

Details of the crystal data and a summary of the intensity data collection parameters for **2**, **3**, **4** are listed in Table S1. The crystals were coated with mineral oil and put on a MicroMount™ (MiTeGen, LLC), and then mounted on diffractometer. Diffraction data were collected on a Bruker Photon or Rigaku HyPix-6000 detectors using Mo$K\alpha$ radiation. The Bragg spots were integrated using CrysAlisPro program package.[15] Absorption corrections were applied. All the following procedure for analysis, Yadokari-XG 2009 was used as a graphical interface.[16] The structure was solved by a direct method with programs of SHELXT and refined by a full-matrix least squares method with the program of SHELXL-2016.[17] Anisotropic temperature factors were applied to all non-hydrogen atoms. The hydrogen atoms were put at calculated positions, and refined applying riding models. The detailed crystallographic data have been deposited with the Cambridge Crystallographic Data Centre: Deposition code CCDC 1975020 (**2**), CCDC 1975021 (**3**), CCDC 1975022 (**4**). A copy of the data can be obtained free of charge via http://www.ccdc.cam.ac.uk/products/csd/request.

Table 3.2 Crystallographic data for **2**, **3**, **4**

	2	**3**	**4**
CCDC #	1975020	1975021	1975022
formula	$C_{59}H_{74}B_2CuLi$	$C_{91}H_{99.5}B_2Cu$	$C_{54}H_{76}B_2Cu_2Li_2$
formula	919.30	1398.04	1011.74
T / K	93	93	93
color	Red	Yellow	Yellow
size / mm	0.33×0.19×0.1	0.25×0.15×0.	0.20×0.14×0.08
crystal	*Triclinic*	*Triclinic*	*Triclinic*
space group	$P\bar{1}$ (#2)	$P\bar{1}$ (#2)	$P\bar{1}$ (#2)
a / Å	11.244(5)	15.2253(5)	11.4670(7)
b / Å	14.932(5)	15.3553(3)	11.7312(7)
c / Å	16.355(5)	17.9283(4)	20.5771(13)
α / °	82.405(5)	75.464(2)	98.763(5)
β / °	73.397(5)	71.410(2)	91.285(5)
γ / °	79.170(5)	75.399(2)	102.150(5)
V / Å^3	2575.6(16)	3777.34(18)	2670.2(3)
Z	2	4	2
D_{calc} / g cm^{-3}	1.185	1.229	1.258
μ / mm^{-1}	0.465	0.612	0.845
F(000)	984	1483	1072
θ range / °	1.914 to	1.611 to	1.9730 to
reflns	19375	27800	20720
Indep reflns	9298	13471	10371
param	645	937	698
GOF on F^2	1.050	1.068	1.041
R_1 [$I >$	0.0646	0.0460	0.0455
wR_2 [$I >$	0.1717	0.1281	0.1165
R_1 (all data)[a]	0.0896	0.0559	0.0592
wR_2 (all	0.2039	0.1450	0.1324
$\Delta\rho_{min,\ max}$ / e	−0.849, 0.845	−0.496,	−0.831, 0.673

[a] $R_1 = \Sigma \, ||Fo| - |Fc|| \, / \, \Sigma \, |Fo|$, [b] $wR_2 = [\Sigma \, \{w(Fo^2 - Fc^2)^2 / \, \Sigma \, w(Fo^2)^2\}]^{1/2}$

3. UV-Vis Absorption and Emission Spectra

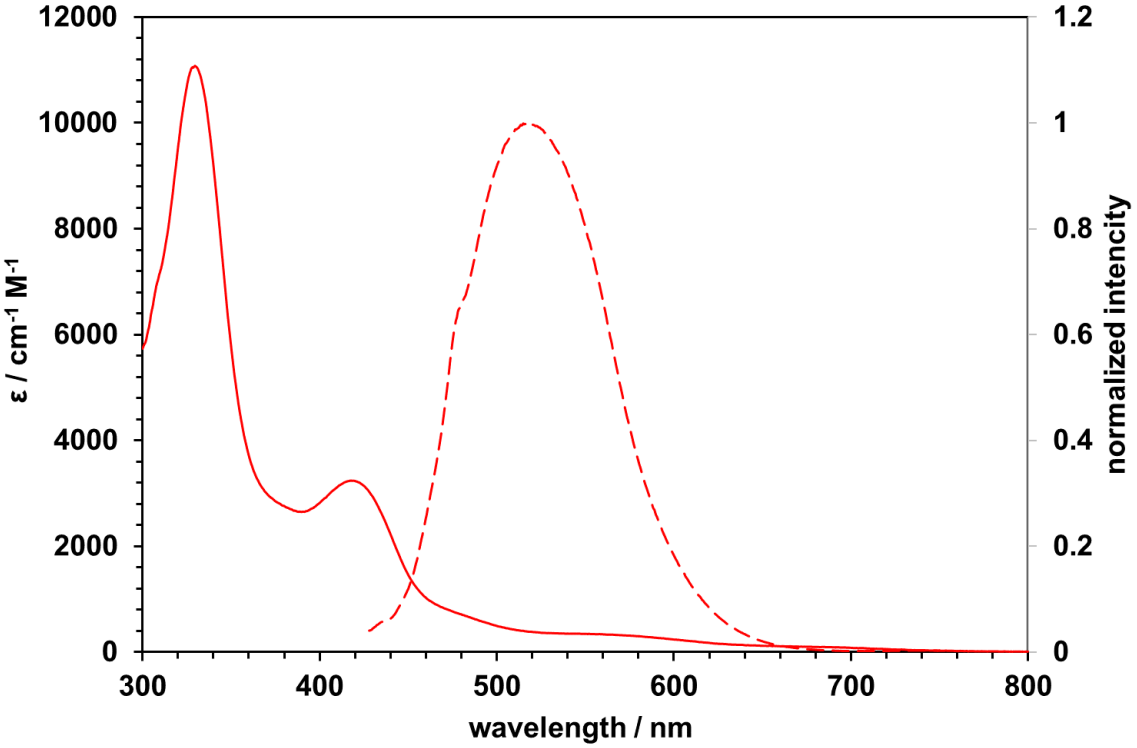

Figure 3.14 UV-Vis absorption spectrum [solid line, λ_{max} = 330 nm ($\varepsilon = 1.1\times10^4$ cm^{-1} M^{-1}), λ_{max} = 418 nm ($\varepsilon = 3.2\times10^3$ cm^{-1} M^{-1})] and emission spectrum (dashed line, λ_{em} = 517 nm, λ_{ex} = 418 nm) of **2** in toluene solution.

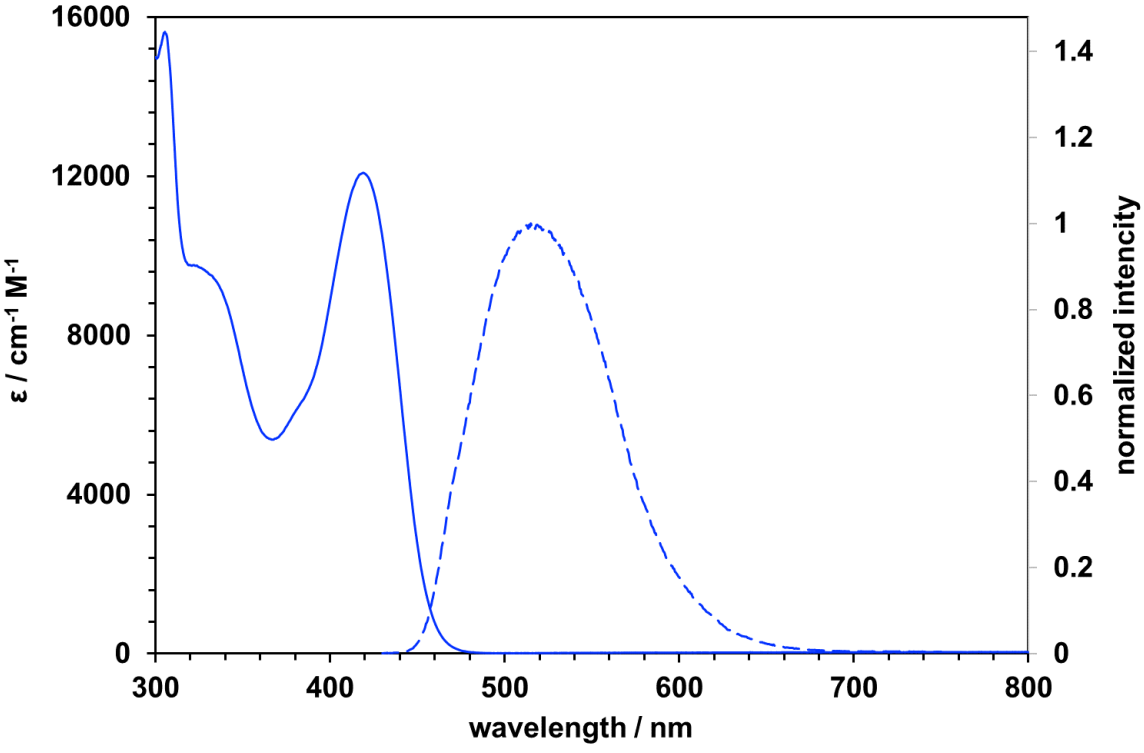

Figure 3.15 UV-Vis absorption spectrum [solid line, λ_{max} = 329 nm ($\varepsilon = 9.6\times10^3$ cm^{-1} M^{-1}), λ_{max} = 419

nm (ε = 1.2×10^4 cm^{-1} M^{-1})] and emission spectrum (dashed line, λ_{em} = 515 nm, λ_{ex} = 420 nm) of **3** in toluene solution.

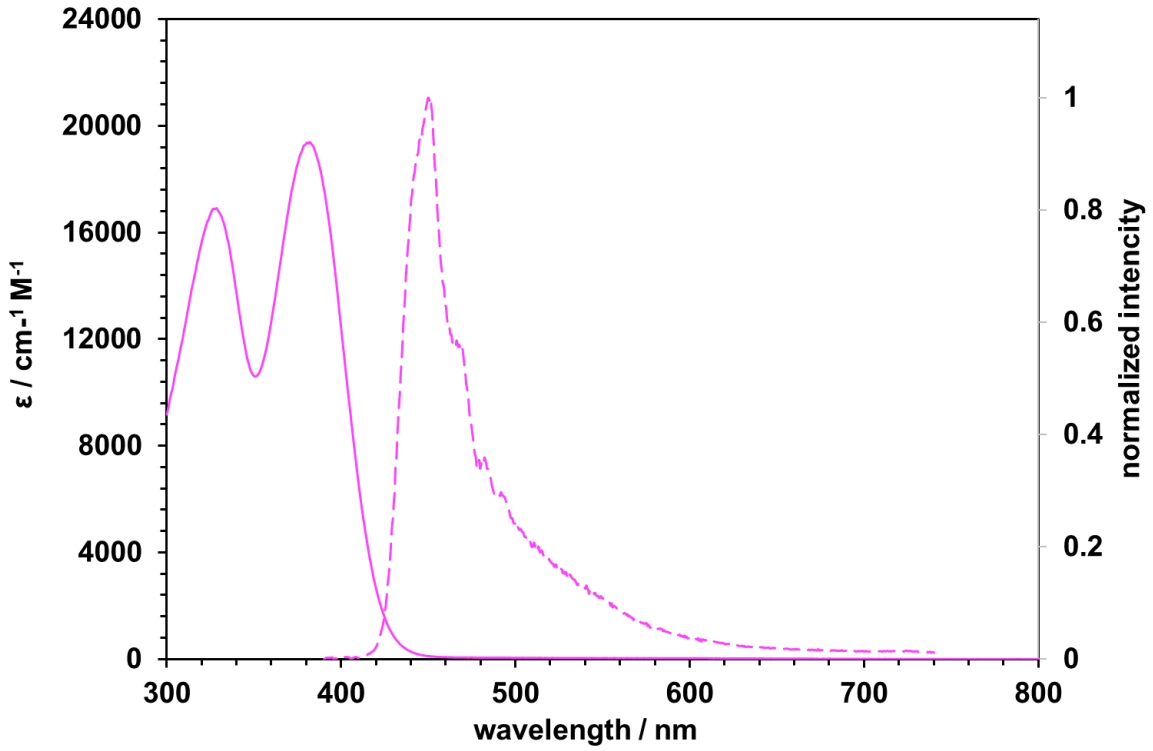

Figure 3.16 UV-Vis absorption spectrum [solid line, λ_{max} = 329 nm (ε = 1.7×10^4 cm^{-1} M^{-1}), λ_{max} = 382 nm (ε = 1.9×10^4 cm^{-1} M^{-1})] and emission spectrum (dashed line, λ_{em} = 451 nm, λ_{ex} = 380 nm) of **4** in THF solution.

XANES spectra

CuCl (Wako), $CuCl_2$ (Wako), and CuCN (TCI) were purchased and used without purification. Appropriated amounts of samples of were diluted with boron nitride, and were packed in a cell (diameter: 4 mmφ) without exposure to air. Cu K-edge XANES spectra were measured in transmission mode at the BL12C station of the Photon Factory at KEK-IMSS (Tsukuba, Japan). The energy current of electrons in the storage ring were 2.5 GeV and 450 mA, respectively. X-rays from the storage ring were monochromatized using a Si(111) double-crystal monochromator, and ionization chambers filled with pure N_2 and N_2/Ar (85/15) gases were used to monitor the incident and transmitted X-rays, respectively. All samples were measured at 298 K. Cu K-edge XANES spectra were analyzed using ATHENA[18] using IFEFFIT (ver. 1.2.11). Threshold energy was tentatively set at the local maximum of the pre-edge peak of Cu K-edge XANES (8980.3 eV for Cu^0 powder),[19] and background was subtracted by the Autobk method.[20]

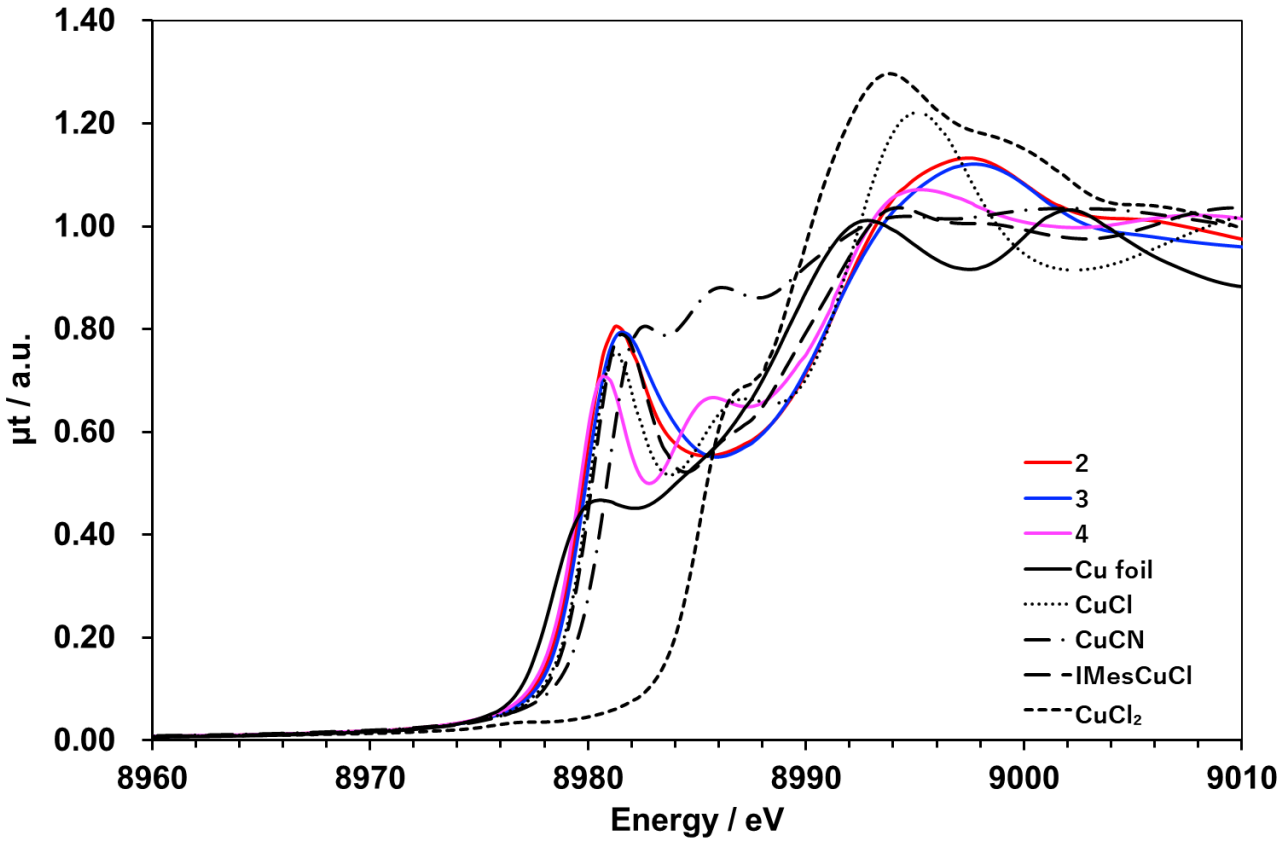

Figure 3.17 XAFS spectra of **2**-**4** and reference compounds.

Theoretical Calculations

DFT calculations were performed by using Gaussian 16, Revision B.01 program package.[21] The geometry optimizations of **2**, **2'**, **3**, **4**, **5** were performed at the B3PW91[22]/Def2SVP[23] level of theory. TD-DFT analysis was conducted with cam-B3LYP[24]/Def2SVP level of theory for optimized structures. The Wiberg bond index (WBI) and natural population analysis (NPA) charge distribution were calculated by natural bond orbital (NBO 6.0) method.[25] Illustrations of NBO are performed by Jmol-NBO Visualization Helper v2.1 and Jmol.

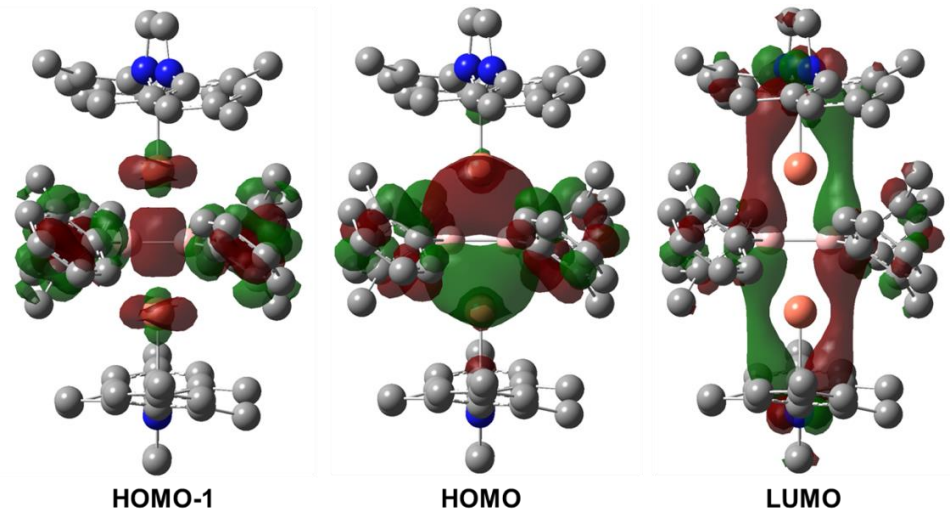

Figure 3.18 Molecular orbitals of compound **3**

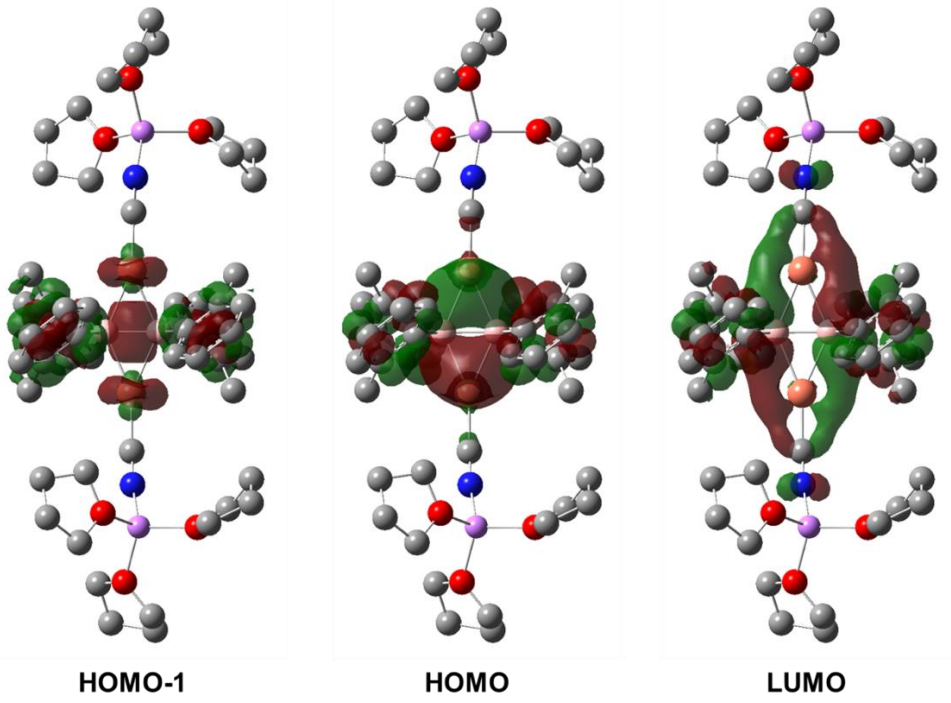

Figure 3.19 Molecular orbitals of compound **4**

Table 3.3 Comparison with optimized structures of crystal structures of **2**, **3**, **4**

compound 2	B1–B2	B1–Cu1	B2–Cu1	B1…Li1	B2…Li1	Cu1–C29
crystal structure	1.685(6)	2.221(5)	2.231(5)	2.27(1)	2.36(1)	1.927(4)
optimized structure	1.6846	2.1678	2.2708	2.2918	2.3618	1.9805

compound 3	B1–B2	B1–Cu1	B2–Cu1	B1–Cu2	B2–Cu2	Cu1–C29	Cu2–C50
crystal structure	1.719(4)	2.178(2)	2.189(3)	2.189(3)	2.186(2)	1.946(2)	1.946(3)
optimized structure	1.7321	2.2218	2.2154	2.2161	2.2234	1.9914	1.9935

compound 4	B1–B2	B1–Cu1	B2–Cu1	B1–Cu2	B2–Cu2	Cu1–C1	Cu2–C2
crystal structure	1.726(4)	2.171(3)	2.135(3)	2.154(3)	2.142(3)	1.897(3)	1.894(3)
optimized structure	1.7293	2.1736	2.1681	2.1868	2.1551	1.9149	1.9153

	C1–N1	N2–C2
crystal structure	1.148(4)	1.153(4)
optimized structure	1.1706	1.1704

Table 3.4 Assignment of main transition mode and predicted spectrum of neutral complex **2** by TD-DFT calculation (nstates = 10)

energy	f	energy	f
2.93 eV 423 nm	0.1712	4.12 eV 301 nm	0.1381
excited state	transition prob.	excited state	transition prob.
HOMO → LUMO	86%	HOMO-7 → LUMO	4%
HOMO → LUMO+1	5%	HOMO-4 → LUMO	3%
HOMO → LUMO+2	4%	HOMO-1 → LUMO	21%
		HOMO → LUMO+3	14%
		HOMO → LUMO+6	4%
		HOMO → LUMO+7	13%
		HOMO → LUMO+9	20%
		HOMO → LUMO+10	6%

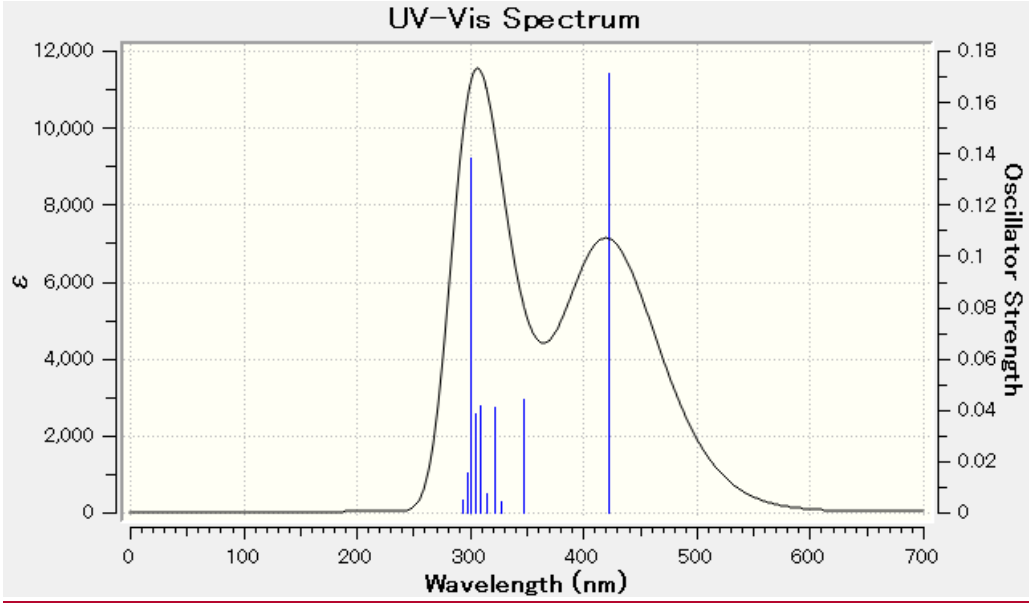

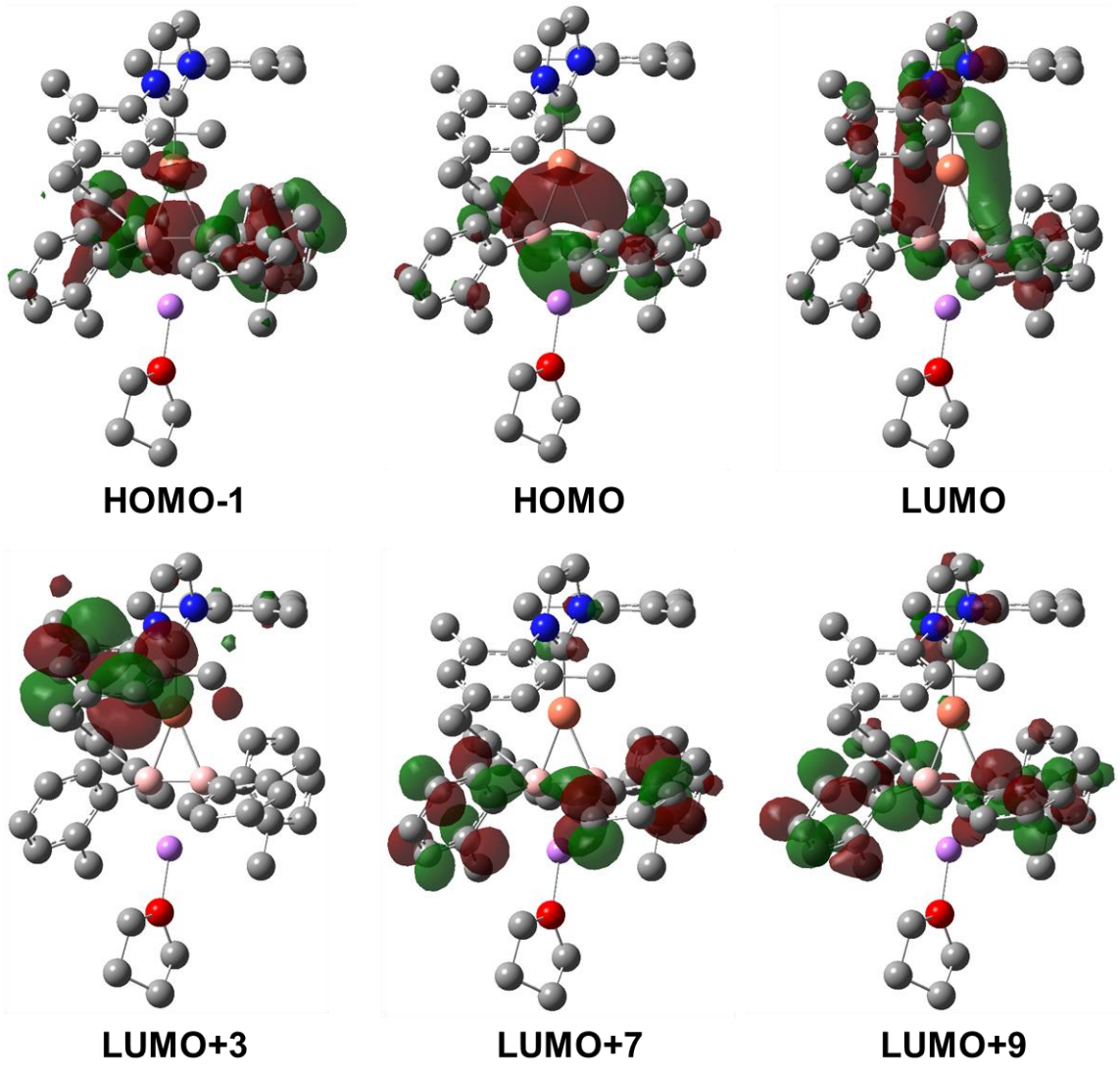

Figure 3.20 Molecular orbitals mainly (>10%) related to calculated transitions of neutral complex **2**

Table 3.5 Assignment of main transition mode and predicted spectrum of anionic complex **2'** by TD-DFT calculation (nstates = 10)

energy	f	energy	f	energy	f
2.08 eV 597 nm	0.0361	3.19 eV 389 nm	0.1045	3.47 eV 357 nm	0.2039
excited state	transition prob.	excited state	transition prob.	excited state	transition prob.
HOMO → LUMO+1	42%	HOMO-1 → LUMO+4	3%	HOMO → LUMO+8	90%
HOMO → LUMO+3	13%	HOMO → LUMO+6	86%	HOMO → LUMO+10	5%
HOMO → LUMO+4	42%	HOMO → LUMO+8	2%		

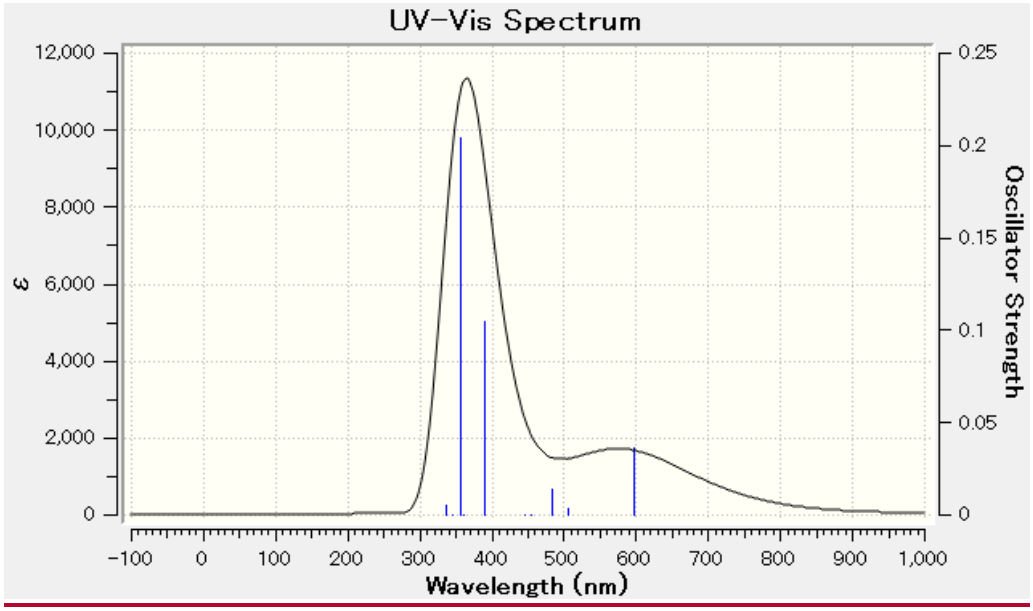

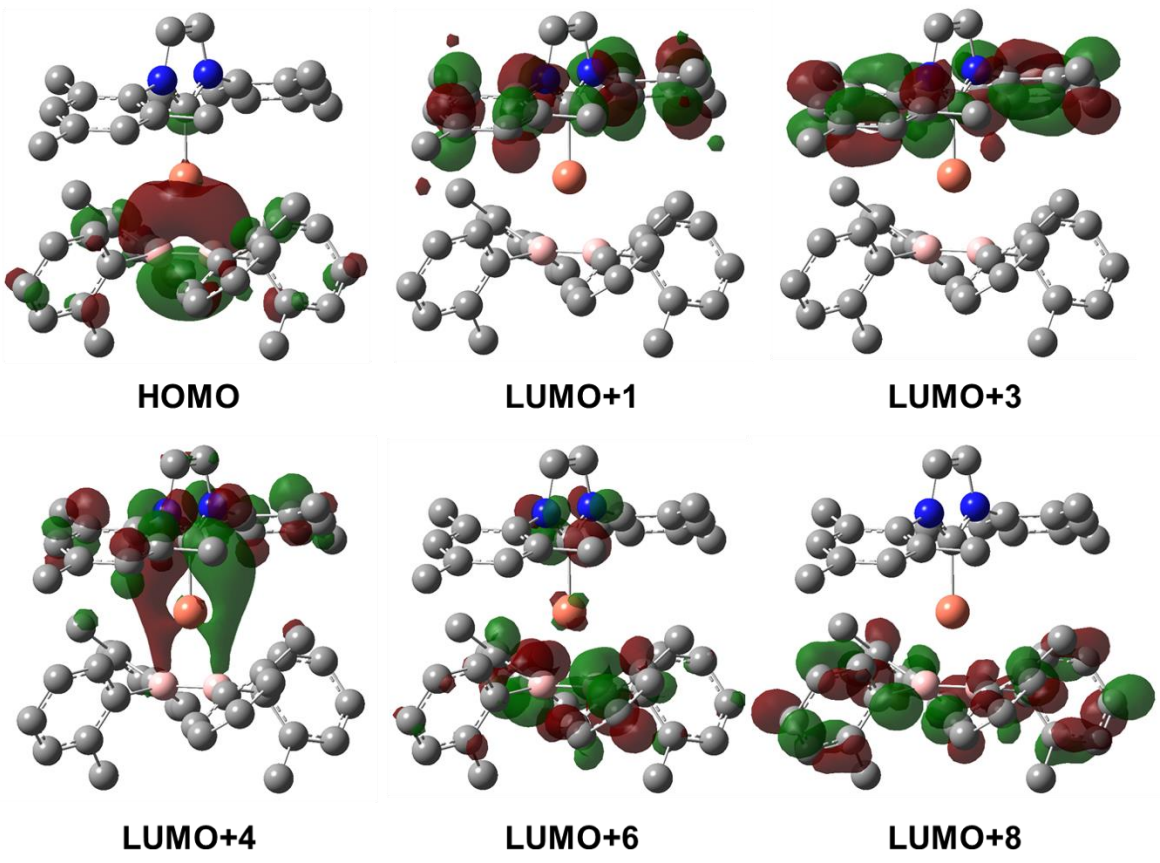

Figure 3.21 Molecular orbitals mainly (>10%) related to calculated transitions of anionic complex **2'**.

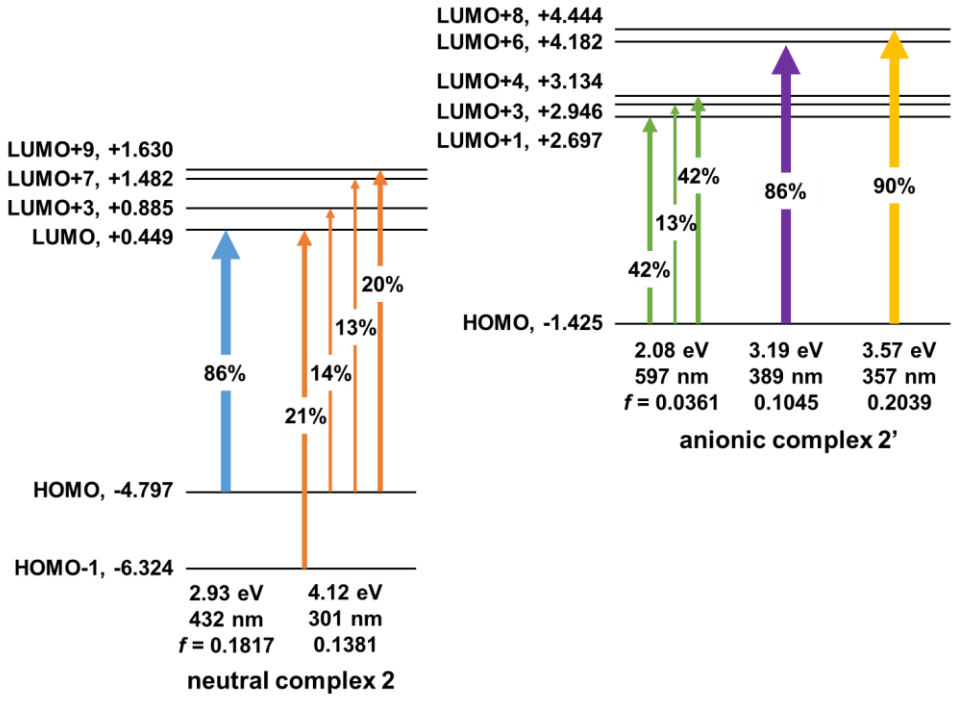

Figure 3.22 Illustration of level of MOs and each transition modes of neutral **2** and anionic complex **2'**.

Table 3.6 Assignment of main transition mode and predicted spectrum of compound **3** by TD-DFT calculation (nstates = 10)

energy	f
3.25 eV 382 nm	0.1677
excited state	transition prob.
HOMO → LUMO	91%
HOMO → LUMO+8	2%

energy	f
3.72 eV 333 nm	0.034
excited state	transition prob.
HOMO-1 → LUMO	6%
HOMO → LUMO+1	15%
HOMO → LUMO+2	30%
HOMO → LUMO+3	3%
HOMO → LUMO+5	17%
HOMO → LUMO+9	21%

energy	f
4.16 eV 298 nm	0.0178
excited state	transition prob.
HOMO-1 → LUMO	5%
HOMO → LUMO+1	21%
HOMO → LUMO+5	30%
HOMO → LUMO+8	3%
HOMO → LUMO+9	4%
HOMO → LUMO+10	17%
HOMO → LUMO+13	3%

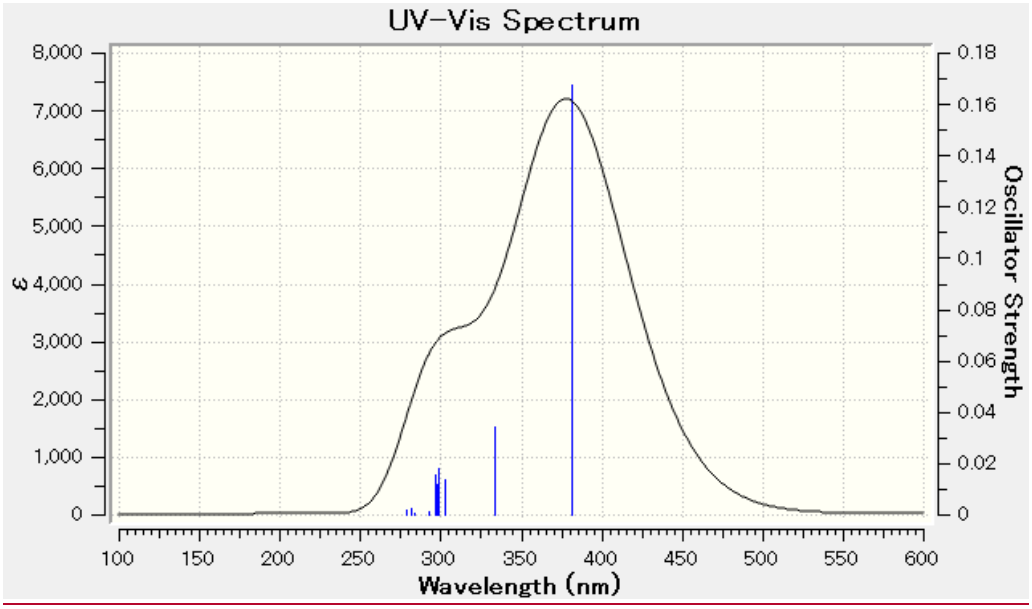

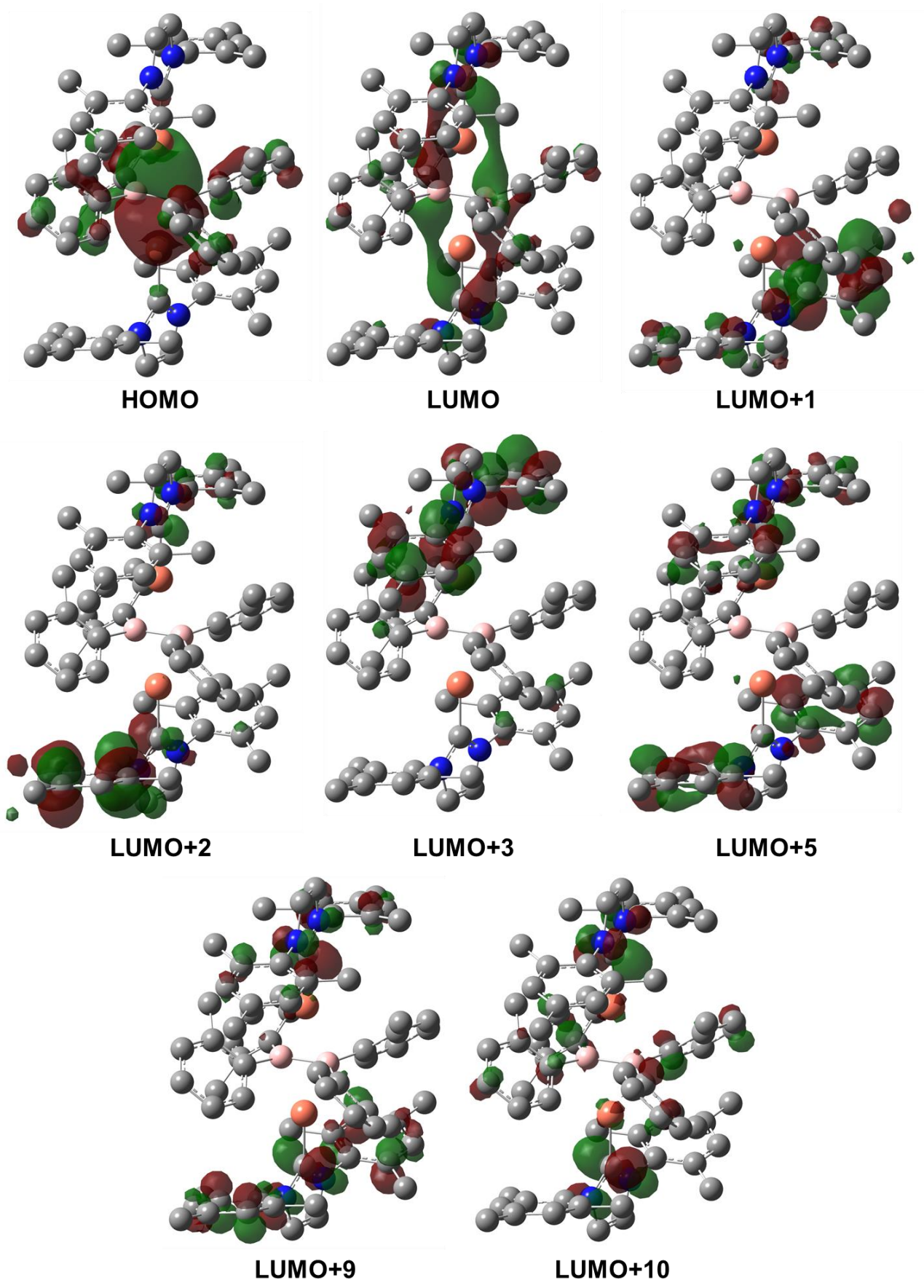

Figure 3.23 Molecular orbitals mainly (>10%) related to calculated transitions of compound **3**

Table 3.7 Assignment of main transition mode and predicted spectrum of compound **4** by TD-DFT calculation (nstates = 10)

energy	f	energy	f	energy	f
3.47 eV 357 nm	0.2957	4.15eV 299 nm	0.1553	4.79 eV 259 nm	0.0582
excited state	transition prob.	excited state	transition prob.	excited state	transition prob.
HOMO → LUMO+2	95%	HOMO-8 → LUMO+2	2%	HOMO → LUMO+5	3%
		HOMO-1 → LUMO+2	51%	HOMO → LUMO+10	16%
		HOMO → LUMO+3	35%	HOMO → LUMO+11	57%

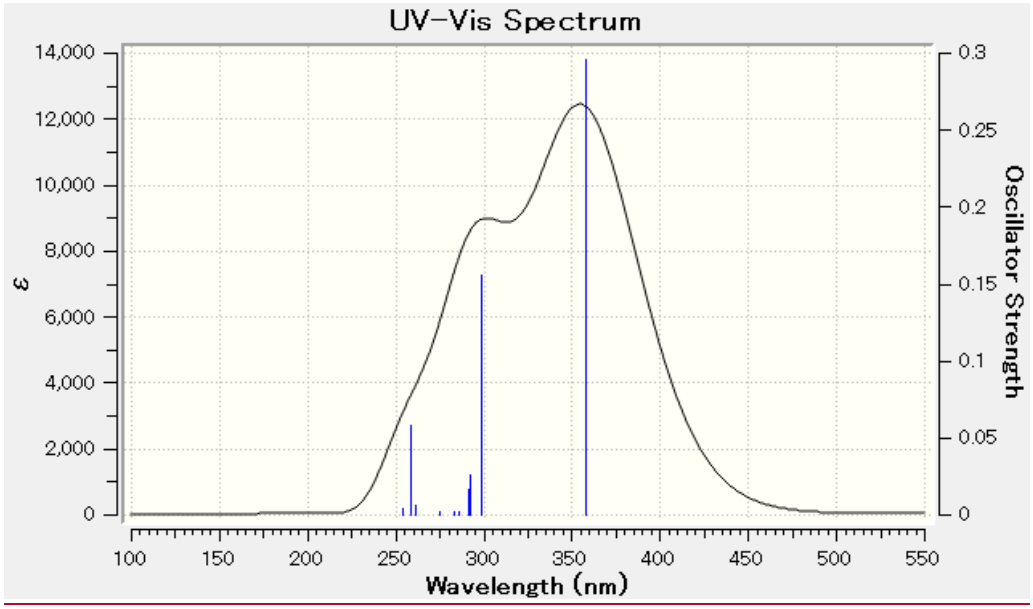

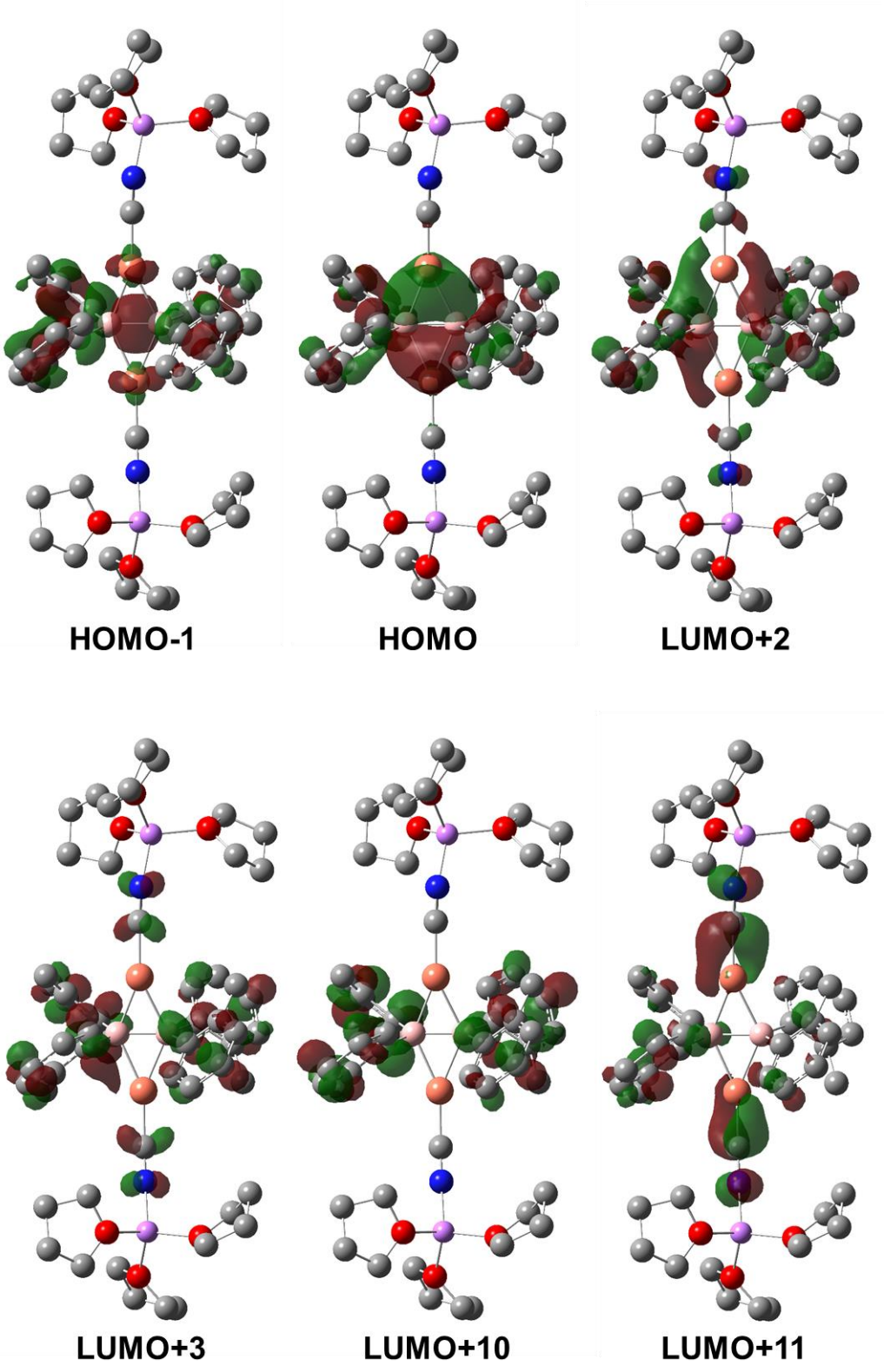

Figure 3.24 Molecular orbitals mainly (>10%) related to calculated transitions of compound **4**

Table 3.8 Selected second order perturbation energies $E^{(2)}$ in NBO analysis of compound **3**

donor NBOs	accecpter NBOs	$E^{(2)}_{ij}$ / kcal mol^{-1}
109, σ(B-B)	297, vacant d(Cu)	17.84
109, σ(B-B)	298, vacant d(Cu)	17.83
110, π(B=B)	297, vacant d(Cu)	31.58
110, π(B=B)	298, vacant d(Cu)	32.22
99, occupied d(Cu)	300, π*(B=B)	6.72
104, occupied d(Cu)	300, π*(B=B)	6.93

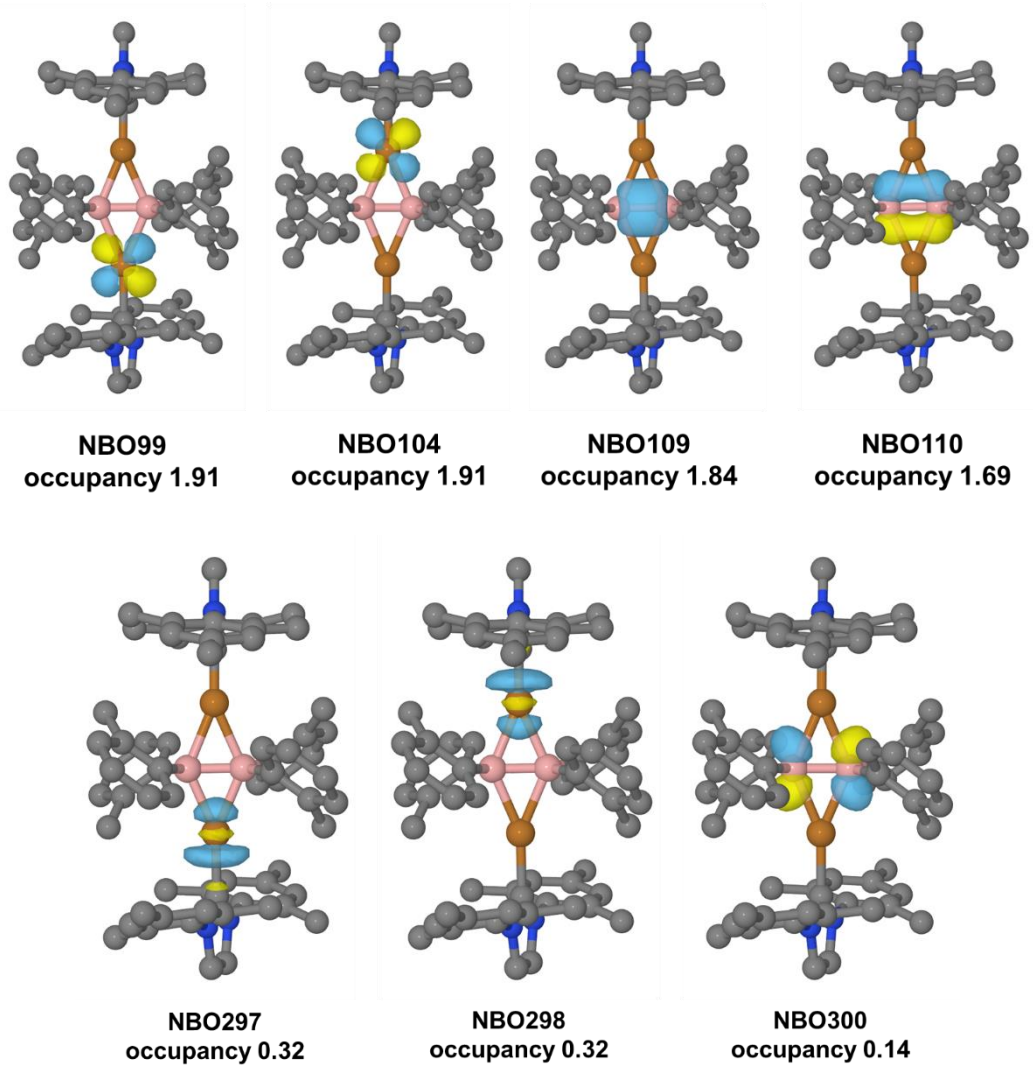

Figure 3.25 NBOs related to the donor-acceptor interaction in **3** summarized in Table S8.

Table 3.9 Selected second order perturbation energies $E^{(2)}$ in NBO analysis of compound **4**

donor NBOs	accecpter NBOs	$E^{(2)}_{ij}$ / kcal mol^{-1}
111, σ(B-B)	269, vacant d(Cu)	20.35
111, σ(B-B)	270, vacant d(Cu)	20.39
112, π(B=B)	269, vacant d(Cu)	43.26
112, π(B=B)	270, vacant d(Cu)	42.86
89, occupied d(Cu)	274, π*(B=B)	7.55
94, occupied d(Cu)	274, π*(B=B)	7.58
88, occupied d(Cu)	280, π*(C≡N)	4.69
89, occupied d(Cu)	281, π*(C≡N)	6.05
93, occupied d(Cu)	283, π*(C≡N)	3.29
94, occupied d(Cu)	284, π*(C≡N)	5.60

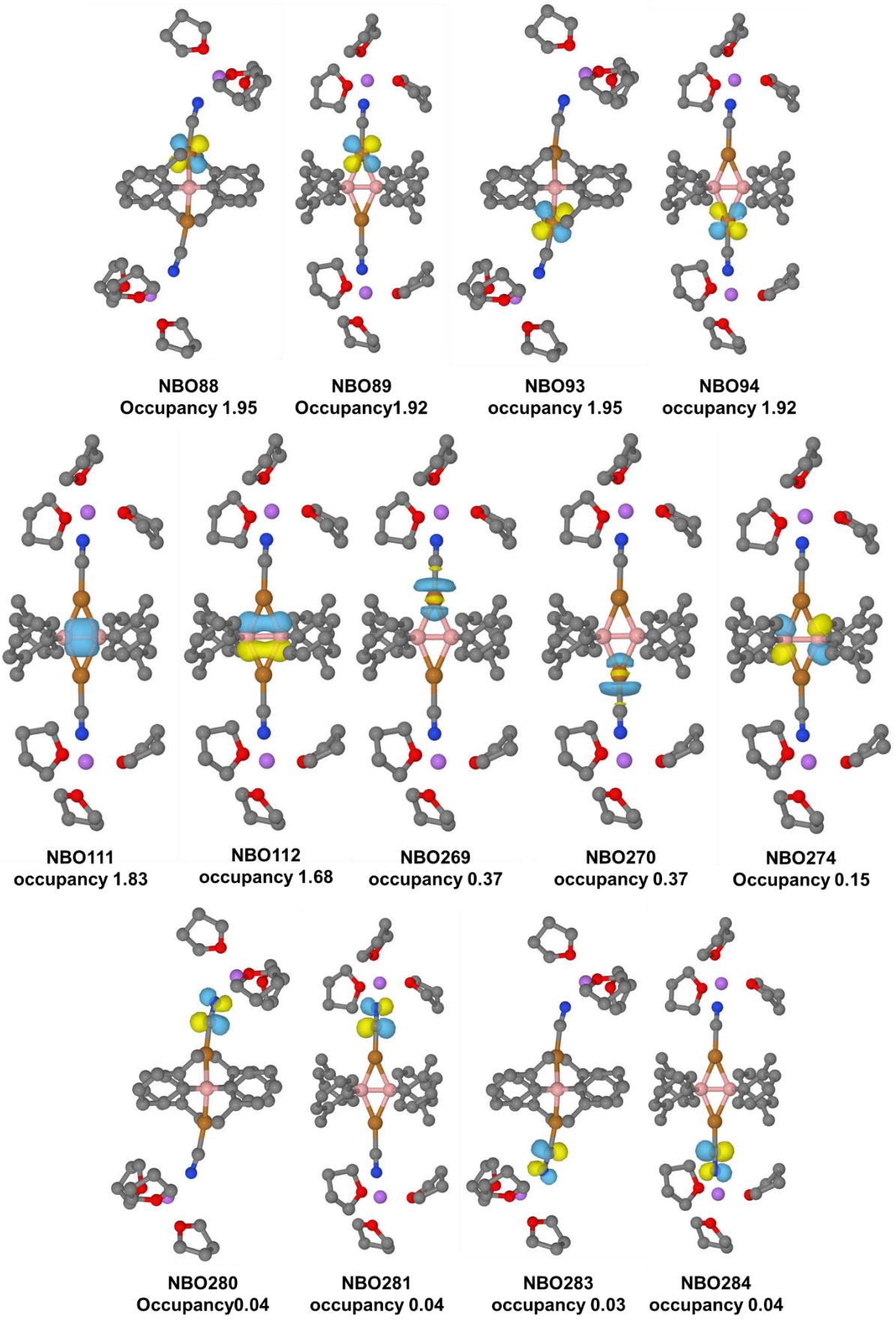

Figure 3.26 NBOs related to the donor-acceptor interaction in **4** summarized in Table S9.

Table 3.10 Selected second order perturbation energies $E^{(2)}$ in NBO analysis of model complex **5**

donor NBOs	accecpter NBOs	$E^{(2)}_{ij}$ / kcal mol^{-1}
39, occipied d(Cu)	107, π*(C=C)	19.27
43, π(C=C)	105, vacant d(Cu)	49.40

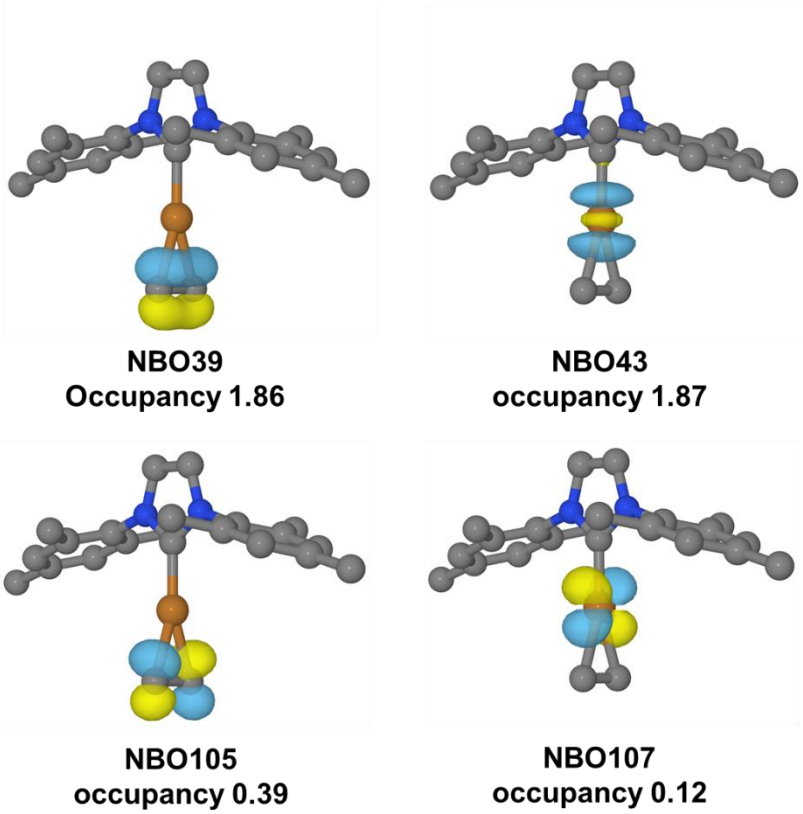

Figure 3.27 NBOs related to the donor-acceptor interaction in **5** summarized in Table S10.

3.6. References

[2] Arrowsmith, H.; Braunschweig, H.; Stennett, T. E. *Angew. Chem. Int. Ed.* **2017**, *56*, 96.

[3] (a) H. Braunschweig, A. Damme, Dewhurst, R. D.; Vargas, A. *Nat. Chem.* **2013**, *5*, 115.
(b) Arnold, N.; Braunschweig, H.; Dewhurst, R. D.; Ewing, W. C. *J. Am. Chem. Soc.* **2016**, *138*, 76.
(c) Bissinger, P.; Braunschweig, H.; Damme, A.; Kupfer, T.; Vargas, A. *Angew. Chem. Int. Ed.* **2012**, *51*, 9931.
(d) Bissinger, P.; Steffen, A.; Vargas, A.; Dewhurst, R. D.; Damme, A.; Braunschweig, H. *Angew. Chem. Int. Ed.* **2015**, *54*, 4362.
(e) Rixin Wang, S.; Arrowsmith, M.; Braunschweig, H.; Dewhurst, R. D.; Paprocki, V.; Winner, L. *Chem. Commun.* **2017**, *53*, 11945.

(f) Wang, S. R.; Arrowsmith, M.; Braunschweig, H.; Dewhurst, R. D.; Dömling, M.; Mattock, J. D.; Pranckevicius, C.; Vargas, A. *J. Am. Chem. Soc*. **2017**, *139*, 10661.
(g) Lu, W.; Kinjo, R. *Chem. Commun.* **2018**, *54*, 8842.
(h) Lu, W.; Kinjo, R. *Chem. Eur. J.* **2018**, *24*, 15656.

[4] Braunschweig, H.; Dellermann, T.; Dewhurst, R. D.; Hupp, B.; Kramer, T.; Mattock, J. D.; Mies, J.; Phukan, A. K.; Steffen, A.; Vargas, A. *J. Am. Chem. Soc.* **2017**, *139*, 4887.

[5] Braunschweig, H.; Dewhurst, R. D.; Jiménez-Halla, J. O. C.; Matito, E.; Muessig, J. H. *Angew. Chem. Int. Ed.* **2018**, *57*, 412.

[6] Mondal, B.; Bag, R.; Ghorai, S.; Bakthavachalam, K.; Jemmis, E. D.; Ghosh, S. *Angew. Chem. Int. Ed.* **2018**, *57*, 8079.

[7] Bertermann, R.; Braunschweig, H.; Constantinidis, P.; Dellermann, T.; Dewhurst, R. D.; Ewing, W. C.; Fischer, I.; Kramer, T.; Mies, J.; Phukan, A. K.; Vargas, A. *Angew. Chem. Int. Ed.* **2015**, *54*, 13090.

[8] Wang, S. R.; Prieschl, D.; Mattock, J. D.; Arrowsmith, M.; Pranckevicius, C.; Stennett, T. E.; Dewhurst, R. D.; Vargas, A.; Braunschweig, H. *Angew. Chem. Int. Ed.* **2018**, *57*, 6347.

[9] Hari Krishna Reddy, K.; Jemmis, E. D. *Dalton Trans.* **2013**, *42*, 10633.

[10] Akiyama, S.; Yamada, K.; Yamashita, M. *Angew. Chem. Int. Ed.* **2019**, *58*, 11806.

[11] Okuno, Y.; Yamashita, M.; Nozaki, K. *Angew. Chem. Int. Ed.* **2011**, *50*, 920.

[12] Segawa, Y.; Yamashita, M.; Nozaki, K. *Angew. Chem. Int. Ed.* **2007**, *46*, 6710.

[13] (a) Laitar, D. S.; Mueller, P.; Sadighi, J. P. *J. Am. Chem. Soc.* **2005**, *127*, 17196.
(b) Kajiwara, T.; Terabayashi, T.; Yamashita, M.; Nozaki, K. *Angew. Chem. Int. Ed.* **2008**, *47*, 6606.

[14] Latendorf, K.; Mechler, M.; Schamne, I.; Mack, D.; Frey, W.; Peters, R. *Eur. J. Org. Chem.* **2017,** *2017*, 4140

[15] CrysAlisPRO *CrysAlisPRO*, Oxford Diffraction/Agilent Technologies UK Ltd: Yarnton, England, **2015**.

[16] Kabuto, C.; Akine, S.; Kwon, E. Release of Software (Yadokari-XG 2009) for Crystal Structure Analyses. *J. Cryst. Soc. Jpn.* **2009,** *51*, 218.

[17] (a) Sheldrick, G. A short history of SHELX. *Act. Cryst. Sec. A* **2008,** *64*, 112.
(b) Sheldrick, G. Crystal structure refinement with SHELXL. *Act. Cryst. Sec. C* **2015,** *71*, 3.

[18] (a) Ravel, B.; Newville, M. ATHENA, ARTEMIS, HEPHAESTUS: data analysis for X-ray absorption spectroscopy using IFEFFIT. *J. Synchrotron Rad.* **2005,** *12*, 537.
(b) Newville, M.; Ravel, B.; Haskel, D.; Rehr, J. J.; Stern, E. A.; Yacoby, Y. Analysis of multiple-scattering XAFS data using theoretical standards. *Physica B* **1995,** *208-209*, 154.

[19] Bearden, J. A.; Burr, A. F. *Rev. Mod. Phys.* **1967,** *39*, 125.

[20] (a) Newville, M. IFEFFIT : interactive XAFS analysis and FEFF fitting. *J. Synchrotron Rad.* **2001,** *8*, 322.
(b) Newville, M.; Līviņš, P.; Yacoby, Y.; Rehr, J. J.; Stern, E. A. Near-edge x-ray-absorption fine

structure of Pb: A comparison of theory and experiment. *Phys. Rev. B* **1993,** *47*, 14126 .

[21] Frisch, M. J.; Trucks, G. W.; Schlegel, H. B.; Scuseria, G. E.; Robb, M. A.; Cheeseman, J. R.; Scalmani, G.; Barone, V.; Petersson, G. A.; Nakatsuji, H.; Li, X.; Caricato, M.; Marenich, A. V.; Bloino, J.; Janesko, B. G.; Gomperts, R.; Mennucci, B.; Hratchian, H. P.; Ortiz, J. V.; Izmaylov, A. F.; Sonnenberg, J. L.; Williams; Ding, F.; Lipparini, F.; Egidi, F.; Goings, J.; Peng, B.; Petrone, A.; Henderson, T.; Ranasinghe, D.; Zakrzewski, V. G.; Gao, J.; Rega, N.; Zheng, G.; Liang, W.; Hada, M.; Ehara, M.; Toyota, K.; Fukuda, R.; Hasegawa, J.; Ishida, M.; Nakajima, T.; Honda, Y.; Kitao, O.; Nakai, H.; Vreven, T.; Throssell, K.; Montgomery Jr., J. A.; Peralta, J. E.; Ogliaro, F.; Bearpark, M. J.; Heyd, J. J.; Brothers, E. N.; Kudin, K. N.; Staroverov, V. N.; Keith, T. A.; Kobayashi, R.; Normand, J.; Raghavachari, K.; Rendell, A. P.; Burant, J. C.; Iyengar, S. S.; Tomasi, J.; Cossi, M.; Millam, J. M.; Klene, M.; Adamo, C.; Cammi, R.; Ochterski, J. W.; Martin, R. L.; Morokuma, K.; Farkas, O.; Foresman, J. B.; Fox, D. J. *Gaussian 16, Revision B.01*, Wallingford, CT, **2016**.

[22] (a) Becke, A. D. Density-functional thermochemistry. III. The role of exact exchange. *J. Chem. Phys.* **1993,** *98*, 5648.

(b) Burke, K.; Perdew, J. P.; Wang, Y., *Electronic Density Functional Theory: Recent Progress and New Directions*. Plenum: **1998**;

(c) Perdew, J. P., *Electronic Structure of Solids '91*. Akademie Verlag: Berlin, **1991**; p 11;

(d) Perdew, J. P.; Chevary, J. A.; Vosko, S. H.; Jackson, K. A.; Pederson, M. R.; Singh, D. J.; Fiolhais, C. *Phys. Rev. B* **1992,** *46*, 6671.

(e) Perdew, J. P.; Chevary, J. A.; Vosko, S. H.; Jackson, K. A.; Pederson, M. R.; Singh, D. J.; Fiolhais, C. *Phys. Rev. B* **1993,** *48*, 4978.

(f) Perdew, J. P.; Burke, K.; Wang, Y. *Phys. Rev. B* **1996,** *54*, 16533.

[23] (a) Weigend, F.; Ahlrichs, R. *Phys. Chem. Chem. Phys.* **2005,** *7*, 3297.

(b) Weigend, F. *Phys. Chem. Chem. Phys.* **2006,** *8*, 1057.

[24] Yanai, T.; Tew, D. P.; Handy, N. C. *Chem. Phys. Lett.* **2004,** *393*, 51.

[25] Glendening, E. D.; Landis, C. R.; Weinhold, F. *J. Comput. Chem.* **2013,** *34*, 1429.

Chapter 4

Diborane(5) Complex Formed by Diborane(4) Dianion

4.1 Introduction

Diborane(6) (B_2H_6) is a dimeric form of the parent borane (BH_3) because of dimerization through 3-center-2-electron bond resulting from electron deficiency of boron.[1] Since diborane(6) has a long distance [1.775(3) Å][2,3] between two boron atoms, it is considered there is no B–B bond in diborane(6). Removal of one proton from B_2H_6 would produce an anionic diborane(5), $[B_2H_5]^-$, having a B–B single bond [Scheme 1(a)], however, it could only be observed in argon matrix at 77K.[4] Replacement of one hydride in the $[B_2H_5]^-$ with a neutral Lewis base would produce base-stabilized neutral diborane(5), which could be isolated by using bulky NHC (*N*-heterocyclic carbene) and aryl substituents.[5,6] Further removal of one proton from $[B_2H_5]^-$ should give dianionic diborane(4) species, $[B_2H_4]^{2-}$, having B=B double bond character.[7] Although the parent $[B_2H_4]^{2-}$ has never been isolated, replacement of hydrides with amino and aryl substituents allowed us to isolate its derivatives.[8-12] These B_2 species in Scheme 1(a) can be stabilized upon complexation with transition metals [Scheme 1(b)]. Metal complexes of $[B_2H_5]^-$ (type A) with Fe, Ru, Os, and Mo have been synthesized by a reaction of metal precursors with borane reagents.[13-16] A similar type-A Ru complex of $[B_2H_3(X)_2]^-$ (X = benzothiazol-2-thione-1-yl) was recently reported.[17] The base-stabilized neutral diborane(5) could also undergo complexation with copper (type B).6 It should be noted that these complexes (types A and B) also could be synthesized by a decomposition of transition metal complex of polyborane.[17,18] As the first example of type C complex, a dinuclear Pt(II)-B2I4 complex was synthesized by a redox reaction between Pt(0) and B_2I_4.[19] We also reported synthesis of dianionic diborane(4)-copper complex as the second example of type C complex by using isolated lithium salt of diborane(4) dianion (**1**) [Scheme 1(c)].[20] Herein, we report the synthesis of anionic diborane(5)-Rh complex **2** as a new member of type A complex by a reaction of the isolated diborane(4) dianion (**1**). The Rh complex **2** involves two distinct Rh atoms in which one Rh atom has aryl group as a substituent formed through C–H bond cleavage of *o*-tolyl group. Furthermore, detailed electronic properties were estimated by DFT calculations.

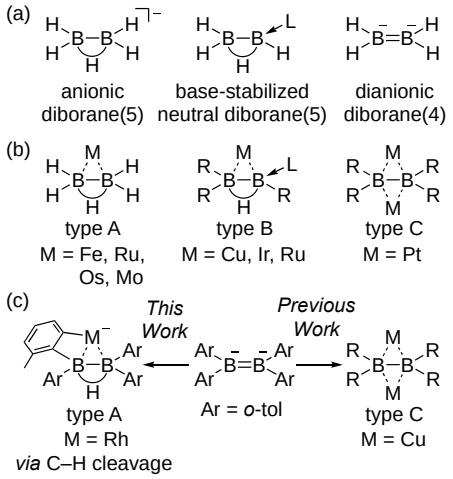

Scheme 4.1 Classification of B_2-based ligand and their transition metal complexes

4.2 The synthesis and Structure of Diborane(5) Complex

Reaction of the lithium salt of diborane(4) dianion (**1**) with $[RhCl(cod)]_2$ afforded an anionic diborane(5)-Rh complex **2** (Scheme 2). In the ^1H NMR spectrum, **2** in C_6D_6 exhibited a characteristic broad signal of the hydride which bridges two boron atoms at $\delta_H = -0.24$ ppm, being in a normal range for the bridging hydride in polyborane complexes (*ca.* $\delta_H = -7 \sim +2$).[17,21-28] Two similar but distinct ^{11}B NMR signals were observed at δ_B = 23, 31 ppm, indicating two boron atoms have similar environment. The molecular structure of **2** was unambiguously confirmed by a single-crystal X-ray diffraction analysis (Figure 2). In the solid state, hydrogen-bridging anionic diborane(5) coordinates to Rh1 in η^2-fashion. It should be noted that one of carbon atoms in *o*-tolyl group also bonded to Rh1 with C–H bond cleavage, which may be a source of the bridging hydride in the anionic diborane(5) moiety. As a result, the geometry of Rh1 is square planer coordinated by 1,5-cyclooctadiene (4-electron donor), tolyl group (2-electron donor), and diborane(5) (2-electron donor). The complex **2** has another rhodium atom, Rh2, binding to the Rh1-attached tolyl group in η^6-fashion. The B–B bond length [1.764(9) Å] in **2** is similar to the B–B bond lengths in the reported anionic diborane(5) complexes (type A) [$Cp_2Mo(B_2H_5)$: 1.796(6) Å,[15] $CpFe(CO)_2(B_2H_5)$: 1.773(8) Å,[16] $Cp^*Ru[B_2H_3(X)_2]$ (X = benzothiazol-2-thione-1-yl): 1.776(4) Å].[17] Two Rh–B bonds in **2** [2.407(7), 2.324(6) Å] are longer than those of poly(hydroborane)-Rh complexes [2.06-2.20 Å],[17,21-28] probably due to the larger steric hindrance of *o*-tolyl groups in **2**. Considering the existence of hydride ligand in anionic diborane(5) moiety and Rh-bonded tolyl group, C–H bond cleavage should be involved in the formation of **2**. A proposed mechanism for the formation of **2** is illustrated in Scheme 3. Considering the nucleophilic reactivity of B=B π-bond in **1** as recently reported, the first step would be a nucleophilic substitution at the Rh atom to form B–Rh bond. The resulting electron-rich Rh(I) complex **3** would undergo an oxidative additon of C–H bond in the *o*-tolyl group to furnish rhodium hydride **4**. The subsequent B–H bond-forming reductive elimination gives arylrhodium **5** having hydroborate moiety. Rotating B–B bond, formation of B–H–B bridge, and coordination of anionic diborane(5) to Rh afford a rhodate complex 6. The electron-rich tolyl group in **6** would be capable for the η^6-coordination to the second equivalent Rh(cod) fragment.

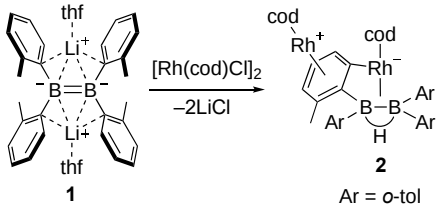

Scheme 2. Synthesis of **2**

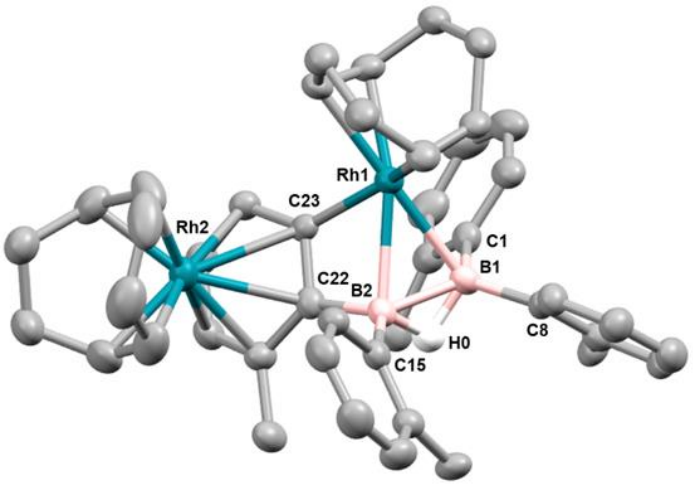

Figure 2. Molecular structure of **2** (thermal ellipsoids set at 50% probability and hydrogen atoms except H0 are omitted for clarity). Selected bond distance (Å): B1–B2 1.764(9), Rh1–B2 2.407(7), Rh1–B1 2.324(6), Rh1–C23 2.032(5), B1–C1 1.61(1), B1–C8 1.619(9), B2–C15 1.59(1), B2–C22 1.598(9).

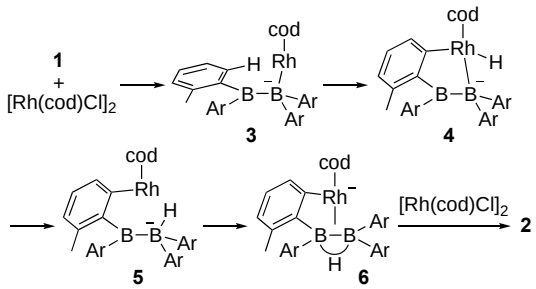

Scheme 3. A proposed mechanism for the formation of **2**

4.3. The characterization of Diborane(5) Complex

The electronic structure of **2** was estimated by UV-Vis spectrum and DFT calculations. A hexane solution of **2** exhibited one absorption maxima at 520 nm with an edge over 700 nm. Structural optimization from the experimentally obtained crystal structure was carried out at M06/def2SVP level of theory with use of ECP for Rh.

At the optimized structure, TD-DFT calculations one large absorption at 503 nm (Figure S6). This absorption was assigned to the transition from HOMO to LUMO+1. HOMO and LUMO+1 show highly delocalized orbitals, thus it is difficult to characterize as a simple transition mode. In molecular orbitals of **2**, highly delocalized B–B or Rh–B bonding interaction were found from HOMO to HOMO-11 (Figure 3 and S4). By NBO analysis, **2** has a large contribution of B–B single bond because the Wiberg bond index of B–B bond is 0.88, and localized orbitals corresponding to the B–B single bond is considerably occupied (occupancy 1.63). In contrast, copper □-complexes of NHC stabilized neutral diborane(5) show low bond order in Mayer bond index (0.38-0.43).[4] Otherwise, NBO corresponding to bonding orbitals of B–H–B shows low occupancy, reflecting normal electron-deficient B–H–B bonding. The main contribution of Rh–B bonding character is coordination from B–B single bond

(NBO65) to *d*-orbital of Rh (NBO183) ($\sigma_{B\text{-}B}$ → vacant *d*-orbital: 46.5 kcal/mol) by second order perturbation theory analysis. DFT study also suggests that the structure of **3** is diborane(4) dianion π-complexes and one rhodium atoms was coordinated from B=B of diborane(4) dianion and C=C of aryl moieties in η^4-fashion.

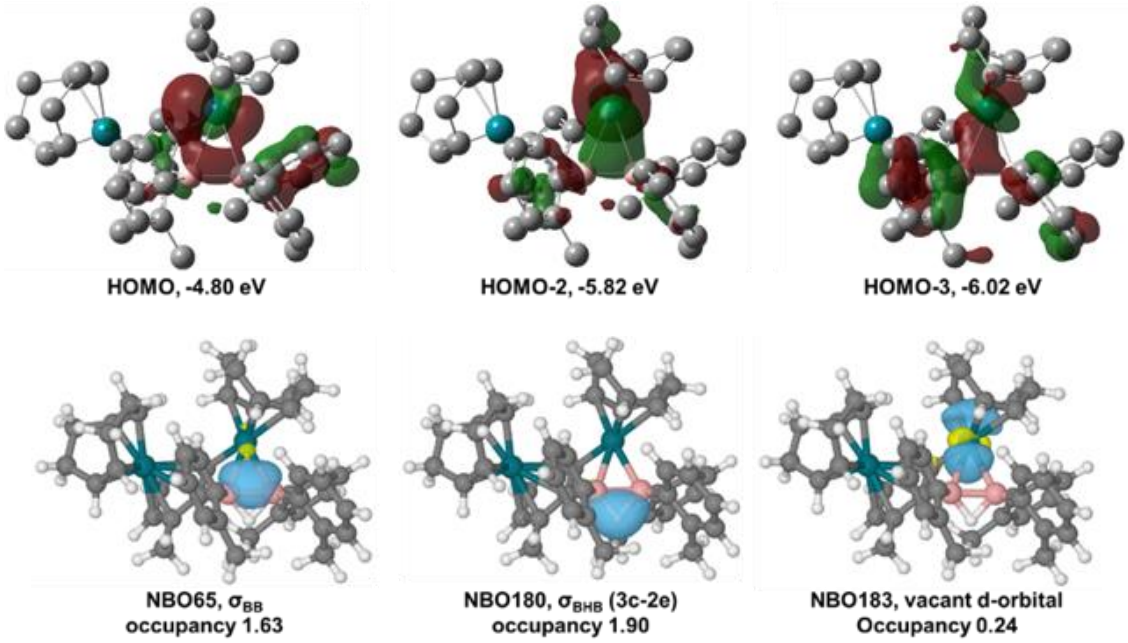

Figure 3. Molecular orbitals and Natural Bonding Orbitals of **2** and each occupancies

4.4 Conclusion

In conclusion, we synthesize and characterization of the rhodium σ-complex of anionic diborane(5). The main contribution of complexation is donation from B-B single bond to Rh vacant d-orbital.

4.5 Experimental Section

General Methods

All manipulations involving the air- and moisture-sensitive compounds were carried out under an argon atmosphere using standard Schlenk and glovebox (Korea KIYON, Korea and ALS Technology, Japan) technique. THF, Et_2O, toluene and *n*-hexane were purified by passing through a solvent purification system (Grass Contour). C_6D_6 was dried by distillation over sodium/benzophenone followed by vacuum transfer. Lithium salt of tetra(*o*-tolyl)diborane(4) dianion **1** was synthesized according to the literature.[12] The nuclear magnetic resonance (NMR) spectra were recorded on a JEOL ECS-400 (399 MHz for ^{1}H, 100 MHz for ^{13}C, 128 MHz for ^{11}B) or a Bruker AVANCE III HD 500 spectrometers (500 MHz for ^{1}H, 128 MHz for ^{13}C). Chemical shifts (δ) are given by definition as dimensionless numbers and relative to ^{1}H or ^{13}C NMR chemical shifts of the residual C_6D_5H for ^{1}H (δ = 7.16), C_6D_6 itself for ^{13}C (δ = 128.0). The ^{11}B NMR NMR spectra were referenced using an external standard of $BF_3(OEt_2)$. The absolute values of the coupling constants are given in Hertz (Hz). Multiplicities are abbreviated as singlet (s), doublet (d), triplet (t), quartet (q), multiplet (m) and broad (br). The

ATR-IR spectra were recorded on an Agilent Cary 630 spectrometer with a resolution of 4 cm^{-1}. Melting points were determined on MPA100 OptiMelt (Tokyo Instruments, Inc.) and were uncorrected. UV-vis absorption spectra were measured with an UV-3600 spectrometer (Shimadzu) using a 1 cm width quartz cell. Elemental analyses were performed on a Perkin Elmer 2400 series II CHN analyzer.

Synthesis of 2, Rh π-complex of anionic diborane(5)

Each toluene solution (each 10 mL) of **1** (63.5 mg, 0.117 mmol) and $[RhCl(cod)]_2$ (57.7 mg, 0.117 mmol) were cooled at −35 °C and solution of **1** was dropwised to Rh complex solution for few min. After stirring at −35 °C for 1 h, resulting solution was filtrated and the volatile was evaporated. The residue was washed with a small amount of Et_2O, crystallized by vapor diffusion method using by THF/pentane to obtained **2** as red crystals (18.5 mg, 20% yield). ^1H NMR (C_6D_6) δ: 8.30 (1H, d, $^3J_{HH}$ = 7 Hz, Ar), 7.91 (1H, d, $^3J_{HH}$ = 7 Hz, Ar), 7.40 (1H, t, $^3J_{HH}$ = 7 Hz, Ar), 7.20-7.03 (8H, m, Ar), 6.91 (1H, t, $^3J_{HH}$ = 7 Hz, Ar), 5.68 (1H, br t, $^3J_{HH}$ = 7 Hz, vinyl), 5.32 (1H, d, $^3J_{HH}$ = 6 Hz, (C_6H_3)MeRh), 5.15 (1H, t, $^3J_{HH}$ = 6 Hz, (C_6H_3)MeRh), 4.85 (1H, d, $^3J_{HH}$ = 6 Hz, (C_6H_3)MeRh), 4.20 (2H, m, vinyl), 3.94 (2H, m, vinyl), 3.86 (1H, m, vinyl), 3.71 (2H, m, vinyl), 3.03 (1H, m, CH_2 of cod), 2.60 (2H, m, CH_2), 2.20 (3H, s, CH_3), 2.16 (3H, s, CH_3), 2.11-1.90 (7H, m, CH_2), 1.76 (1H, m, CH_2), 1.67 (3H, m, CH_3), 1.63 (2H, m, CH_2), 1.52 (3H, s, CH_3), 1.51 (2H, m, CH_2), −0.24 (1H, br s, BHB). $^1H\{^{11}B\}$ (C_6D_6) δ: −0.24 (1H, br d, BHB). NMR (C_6D_6)$^{13}C\{^1H\}$ (C_6D_6) δ: 145.24 (1C, 4° Ar), 144.99 (1C, 4° Ar), 142.77 (1C, 4° Ar), 140.19 (1C, 4° Ar), 139.86 (1C, 4° Ar), 137.90 (1C, 4° Ar), 136.68 (1C, 3° Ar), 134.24 (1C, 3° Ar), 132.42 (1C, 3° Ar), 130.10 (1C, 3° Ar), 129.54 (1C, 3° Ar), 129.34 (1C, 3° Ar), 129.02 (1C, 3° Ar), 128.57 (1C, 4° Ar) 126.77 (1C, 3° Ar), 125.88 (1C, d, $^2J_{C–Rh}$ = 45 Hz, 3° Ar), 125.13 (1C, 4° Ar), 124.00 (1C, 3° Ar), 123.86 (1C, 3° Ar), 123.81 (1C, 3° Ar), 114.55 (1C, 4° Ar), 101.23 (1C, d, $^1J_{C–Rh}$ = 3 Hz, 3° Ar–Rh), 98.89 (1C, d, $^1J_{C–Rh}$ = 3 Hz, 3° Ar–Rh), 98.09 (1C, d, $^1J_{C–Rh}$ = 4 Hz, 3° Ar–Rh), 92.50 (1C, d, $^1J_{C–Rh}$ = 9 Hz, vinyl), 85.89 (1C, d, $^1J_{C–Rh}$ = 11 Hz, vinyl), 82.67 (1C, d, $^1J_{C–Rh}$ = 5 Hz, vinyl), 81.91 (1C, d, $J_{C–Rh}$ = 11 Hz, vinyl), 75.44 (2C, d, $^1J_{C–Rh}$ = 13 Hz, vinyl), 74.73 (2C, d, $^1J_{C–Rh}$ = 15 Hz, vinyl), 37.32 (1C, CH_2), 34.81 (1C, CH_2), 32.05 (2C, CH_2), 31.13 (2C, CH_2), 28.09 (1C, CH_2), 27.58 (1C, CH_2), 24.13 (1C, CH_2), 23.82 (1C, CH_3), 22.42 (1C, CH_3), 21.43 (1C, CH_3), 16.41 (1C, CH_3). $^{11}B\{^1H\}$ NMR (C_6D_6) δ 23, 3. mp. 130-140 °C (decomp); Anal. Calc. for $C_{44}H_{52}B_2Rh_2$: C, 65.38; H, 6.48; N, 0; Found: C, 65.74; H, 6.82; N, 0.02.

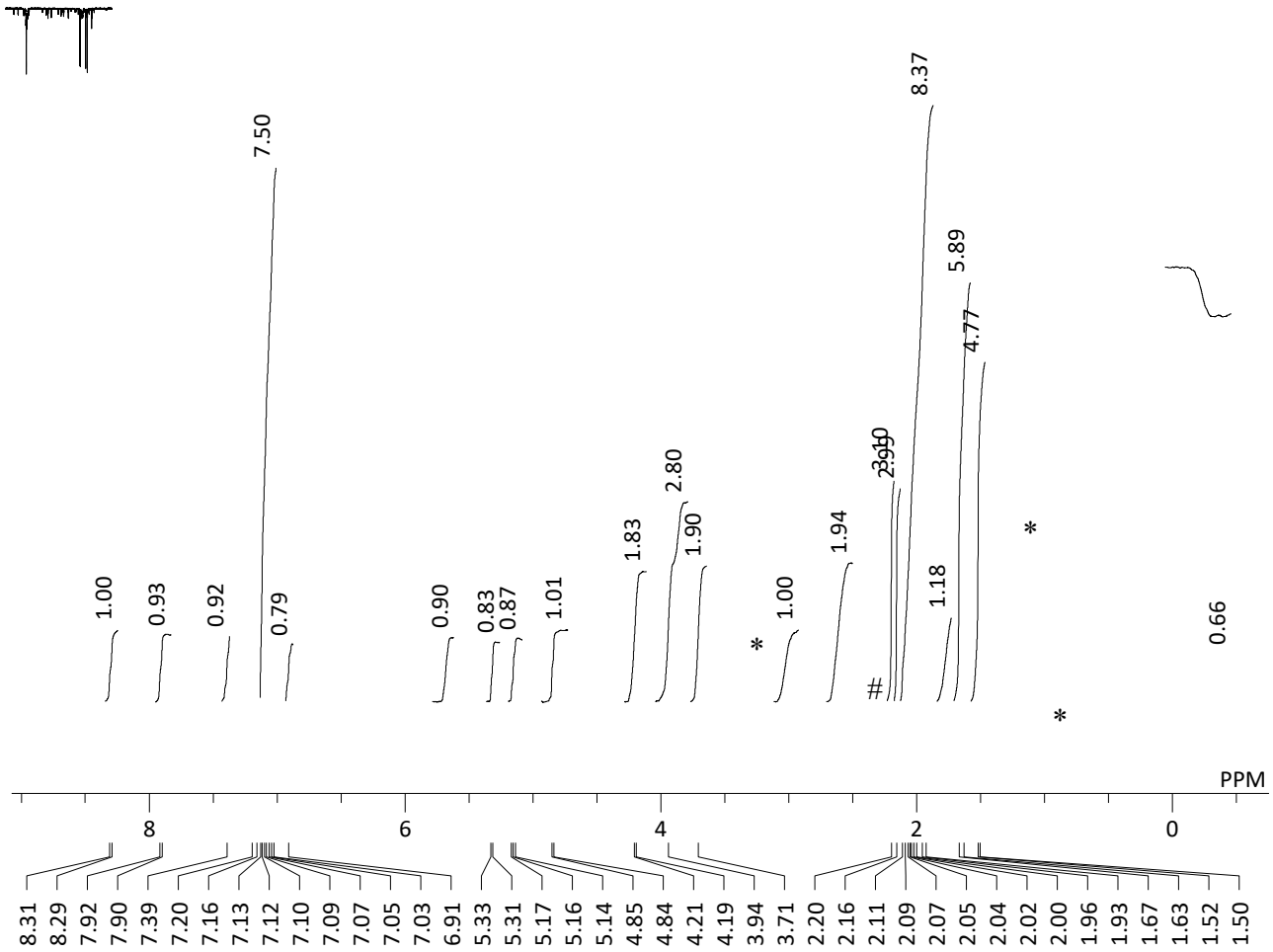

Figure S1. ^{1}H NMR (C_6D_6) spectrum of **2** (signals of hexane or Et_2O are marked by *, an unidentified product is marked by #)

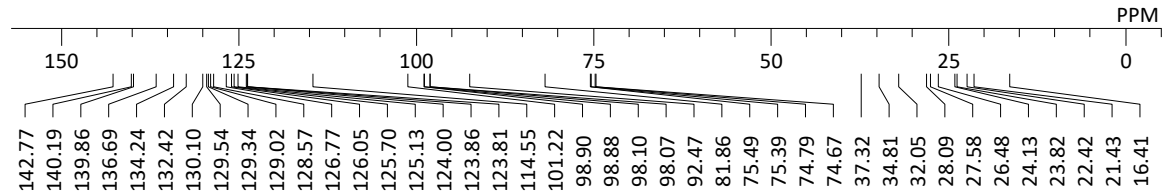

Figure S2. $^{13}C\{^{1}H\}$ NMR (C_6D_6) spectrum of **2**

X-ray Crystallographic Analysis

Details of the crystal data and a summary of the intensity data collection parameters for **2** are listed in Table S1. The crystals were coated with mineral oil and put on a MicroMount™ (MiTeGen, LLC), and then mounted on diffractometer. Diffraction data were collected on a Bruker Photon or Rigaku HyPix-6000 detectors using Mo$K\alpha$ radiation. The Bragg spots were integrated using CrysAlisPro program package.[2] Absorption corrections were applied. All the following procedure for analysis, Yadokari-XG 2009 was used as a graphical interface.[30] The structure was solved by a direct method with programs of SHELXT and refined by a full-matrix least squares method with the program of SHELXL-2016.[31] Anisotropic temperature factors were applied to all non-hydrogen atoms. The hydrogen atoms were put at calculated positions, and refined applying riding models. The detailed crystallographic data have been deposited with the Cambridge Crystallographic DataCentre: Deposition code CCDC (**2**). A copy of the data can be obtained free of charge via http://www.ccdc.cam.ac.uk/products/csd/request.

Table S1. Crystallographic data for **2**

	2
CCDC #	
formula	$C_{44}H_{52}B_2Rh_2$
formula weight	808.29
T / K	93
color	Red
size / mm	0.08×0.07×0.01
crystal system	*Monoclinic*
space group	$P2_1/n$ (#14)
a / Å	16.2471(6)
b / Å	12.5202(4)
c / Å	18.2440(8)
α / °	90
β / °	106.998(4)
γ / °	90
V / Å^3	3549.0(2)
Z	4
D_{calc} / g cm^{-3}	1.513
μ / mm^{-1}	0.962
F(000)	1664
θ range / °	1.994 to 25.999
reflns collected	20476
Indep reflns	11969
param	441
GOF on F^2	1.029
R_1 [$I > 2\sigma(I)$][a]	0.0592
wR_2 [$I > 2\sigma(I)$][b]	0.1440
R_1 (all data)[a]	0.0792
wR_2 (all data)[b]	0.1610
$\Delta\rho_{min,\ max}$ / e Å^{-3}	−1.435, 3.006

[a] $R_1 = \Sigma\ ||Fo| - |Fc|| / \Sigma\ |Fo|$, [b] $wR_2 = [\Sigma\ \{w(Fo^2 - Fc^2)^2 / \Sigma\ w(Fo^2)^2\}]^{1/2}$

UV-Vis Absorption and Emission Spectrum

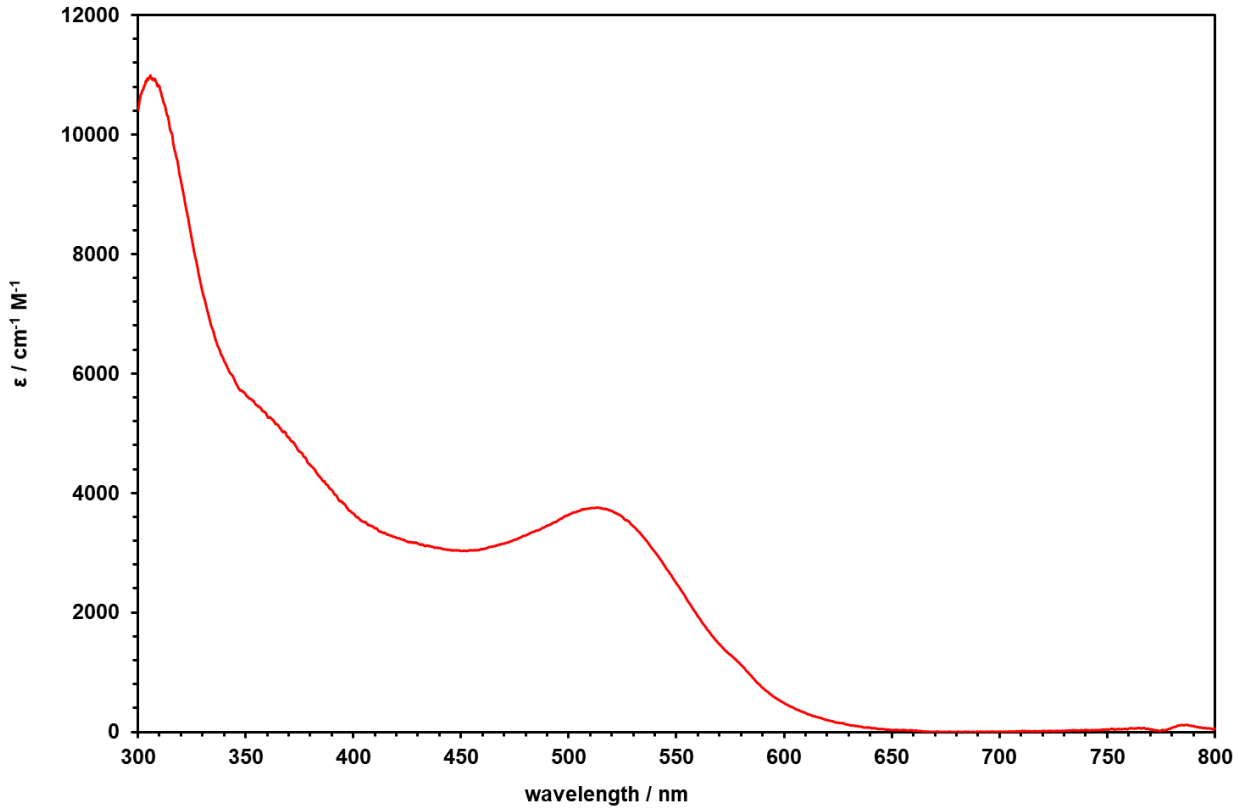

Figure S3. UV-Vis absorption spectrum of **2** (toluene solution)

5. Theoretical Calculations

DFT calculations were performed by using Gaussian 16, Revision B.01 program package.[32] The geometry optimizations of **2**, **3**, **4** were performed at the M06[6]/Def2SVP with ECP[7] level of theory. TD-DFT analysis was conducted with B3PW91[35]/Def2SVP level of theory for optimized structures. The Wiberg bond index (WBI) and natural population analysis (NPA) charge distribution were calculated by natural bond orbital (NBO 6.0) method.[36] Illustrations of NBO are performed by Jmol-NBO Visualization Helper v2.1 and Jmol.

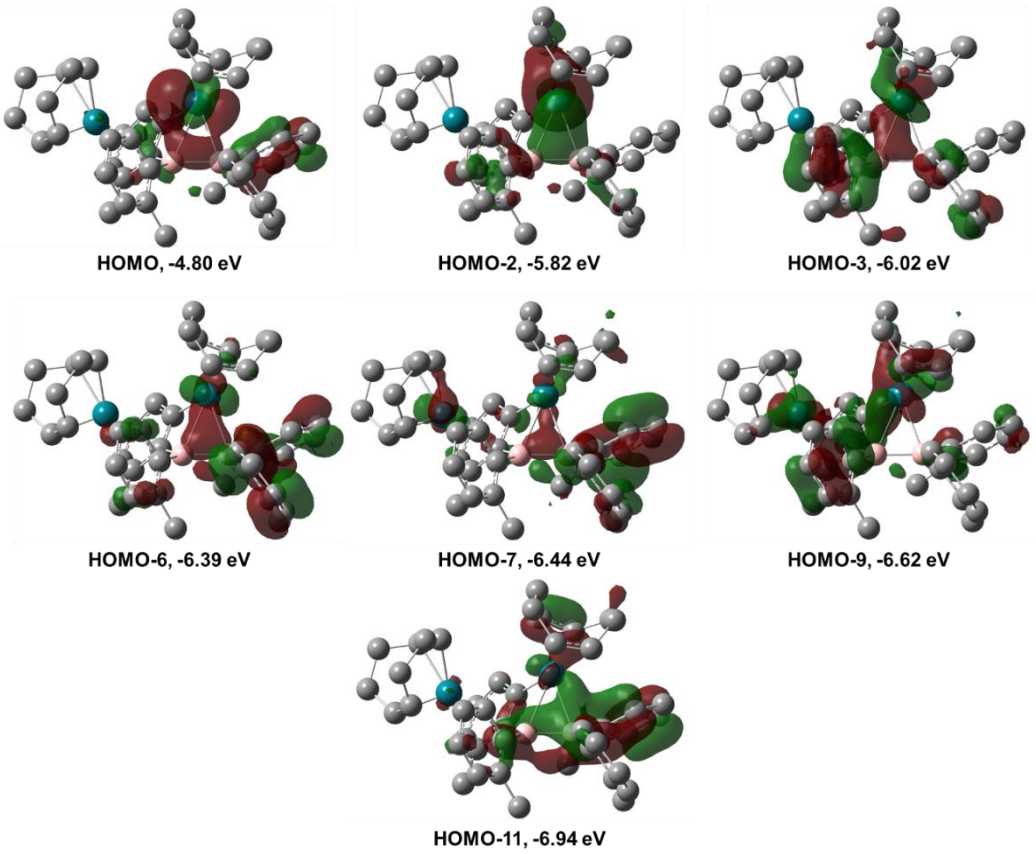

Figure S4. Molecular Orbitals of **2** Related to Rh–B Interaction

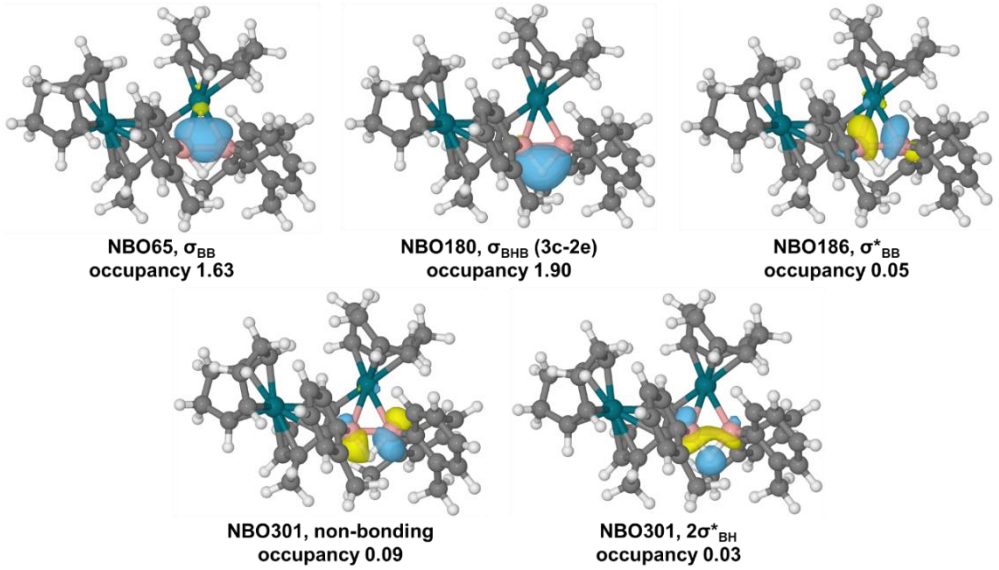

Figure S5. Natural Bonding Orbitals of **2** for Diborane(5) Moiety

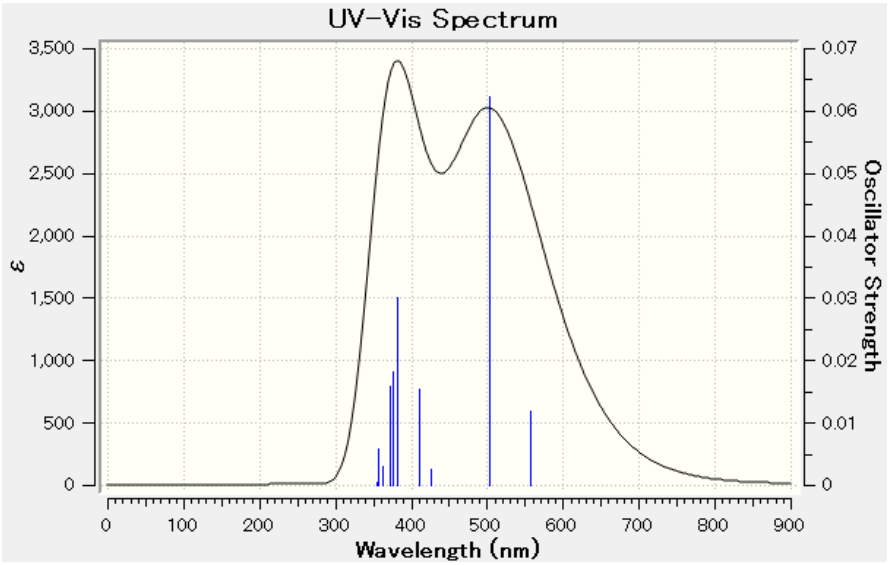

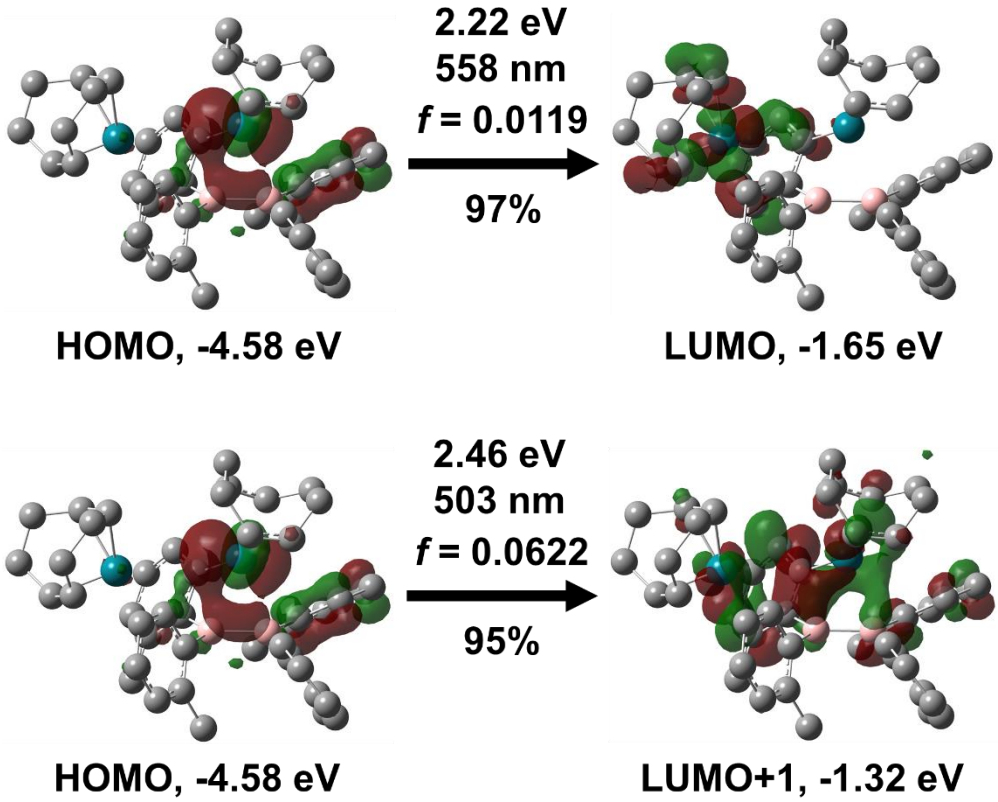

Figure S6. Predicted spectrum and assignment of UV-Vis spectrum of **2** by TD-DFT calculation

4.6. Reference

[1] W. N. Lipscomb, *Angew. Chem.* **1977**, *89*, 685-696.

[2] L. S. Bartell, B. L. Carroll, *J. Chem. Phys.* **1965**, *42*, 1135-1139.

[3] K. Kuchitsu, *J. Chem. Phys.* **1968**, *49*, 4456-4462.

[4] M.-C. Liu, H.-F. Chen, W.-J. Huang, C.-H. Chin, S.-C. Chen, T.-P. Huang, Y.-J. Wu, *J.*

Chem. Phys. **2016**, *145*, 074314.
[5] P. Bissinger, H. Braunschweig, A. Damme, R. D. Dewhurst, T. Kupfer, K. Radacki, K. Wagner, *J. Am. Chem. Soc.* **2011**, *133*, 19044-19047.
[6] S. R. Wang, D. Prieschl, J. D. Mattock, M. Arrowsmith, C. Pranckevicius, T. E. Stennett, R. D. Dewhurst, A. Vargas, H. Braunschweig, *Angew. Chem. Int. Ed.* **2018**, *57*, 6347-6351.
[7] E. Kaufmann, P. v. R. Schleyer, *Inorg. Chem.* **1988**, *27*, 3987-3992.
[8] A. Moezzi, M. M. Olmstead, P. P. Power, *J. Am. Chem. Soc.* **1992**, *114*, 2715-2717.
[9] A. Moezzi, R. A. Bartlett, P. P. Power, *Angew. Chem. Int. Ed. Engl.* **1992**, *31*, 1082-1083.
[10] T. Kaese, A. Hübner, M. Bolte, H.-W. Lerner, M. Wagner, *J. Am. Chem. Soc.* **2016**, *138*, 6224-6233.
[11] T. Kaese, T. Trageser, H. Budy, M. Bolte, H.-W. Lerner, M. Wagner, *Chem. Sci.* **2018**, *9*, 3881-3891.
[12] S. Akiyama, K. Yamada, M. Yamashita, *Angew. Chem. Int. Ed.* **2019**, *58*, 11806-11810.
[13] G. Medford, S. G. Shore, *J. Am. Chem. Soc.* **1978**, *100*, 3953-3954.
[14] J. S. Plotkin, S. G. Shore, *J. Organomet. Chem.* **1979**, *182*, C15-C19.
[15] P. D. Grebenik, M. L. H. Green, M. A. Kelland, J. B. Leach, P. Mountford, G. Stringer, N. M. Walker, L.-L. Wong, *J. Chem. Soc., Chem. Commun.* **1988**, 799-801.
[16] T. J. Coffy, G. Medford, J. Plotkin, G. J. Long, J. C. Huffman, S. G. Shore, *Organometallics* **1989**, *8*, 2404-2409.
[17] S. A. R, D. K. Roy, B. Mondal, Y. K, A. C, K. Saha, B. Varghese, S. Ghosh, *Angew. Chem. Int. Ed.* **2014**, *53*, 2873-2877.
[18] R. Macías, T. P. Fehlner, A. M. Beatty, *Organometallics* **2004**, *23*, 2124-2136.
[19] H. Braunschweig, R. D. Dewhurst, J. O. C. Jiménez-Halla, E. Matito, J. H. Muessig, *Angew. Chem. Int. Ed.* **2018**, *57*, 412-416.
[20] S. Akiyama, M. Yamashita, *Organometallics* **2020**, *39*, accepted.
[21] X. Lei, M. Shang, T. P. Fehlner, *J. Am. Chem. Soc.* **1998**, *120*, 2686-2687.
[22] H. Yan, A. M. Beatty, T. P. Fehlner, *Angew. Chem. Int. Ed.* **2001**, *40*, 4498-4501.
[23] H. Yan, A. M. Beatty, T. P. Fehlner, *Organometallics* **2002**, *21*, 5029-5037.
K. Roy, S. K. Bose, R. S. Anju, V. Ramkumar, S. Ghosh, *Inorg. Chem.* **2012**, *51*, 10715-10722.
[25] D. K. Roy, S. K. Bose, S. A. R, B. Mondal, R. V, S. Ghosh, *Angew. Chem. Int. Ed.* **2013**, *52*, 3222-3226.
[26] D. K. Roy, R. Jagan, S. Ghosh, *J. Organomet. Chem.* **2014**, *772-773*, 242-247.
[27] D. K. Roy, B. Mondal, S. A. R, S. Ghosh, *Chem. Eur. J.* **2015**, *21*, 3640-3648.
[28] K. Barik, M. G. Chowdhury, S. De, P. Parameswaran, S. Ghosh, *Eur. J. Inorg. Chem.* **2016**, *2016*, 4546-4550.
[29] CrysAlisPRO *CrysAlisPRO*, Oxford Diffraction/Agilent Technologies UK Ltd: Yarnton, England, **2015**.

[30] Kabuto, C.; Akine, S.; Kwon, E. Release of Software (Yadokari-XG 2009) for Crystal Structure Analyses. *J. Cryst. Soc. Jpn.* **2009,** *51*, 218-224.

[31] (a) Sheldrick, G. A short history of SHELX. *Act. Cryst. Sec. A* **2008,** *64*, 112-122; (b) Sheldrick, G. Crystal structure refinement with SHELXL. *Act. Cryst. Sec. C* **2015,** *71*, 3-8.

[32] Frisch, M. J.; Trucks, G. W.; Schlegel, H. B.; Scuseria, G. E.; Robb, M. A.; Cheeseman, J. R.; Scalmani, G.; Barone, V.; Petersson, G. A.; Nakatsuji, H.; Li, X.; Caricato, M.; Marenich, A. V.; Bloino, J.; Janesko, B. G.; Gomperts, R.; Mennucci, B.; Hratchian, H. P.; Ortiz, J. V.; Izmaylov, A. F.; Sonnenberg, J. L.; Williams; Ding, F.; Lipparini, F.; Egidi, F.; Goings, J.; Peng, B.; Petrone, A.; Henderson, T.; Ranasinghe, D.; Zakrzewski, V. G.; Gao, J.; Rega, N.; Zheng, G.; Liang, W.; Hada, M.; Ehara, M.; Toyota, K.; Fukuda, R.; Hasegawa, J.; Ishida, M.; Nakajima, T.; Honda, Y.; Kitao, O.; Nakai, H.; Vreven, T.; Throssell, K.; Montgomery Jr., J. A.; Peralta, J. E.; Ogliaro, F.; Bearpark, M. J.; Heyd, J. J.; Brothers, E. N.; Kudin, K. N.; Staroverov, V. N.; Keith, T. A.; Kobayashi, R.; Normand, J.; Raghavachari, K.; Rendell, A. P.; Burant, J. C.; Iyengar, S. S.; Tomasi, J.; Cossi, M.; Millam, J. M.; Klene, M.; Adamo, C.; Cammi, R.; Ochterski, J. W.; Martin, R. L.; Morokuma, K.; Farkas, O.; Foresman, J. B.; Fox, D. J. *Gaussian 16, Revision B.01*, Wallingford, CT, 2016.

[33] Y. Zhao, Y.; Truhlar, D. G. The M06 suite of density functionals for main group thermochemistry, thermochemical kinetics, noncovalent interactions, excited states, and transition elements: two new functionals and systematic testing of four M06-class functionals and 12 other functionals. *Theor. Chem. Acc.* **2008**, 120, 215-241.

[34] (a) Becke, A. D. Density-functional thermochemistry. III. The role of exact exchange. *J. Chem. Phys.* **1993,** *98*, 5648-5652; (b) Burke, K.; Perdew, J. P.; Wang, Y., *Electronic Density Functional Theory: Recent Progress and New Directions*. Plenum: 1998; (c) Perdew, J. P., *Electronic Structure of Solids '91*. Akademie Verlag: Berlin, 1991; p 11; (d) Perdew, J. P.; Chevary, J. A.; Vosko, S. H.; Jackson, K. A.; Pederson, M. R.; Singh, D. J.; Fiolhais, C. Atoms, molecules, solids, and surfaces: Applications of the generalized gradient approximation for exchange and correlation. *Phys. Rev. B* **1992,** *46*, 6671-6687; (e) Perdew, J. P.; Chevary, J. A.; Vosko, S. H.; Jackson, K. A.; Pederson, M. R.; Singh, D. J.; Fiolhais, C. Erratum: Atoms, molecules, solids, and surfaces: Applications of the generalized gradient approximation for exchange and correlation. *Phys. Rev. B* **1993,** *48*, 4978-4978; (f) Perdew, J. P.; Burke, K.; Wang, Y. Generalized gradient approximation for the exchange-correlation hole of a many-electron system. *Phys. Rev. B* **1996,** *54*, 16533-16539.

[35] (a) Weigend, F.; Ahlrichs, R. Balanced basis sets of split valence, triple zeta valence and quadruple zeta valence quality for H to Rn: Design and assessment of accuracy. *Phys. Chem. Chem. Phys.* **2005,** *7*, 3297-3305; (b) Weigend, F. Accurate Coulomb-fitting basis sets for H to Rn. *Phys. Chem. Chem. Phys.* **2006,** *8*, 1057-1065.

[36] Glendening, E. D.; Landis, C. R.; Weinhold, F. NBO 6.0: Natural bond orbital analysis

program. *J. Comput. Chem.* **2013,** *34*, 1429-1437.

Chapter 5

Synthesis of Triborylmethane Using by Diborane(4) Dianion

5.1 Introduction

The feature of trigonal boron is the presence of vacant p-orbital. Particularly, boron with no adjacent lone pair is efficient π-acceptor. One of the most popular π-acceptor is a dimesitylboryl group (Mes_2B).[1)] Because this boryl group is easily available and metastable for moisture, it is sometimes used in a luminescent material based on charge transfer transition.[2)] In many cases, the Mes_2B group is introduced by the nucleophilic attack to Mes_2BF.[3)] On the other hand, the Mes_2B group is used for the enhancement of the acidity of the C–H bond. Actually, the deprotonation by mesityllithium of methyl C–H of Mes_2BMe was reported.[4)] In chapter 2, the reactivity of diboran(4) dianion as a synthetic equivalent of diarylboryl anion was described.[5),6)] In this chapter 6, the diarylboryl group introduced by diborane(4) dianion is utilized for the synthesis of triborylmethane.

5.2 Synthesis of Triborylmethane

The active methylene in bis(diarylboryl)methane **1** was deprotonated with KHMDS to afford bis(diarylboryl)methylpotassium **2** as a yellow solid (Scheme 5.1). Potassium salt **2** is potassium carbanion, however, it is stable in THF solution. ^{1}H NMR spectrum of THF solution of **2** shows non-equivalent four signals of aryl proton, indicating free rotation of C–B bond between boryl group and center carbon is slow or nothing. The addition of cryptand into the THF solution of **2** gave a potassium cation free **2'**, which is the almost colorless solution. The preliminary data of the molecular structure of 2' was obtained by X-ray analysis. Considering this color changing, the ionic interaction between the *o*-tolyl group and potassium cation might cause the yellow color of **2**.

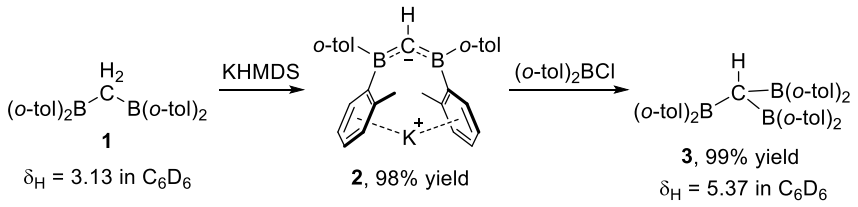

Scheme 5.1 The synthesis of **2** and **3**

A single-crystal X-ray diffraction analysis revealed the structure of **2** (Figure 5.1). The potassium cation is bind to three *o*-tolyl groups in two η^6- and one η^3-fashion. Three planes around two boron atoms and one center carbon atom are almost coplanar. The C–B bond [1.489(4), 1.476(4) Å] of the present potassium salt **2** was shorter than that of the bis(diarylboryl)methane [1.581(2), 1.577(2) Å], indicating the delocalization of the negative charge on the carbon atom to the boron atom. The reaction of the potassium salt **2** with $(o\text{-tol})_2BCl$ gave a tris(diarylboryl)methane **3**. The ^{1}H NMR spectra of methylene or methine protons of **2** and **3** exhibit higher-field shifted signals (**2**: δ_H = 3.13, **3**: δ_H = 5.37) than those of Bpin analogues,[6),7)] indicating strong negative hyperconjugation of diarylboryl group. To synthesize highly stabilized triborylmethyl anion, the reaction of **2** with 1 equivalent of KHMDS was conducted. However, the only complex mixture was obtained and target

compound was not generated.

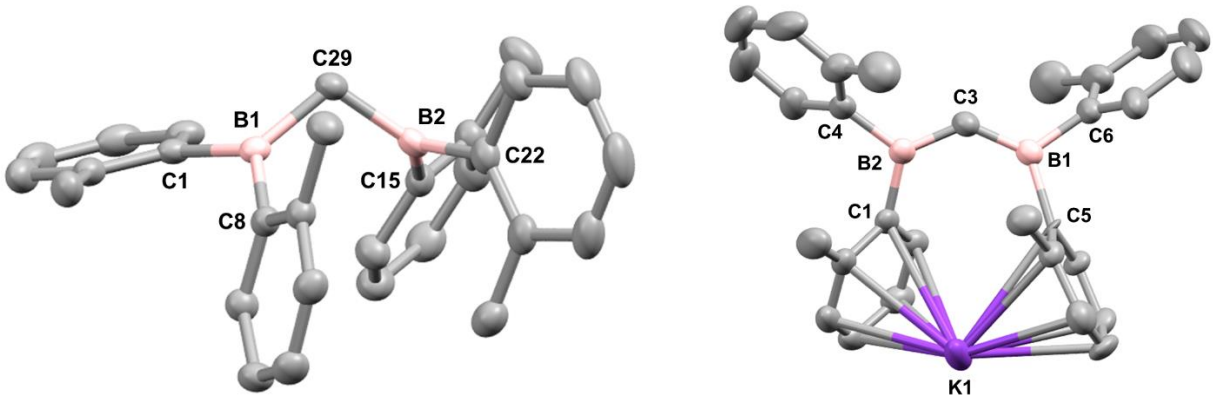

Figure 5.1 The molecular structure of **1** (right) and **3** (left) (thermal ellipsoids set at 50% probability and hydrogen atoms are omitted for clarity).

5.3 Conclusion

The strong negative hyperconjugation in **2** and **3** based on vacant p-orbital on di(*o*-tolyl)boryl group was observed by NMR spectroscopy and X-ray analysis. The negative hyperconjugation efficiently stabilizes potassium salt of carbanion species **2**.

5.4 Experimental Section

General Methods

All manipulations involving the air- and moisture-sensitive compounds were carried out under an argon atmosphere using standard Schlenk and glovebox (Korea KIYON, Korea and ALS Technology, Japan) technique. THF, Et_2O, toluene and *n*-hexane were purified by passing through a solvent purification system (Grass Contour). C_6D_6 was dried by distillation over sodium/benzophenone followed by vacuum transfer. Lithium salt of tetra(*o*-tolyl)diborane(4) dianion **1** was synthesized according to the literature.[12] The nuclear magnetic resonance (NMR) spectra were recorded on a JEOL ECS-400 (399 MHz for ^{1}H, 100 MHz for ^{13}C, 128 MHz for ^{11}B) or a Bruker AVANCE III HD 500 spectrometers (500 MHz for ^{1}H, 128 MHz for ^{13}C). Chemical shifts (δ) are given by definition as dimensionless numbers and relative to ^{1}H or ^{13}C NMR chemical shifts of the residual C_6D_5H for ^{1}H (δ = 7.16), C_6D_6 itself for ^{13}C (δ = 128.0). The ^{11}B NMR spectra were referenced using an external standard of $BF_3(OEt_2)$. The absolute values of the coupling constants are given in Hertz (Hz). Multiplicities are abbreviated as singlet (s), doublet (d), triplet (t), quartet (q), multiplet (m) and broad (br). The ATR-IR spectra were recorded on an Agilent Cary 630 spectrometer with a resolution of 4 cm^{-1}. Melting points were determined on MPA100 OptiMelt (Tokyo Instruments, Inc.) and were uncorrected. UV-vis absorption spectra were measured with an UV-3600 spectrometer (Shimadzu) using a 1 cm width quartz cell. Elemental analyses were performed on a Perkin Elmer 2400 series II CHN analyzer.

Synthesis of 2, potassium salt of diborylmethyl anion

Hexane 2 mL was added to the mixture of 1 (43.6 mg, 0.109 mmol) and KHMDS (21.9 mg, 0.110 mmol). After stirring at RT for 2 h, the volatile was evaporated and the yellow residue was washed with a large amount of hexane. After drying the yellow residue, 2 was obtained as a pure yellow powder (98% yield). By slow evaporation from THF solution of 2, yellow single crystals suitable for X-ray analysis was obtained. ^{1}H NMR (C_6D_6) δ: 7.05 (2H, br, Ar), 6.08 (2H, br, Ar), 6.59 (6H, br, Ar), 6.21 (6H, br, Ar), 4.52 (1H, s, methine). ^{11}B{^{1}H} (THF) δ: 57. Anal. Calc. for $C_{29}H_{29}B_2K$: C, 79.48; H,6.67; N, 0; Found: C, 79.12; H, 6.75; N, 0.06.

Synthesis of 3, triborylmethane

The mixture of THF 0.5 mL and **2** (23.1 mg, 0.577 mmol) was added to the mixture of THF 0.5 mL and (*o*-tol)$_2$BCl (12.9 mg, 0.564 mmol). After stirring at RT for 10 min, the resulting solution was filtrated. The solution was evaporated and the residue was washed with a small amount of hexane. The white power was obtained as a **3** (33.7 mg, 99% yield). ^{1}H NMR (THFnoD) δ: 7.83 (6H, m, Ar), 7.05 (12H, m, Ar), 6.81 (6H, m, Ar), 5.37 (1H, s, methine), 1.68 (18H, s, CH_3). ^{11}B{^{1}H} (THF) δ: 79 (br). Anal. Calc. for $C_{43}H_{43}B_3$: C, 87.21; H, 7.32; N, 0; Found: C, 87.35; H, 7.25; N, 0.03.

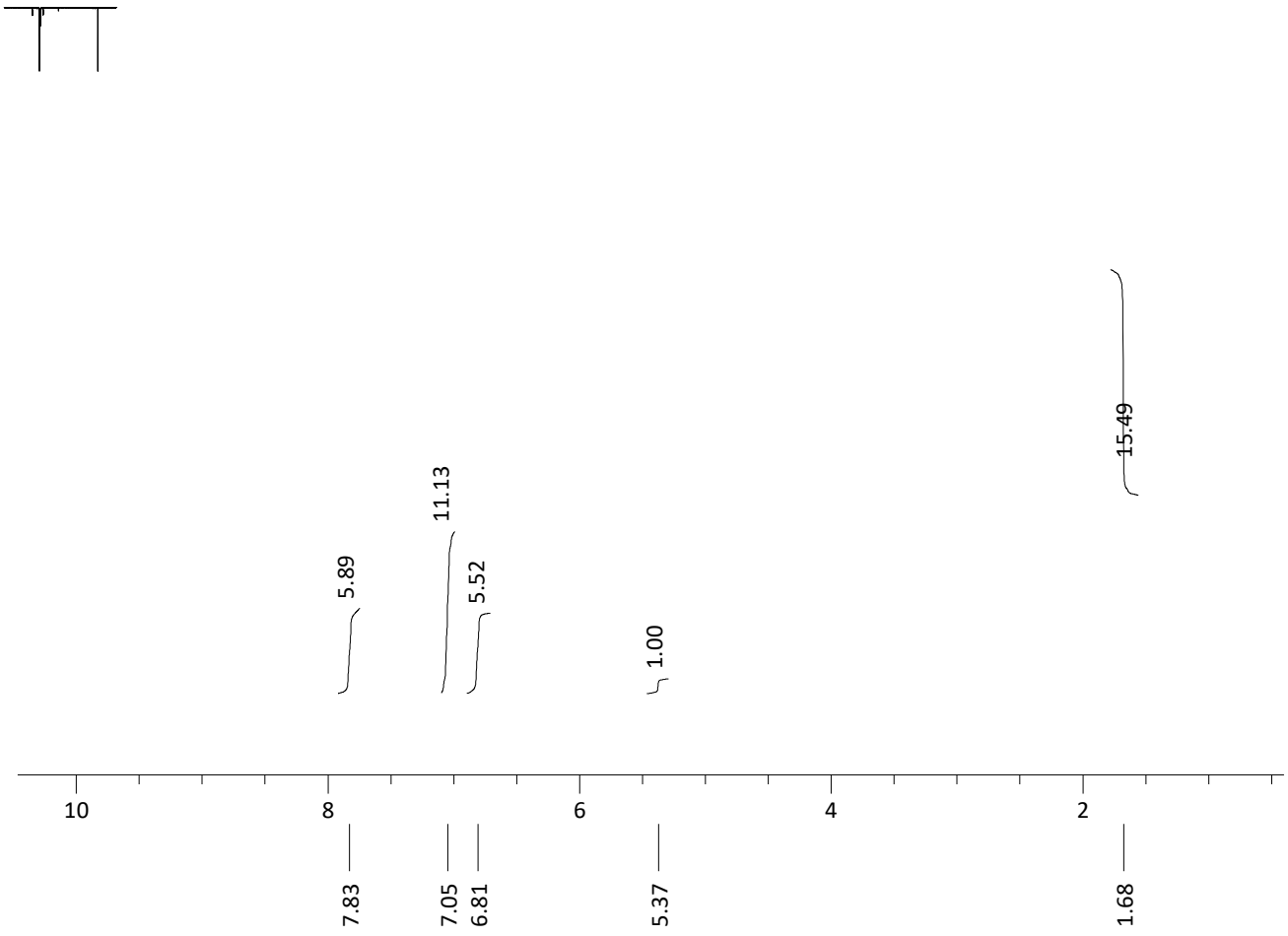

X-ray Crystallographic Analysis

Details of the crystal data and a summary of the intensity data collection parameters for **2** are listed in Table S1. The crystals were coated with mineral oil and put on a MicroMount™ (MiTeGen, LLC), and then mounted on diffractometer. Diffraction data were collected on a Bruker Photon or Rigaku HyPix-6000 detectors using Mo$K\alpha$ radiation. The Bragg spots were integrated using CrysAlisPro program package.[2] Absorption corrections were applied. All the following procedure for analysis, Yadokari-XG 2009 was used as a graphical interface.[30] The structure was solved by a direct method with programs of SHELXT and refined by a full-matrix least squares method with the program of SHELXL-2016.[31] Anisotropic temperature factors were applied to all non-hydrogen atoms. The hydrogen atoms were put at calculated positions, and refined applying riding models. The detailed crystallographic data have been deposited with the Cambridge Crystallographic DataCentre: Deposition code CCDC (**1**), (**3**). A copy of the data can be obtained free of charge via http://www.ccdc.cam.ac.uk/products/csd/request.

Table S1. Crystallographic data for **1**, **3**

	1	**3**
CCDC #		
formula	$C_{29}H_{30}B_2$	$C_{29}H_{29}B_2K$
formula weight	400.15	438.24
T / K	93	93
color	colorless	Yellow
size / mm	0.30×0.26×0.20	0.11×0.10×0.80
crystal system	*Triclinic*	*Monoclinic*
space group	*P*-1 (#2)	$P2_1/n$ (#14)
a / Å	10.8011(5)	10.7599(5)
b / Å	11.2843(3)	16.7798(6)
c / Å	11.3930(4)	14.1769(5)
α / °	68.347(3)	90
β / °	64.967(4)	102.774(4)
γ / °	80.057(3)	90
V / Å^3	1169.16(9)	2496.27(18)
Z	2	4
D_{calc} / g cm^{-3}	1.137	1.166
μ / mm^{-1}	0.063	0.227
F(000)	428	928
θ range / °	1.942 to 27.499	1.909 to 27.494
reflns collected	14090	18746
Indep reflns	8221	5615
param	284	351
GOF on F^2	1.061	1.062
R_1 [$I > 2\sigma(I)$][a]	0.0567	0.0755
wR_2 [$I > 2\sigma(I)$][b]	0.1306	0.2111
R_1 (all data)[a]	0.0567	0.1008
wR_2 (all data)[b]	0.1306	0.2260
$\Delta\rho_{min,\ max}$ / e Å^{-3}	−0.215, 0.396	−0.466, 1.405

5.5 References

[1)] (1) Yamaguchi, S.; Wakamiya, A. *Pure and Applied Chemistry* **2006**, *78*, 1413.

[2)] (a) Yamaguchi, S.; Akiyama, S.; Tamao, K. *J. Am. Chem. Soc.* **2000**, *122*, 6335. (b) Glogowski, M. E.; Williams, J. L. R. *J. Organomet. Chem.* **1981**, *216* , 1–8. (c) Collings, J. C.; Poon, S.-Y.; Le Droumaguet, C.; Charlot, M.; Katan, C.; Pålsson, L.-O.; Beeby, A.; Mosely, J. A.; Kaiser, H. M.; Kaufmann, D.; Wong, W.-Y.; Blanchard-Desce, M.; Marder, T. B. *Chem. Eur. J.* **2009**, *15*, 198–208. (e) Fu, G.-L.; Zhang, H.-Y.; Yan, Y.-Q.; Zhao, C.-H. *J. Org. Chem.* **2012**, *77*, 1983

[3)] Li, C.; Mellerup, S. K.; Wang, X.; Wang, S. *Organometallics*, **2018**, *37*, 3360.

[4)] Pelter, A.; Drake, R.; Stewart, M. J. *Tetrahedron Lett.* **1989**, *30*, 3085.

[5)] Tsukahara, N.; Asakawa, H.; Lee, K.-H.; Lin, Z.; Yamashita, M., *J. Am. Chem. Soc.* **2017,** *139*, 2593.

[6)] Akiyama, S.; Yamada, K.: Yamashita, M. *Angew. Chem. Int. Ed.* **2019**, *58*, 11806.

[7)] Zhang, Z.-Q.; Yang, C.-T.; Liang, L.-J.; Xiao, B.; Lu, X.; Liu, J.-H.; Sun, Y.-Y.; Marder, T. B.; Fu, Y. *Org. Lett.* **2014**, *16*, 6342.

[8)] Yamamoto, T.; Ishibashi, A.; Suginome, M. *Org. Lett.* **2019**, *21*, 6235.

Chapter 6

Conclusion

Conclusion

In this thesis, the author has revealed the synthesis and reactivity of chemistry of diborane(4) dianion and its transition metal complexes. By the synthesis and full characterization of diborane(4) dianion, the double bond character, the ionic interaction between a B=B double bond and lithium cation, and high occupied π-orbital of diborane(4) dianion was investigated. In particular, the reactivity of diborane(4) dianion as a two synthetic equivalent of diarylborylanion implies the possibility of dicarbon-substituted borylanion having vacant π-orbital. In the complexation of diborane(4) dianion with copper, the ability of σ-donation and π-backdonation was investigated. As a result, dianionic diborane(4) ligand show strong s-donation and very weak π-backdonation. This property of diborane(4) dianion as a ligand reflects the low electronegativity of boron. Also, the diborane(4) dianion ligand transformed into anionic diborane(5) via aryl C–H activation on rhodium. The substituents introduced by diborane(4) dianion are useful for the strong π-accepter based on vacant p-orbital of diarylboryl group. Actually, the localization of the lone pair of carbanion was observed in the molecular structure. The achievement of the new reagent of equivalent boryl anion with vacant p-orbitals is important for various and unique boron compounds.

Publication List

Original Paper

[1] Akiyama, S.; Yamada, K.; Yamashita, M.

"Reactivity of A Tetra(*o*-tolyl)diborane(4) Dianion as Diarylboryl Anion"

Angewante Chemie. Internaltionl. Edition **2019**, *58,* 11806-11810.

[2] Akiyama, S.; Ikemoto, S.; Muratsugu, S.; Tada, M.; Yamashita, M.

"Copper Complexes Bearing A Dianionic Diborane(4) Ligand: Synthesis and Evaluation of the Donor Property."

Organometallics **2020,** *39,* in press. doi:10.1021/acs.organomet.0c00027

Other Publication List

[3] Katsuma, Y.; Wu, L.; Lin, Z.; Akiyama, S.; Yamashita, M.

"Reactivity of Highly Lewis-Acidic Diborane(4) toward C≡N Triple and N=N Double Bonds: Uncatalyzed Addition and N=N Bond Cleavage Reactions"

Angewante Chemie. Internaltionl. Edition **2019**, *58*, 317-321.

Acknoledgment

All the works have been done under supervision of Professor Makoto Yamashita. First of all, the author would like to thank Professor Makoto Yamashita for his advice, ideas, patience, encouragement and the best environment for investigation. The author would like to thank Senior assistant professor Jun-ichi Ito, Assistant Professor Katsunori Suzuki, Special assistant Professor Ryo Nakano for their advice and encouragement.

The author is appreciative to the members of Ph. D. committee, Professor Hiroshi Shinokubo, Professor Shigehiro Yamaguchi, for their instructive and helpful discussions.

The author is sincely grateful to the members of Yamashita laboratory, Secretary Shiho Takeyasu, Dr. Shogo Morisako, Dr. Taichi Nakamura, Dr. Enrique H. Kwan, Mr. Kengo Sugita, Mr. Haruki Kisu, Mr. Yuhei Katsuma, Mr. Shin Nakayama, Mr. Jun Kobayashi, Mr. Satoshi Kurumada, Mr. Ding Tao, Mr. Masaki Kuno, Ms. Wakano Taniguchi, Ms. Yasuho Namba, Mr. Kaito Yamada, Ms. Lee Ming Min, Mr. Kazuyoshi Asaka, Ms. Aoi Okamura, Ms. Akemi Kobayashi, Ms. Akane Suzuki, Ms. Yuna Yonekawa, Ms. Lee Hyejin, Ms. Yuria Otsuka, Mr. Katsumi Sato, Mr. Ryotaro Yamanashi, Mr. Zeng Wenhao.

Finally, the author is most grateful to his friend, Mr. Daisuke Kasori, Mr. Yoshiaki Yoichi, and his family, Mr. Tetsuharu Akiyama, Ms. Narumi Akiyama, Mr. Koji Akiyama for heart-warming encouragement through the research.

2020, February

Seiji Akiyama